Chair of Geology and Economic Geology

Master's Thesis

Alteration Processes as Exploration Parameter for Lead-Zinc Ores in the Graz Paleozoic

Sandro Rohrhofer, BSc

March 2025

AFFIDAVIT

I declare on oath that I wrote this thesis independently, did not use any sources and aids other than those specified, have fully and truthfully reported the use of generative methods and models of artificial intelligence, and did not otherwise use any other unauthorized aids.

I declare that I have read, understood and complied with the "Preamble on Integrity in Academic Study, Teaching, and Research Operations" of the Montanuniversität Leoben.

Furthermore, I declare that the electronic and printed versions of the submitted thesis are identical in form and content.

Date

(The original signature is kept at the university)

Acknowledgements

Having reached the end of my studies, I would like to express my deepest gratitude to my parents for their tireless support during all these years at the Montanuniversität Leoben, as they made the path to this thesis and its completion possible in the first place. I would also like to thank all my relatives and friends who have given me the strength to complete this degree by having a great time together.

I would especially like to thank my supervisor Univ.-Prof. Mag.rer.nat. Dr.mont Frank Melcher for his professional support, the sharing of his wealth of experience in writing scientific papers and the very collegial atmosphere.

A big thank you goes to Annika Geringer for the organization and administration of the project as well as to Dr. Leopold Weber and Dr. Ralf Schuster for their expertise regarding the Pb-Zn-Ag-Ba mineralization and the geology of the Paleozoic of Graz. I would also like to thank all other members of the project for their professional contribution. Apart from the project, recognition for expert support is due to Ao.Univ.-Prof. Mag. et Dr.rer.nat. Gerd Rantitsch, and Ass.Prof. Dipl.-Ing. Dr.mont. Heinz Mali. I would like to thank Ivaylo Martinov for sample preparation and all the staff at the Department of Geology and Economic Geology at the Montanuniversität Leoben for the excellent working atmosphere.

I would like to thank Priv.-Doz. Dr. Etienne Skrzypek from the Institute of Earth Sciences at the University of Graz for carrying out microprobe analyses.

Looking back at my time as a student at the Montanuniversität Leoben, I realize once again that I have matured in terms of perseverance, structured thinking and accuracy and that I have been given the tools to succeed in my future career - I appreciate that.

Danksagung

Am Ende meines Studiums angekommen, möchte ich meinen Eltern für ihre unermüdliche Unterstützung in all den Jahren an der Montanuniversität Leoben den größten Dank aussprechen, da sie den Weg hin zu dieser Arbeit und zum Fertigstellen erst ermöglicht haben. Herzlicher Dank gilt auch all meinen Verwandten und Freunden, die mir durch die gemeinsame Zeit Kraft für das Abschließen dieses Studiums gegeben haben.

Besonders möchte ich meinem Betreuer Univ.-Prof. Mag.rer.nat. Dr.mont Frank Melcher für die fachlichen Hilfestellungen, das Weitergeben seines Erfahrungsschatzes für das Verfassen wissenschaftlicher Arbeiten und der überaus kollegialen Atmosphäre danken.

Ein großes Dankeschön gilt Annika Geringer für die Organisation und Administration des Projektes sowie Dr. Leopold Weber und Dr. Ralf Schuster für deren Expertise hinsichtlich der Pb-Zn-Ag-Ba Vererzungen und der Geologie des Grazer Paleozoikums. Ich bedanke mich auch bei allen weiteren Projektangehörigen für deren fachlichen Beitrag. Abseits des Projektes gilt Anerkennung für fachkundige Unterstützung Ao.Univ.-Prof. Mag. et Dr.rer.nat. Gerd Rantitsch, und Ass.Prof. Dipl.-Ing. Dr.mont. Heinz Mali. Ein Dankeschön möchte ich Ivaylo Martinov für die Probenpräparation aussprechen sowie allen Mitarbeitern des Lehrstuhls für Geologie und Lagerstättenlehre an der Montanuniversität Leoben für das großartige Arbeitsklima.

Bei Priv.-Doz. Dr. Etienne Skrzypek vom Institut für Erdwissenschaften der Universität Graz bedanke ich mich für die Durchführung von Mikrosondenanalysen zur Altersdatierung.

Mit dem Blick zurück an meine Studienzeit an der Montanuniversität Leoben wird mir einmal mehr bewusst, dass in mir ein Reifeprozess hin zu Durchhaltevermögen, strukturiertem Denken und Genauigkeit stattgefunden hat und es wurde mir das Werkzeug in die Hände gelegt, um Erfolg im zukünftigen Beruf haben zu können – das weiß ich zu schätzen.

Abstract

The Graz Paleozoic is part of the Drauzug-Gurktal nappe system in the Austroalpine unit of the eastern Alps (Austria). It consists of Silurian to Carboniferous metasedimentary successions representing a differentiated basin evolution. Stratiform SEDEX-type Pb-Zn-Ag-Ba occurrences are situated in the Schönberg formation of the Schöckl nappe and are hosted by polyphase deformed greenschist facies metapelitic, metacarbonate and metavolcanoclastic lithologies. Alteration zones and elemental zonation surrounding sulphide mineralisation were investigated. For this purpose, drill core sections with sulphide ore horizons of a 1970-80s exploration program at Haufenreith and Guggenbach as well as from former mining districts were analysed. The investigated sulphide ore horizons are composed of mainly galena, sphalerite, pyrite, pyrrhotite and in parts of baryte and magnetite. Minor ore phases are chalcopyrite, ullmannite, pentlandite, Ni-Co-Fe sulpharsenides, argentiferous phases such as hessite and argentopentlandite, and other rare ore minerals. These major and minor ore phases are also present disseminated or in veinlets in small quantities throughout the alteration zone. The alteration zone around sulphide mineralisation forms a diffuse halo within metamorphosed background sedimentation. It occurs both in the footwall and hanging wall of ore horizons indicating vent proximal ore deposition and is traceable for tens of metres even in weakly mineralised ore horizons of drill cores. Albitization occurs commonly beneath ore horizons. Carbonate alteration is present mainly but not exclusively in the hanging wall of sulphide mineralisation and consists of dominating dolomite-ankerite, and minor siderite. The chemical compositions of ferrous carbonates, chlorite and white mica in the alteration zone show a general enrichment in Fe as well as Mg. Carbonates are additionally enriched in Mn. A zone of initial Mg enrichment at the outer rim of the alteration zone is followed by an inner zone with Mg depletion as well as Fe enrichment peaking at sulphide mineralisation, where carbonates become Mn enriched. Moreover, Ba bearing white mica is present in the alteration zone reaching highest Ba concentrations at the location of mineralisation. Barium rich feldspar, celsian and hyalophane, is present in samples of the mineralisation at Arzwaldgraben and Peggau-Taschen as well as in drill cores from Haufenreith, where they are accompanied by K-feldspar, which sometimes occurs also as minor constituent of ore horizons and in sulphide veinlets as gangue phase. High Field Strength Element (HFSE) and Rare Earth Element (REE) rich phases frequently accompany ore and alteration minerals. Observed HFSE minerals are rutile, ilmenite, titanite, (urano-)thorite, zircon and others. Discrete niobium rich minerals are columbite-(Fe) and euxenite-(Y), which are exclusively associated with ore horizons at the Kaltenberg-Burgstall district. REE minerals encompass abundant monazite-(Ce), minor fluorocarbonates and xenotime-(Y) as well as rare allanite-(Ce). Besides, fluorapatite occurs often with HFSE and REE minerals. Observed alteration mineralogy and the frequency of alteration related phases correlate well with whole rock geochemistry of investigated drill cores. The detailed mineralogical and geochemical investigation of drill core material illustrates type and extent of wall rock alteration associated with the metamorphosed stratiform sulphide ore and can be applied as a tool in regional exploration programs.

Zusammenfassung

Das Grazer Paläozoikum gehört zum Drauzug-Gurktal-Deckensystem und ist Teil des Ostalpin der Ostalpen (Österreich). Die Lithologien setzen sich aus sedimentären Abfolgen einer differenzierten Beckenentwicklung des Silur bis Karbon zusammen. Die stratiformen Pb-Zn-Ag-Ba-Vorkommen, die dem SEDEX-Lagerstättentyps zugeschrieben werden, befinden sich in mehrfach deformierten und grünschieferfaziell überprägten Metapeliten und Metavulkanoklastika innerhalb der Schönberg-Formation der Schöckl-Decke. Im Zuge dieser Arbeit wurden Untersuchungen durchgeführt, um Alterationserscheinungen als auch Elementzonierungen im Bereich von Sulfiderzlagen zu identifizieren. Zu diesem Zweck wurden Bohrkerne aus Haufenreith und Guggenbach eines Explorationsprojektes aus den 1970-80er Jahren als auch Handstücke aus ehemaligen Bergbaugebieten beprobt und analysiert. Die untersuchten Sulfiderze bestehen hauptsächlich aus Bleiglanz, Sphalerit, Pyrit, Pyrrhotin und teilweise aus Baryt und Magnetit. Untergeordnete Erzphasen sind Chalkopyrit, Ullmannit, Pentlandit, Ni-Co-Fe-Arsensulfide, silberhaltige Phasen wie Hessit und Argentopentlandit sowie andere selten vorkommende Erzphasen. Diese Erzminerale kommen auch in kleinerem Ausmaß in der gesamten Alterationszone disseminiert oder innerhalb von Äderchen vor. Die Alterationszone um die stratiformen Vererzungen bildet einen diffusen Hof bestehend aus Alterationsphasen der Mineralisation, welche die sedimentären und vulkanoklastischen Nebengesteine überprägt. Sie tritt sowohl im Liegenden als auch im Hangenden von Erzhorizonten auf, was eine proximale Ausfällung von Erzphasen widerspiegelt, und ist selbst in sehr geringmächtigen Erzschnüren in den Bohrkernen über dutzende Meter nachweisbar. Albitisierung tritt häufig im Liegenden von Erzhorizonten auf. Die Karbonat-Alteration ist hauptsächlich, aber nicht ausschließlich, im Hangenden der Vererzung ausgebildet und besteht überwiegend aus der Dolomit-Ankerit-Serie sowie untergeordnet Siderit. Die chemische Zusammensetzung von Karbonaten, Chlorit und Hellglimmer in der Alterationszone zeigt eine allgemeine Anreicherung von Fe und in Karbonaten kommt es zu einem zusätzlichen Mn-Einbau. Karbonate sind Mg-reich in der äußeren Alterationszone, gefolgt von einer inneren Fe-Anreichung, die ihr Maximum in der Vererzung erreicht, wobei diese in der Nähe von Erzhorizonten auch Mn-führend sind. Weiters ist in der Alterationszone Ba-haltiger Hellglimmer vorhanden, der im Erz die höchsten Ba-Konzentrationen erreicht. Ba-reiche Feldspäte, Celsian und Hyalophan, sind in Proben der Mineralisationen von Arzwaldgraben, Peggau-Taschen und von Bohrkernen aus Haufenreith vorhanden, wo diese von Kalifeldspat, begleitet werden, der manchmal auch in geringerem Ausmaß in Erzhorizonten und sulfidhaltigen Äderchen als Gangphase auftritt. Minerale der HFSE (High Field Strength Elemente) und SEE (Seltenerdelemente) begleiten Erz- und Alterationsminerale häufig. Zu den beobachteten HFSE-Mineralen gehören Rutil, Ilmenit, Titanit, (Uran-)Thorit, Zirkon und andere Seltene. Diskrete Niob-reiche Minerale sind Columbit-(Fe) und Euxenit-(Y), die ausschließlich in Verbindung mit Erzhorizonten im Revier Kaltenberg-Burgstall vorkommen. Zu den SEE-Mineralen gehören Monazit-(Ce), untergeordnet Fluorokarbonate und Xenotim-(Y) sowie seltener Allanit-(Ce). Außerdem tritt Fluorapatit häufig mit HFSE- und SEE-Phasen auf. Die beobachtete Alterationsmineralogie und die Häufigkeit der alterationsbezogenen Phasen korrelieren gut mit der Gesamtgesteinschemie der untersuchten Bohrkerne. Die detaillierte mineralogische und

geochemische Untersuchung des Bohrkernmaterials veranschaulicht Art und Ausmaß der mit dem metamorphisierten stratiformen Sulfiderz assoziierten Nebengesteinsalteration, und kann als Hilfsmittel in regionalen Explorationsprogrammen eingesetzt werden.

Table of Contents

Table of Figures

List of Tables

1 Introduction

Sedimentary exhalative/SEDEX deposits are the most important source of Pb & Zn and make up more than 50% of the known resources and a quarter of total production (Goodfellow, 2004). There are 121 known deposits, which occur mainly in Australia, America, and Asia. Twelve of these deposits exceed 100 Mt total tonnage of contained Pb and Zn metal and some also hold considerable amounts of Ag (Taylor *et al.*, 2009). These massive sulphide deposits can also host important byproducts; for instance, Cu orebodies are part of the Mount Isa, Australia (Finlow-Bates & Stumpfl, 1979), and Rammelsberg, Germany (Sperling & Walcher, 1990), deposits. Some deposits exhibit thick baryte layers, e.g. Meggen, Germany (Krebs, 1981), and there are a few known mineralisation with syngenetic Au occurrences (Emsbo, 2000). Furthermore, SEDEX deposits are associated with rift-controlled sedimentary basin environments (Lydon, 2004a). The age distribution of deposits shows two main geological time periods of formation at the boundary of the Paleo- and Mesoproterozoic as well as in the Paleozoic era (Taylor et al., 2009).

The Graz Paleozoic hosts a number of SEDEX-type Pb/Zn occurrences within fine-grained metasediments. They are the basis of a long history of mining activity in the area stretching back to medieval times with the first mentioning of Arzberg, an important centre of former mining, in 1200 A.D.. There were several boom and bust cycles in the course of ore extraction in the region, but during the 17/1800s a rise in activity took place, albeit mining declined with the first world war and was abandoned in the first half of the 20th century completely (Weber, 1990). In the 1970s exploration commenced by “Bleiberger Bergwerks Union”. Drilling, mapping, geochemical & geophysical studies were carried out, which identified the area between the villages Guggenbach and Großstübing as the most promising. At Großstübing, an exploration adit (“Silberberg”) was excavated beginning in 1983 and layers of massive Zn ore, massive Pb ore and baryte were found reaching over 1 m in thickness each (Weber, 1990). However, these findings did not lead to a revival of mining but instead provided the impetus to conduct further investigations, to deepen the geological understanding of these deposits, and to identify the potential of metal deposits in the Graz Paleozoic.

Therefore, the project “MRI_SEDEXPOT - SEDEX deposits in the Graz Paleozoic – investigations to the exploration potential with the Arzberg deposit as calibration region” was initiated by GeoSphere Austria in cooperation with the Chair of Geology and Economic Geology at the Montanuniversität Leoben. Its aim is to identify hydrothermal alteration phenomena, element zonation around mineralisation, and studies are carried out on stream sediments & water samples. This thesis is part of this project and addresses hydrothermal alteration and elemental zonation and summarizes scientific findings gathered during the investigations of rock samples from different locations with known Pb/Zn occurrences and drill cores from the exploration program of the 1970-80s.

1.1 Characteristics of SEDEX deposits

SEDEX deposits form in an extensional tectonic regime. In general, there are two main settings: failed rifts of continental crust or passive margin environments of oceanic domains (Leach *et al.*, 2005). The former is found with Proterozoic deposits of the northern Australian basins, which occur especially in post-rift or syn-inversion sediment successions overlaying basal syn-rift units, which rarely host SEDEX mineralisation. Initial submarine basin inversion occurred contemporaneously with the Isan Orogeny, which reactivated a network of existing intrabasinal extensional faults of the rift phase, creating pathways for fluids transporting metals from volcanic and juvenile siliciclastic syn-rift sequences, which otherwise would be sealed by younger carbonatic sediments, to or near the seafloor (Gibson *et al.*, 2016). The latter extensional setting is found in deposits within the Palaeozoic Selwyn basin in north-eastern Canada and shows analogous fluid source and transport mechanisms. These deposits were generated at a hyper-extended continental margin from brines in deep seated immature clastic sediments of the syn-rift phase, where these lithologies acted as an aquifer which in turn got capped by thermally insulating impermeable fine-grained successions of the following sag phase. Fault opening as a result of brittle deformation at the hyper-extended margin tapped the reservoir and acted as conduits for ascending metalliferous fluids forming the massive sulphide deposits (Rodríguez *et al.*, 2021). However, SEDEX deposits may also form during the early stages of the post-rift phase of the passive margin, like the Rammelsberg deposit in Germany. A drastic subsidence event caused by the combination of thermal and tectonic subsidence initiated a circulation of metal enriched brines enclosed in the sedimentary basin fill and seismic pumping moved these fluids along a fault zone to hydrothermal vents at the basin margin where the Rammelsberg deposit was located (Moreno *et al.*, 2019).

Both tectonic environments, where SEDEX deposits form, have the same principal sedimentary sequences. The stratigraphy starts with a 4 to 15 km thick basal rift-related sediment accumulation of clastic terrigenous sediments, such as conglomerates, red beds, sandstones, turbiditic sediments, and to a lesser extent also remnants of volcanic activity during the initial opening of the basin. These successions were then covered by transgressive shales/siltstones and shallow-water carbonates derived from platforms at the basin margins (Emsbo, 2009). The deposits are part of the upper sediment pile from the sag-phase and are hosted by black shales or mudstones and micritic limestones with high organic matter contents deposited in a reduced sedimentation setting. In the case of passive margin environments, carbonate platforms at the margins record very low siliciclastic sedimentary input, which favours organic carbon preservation and thus anoxic conditions at the seafloor (Leach *et al.*, 2005; Emsbo, 2009). Furthermore, an important feature of these basins with SEDEX deposits is syn-sedimentary faulting and the deposition of fault-related debris material in fine-grained deep-water sediments of the host rock. Additionally, the formation of subbasins links all SEDEX deposits (Leach *et al.*, 2005).

The exact genesis of SEDEX deposits is still disputed and several models have been proposed (Emsbo, 2009), and by way of example span from traditional syn-sedimentary (Finlow-Bates & Stumpfl, 1979; Large *et al.*, 2005) to epigenetic syn-deformational models (Cave, 2022) for the Mount Isa region (Australia). However, for most and especially all giant (>10 Mt of metal) sediment-hosted base metal deposits of different types rifting in a 200 km wide transitional zone from high to low lithospheric thickness seems to be fundamental since the boundary of cratonic lithosphere enables long-lived lithospheric edge stability as well as a low geothermal heat flow,

and combined with high subsidence rates accumulating thick sediment piles extend the depth for fluid circulation (Hoggard *et al.*, 2020). Nevertheless, evaporated seawater as complexing agent from basin margins in low latitudes with corresponding climatic conditions played a vital part in the formation of mineralisation. Penetration of cold fluids to great depths of several kilometres occurred in order to reach temperatures high enough for metal leaching from rift-phase sediments or even basement lithologies (Wilkinson, 2014). A fluid convection, facilitated by high temperatures and/or mixing of colder seawater with highly saline evaporitic seawater to reduce the density of brines, thus enhances the possibility of movement and the displacement of basin fluids at more moderate temperatures, and drove the upwelling of hydrothermal fluids and the discharge at the seafloor or the infiltration along shallow permeable strata (Wilkinson, 2014). Furthermore, fault-controlled subbasins acted as traps for vented metalliferous fluids, which then precipitated ore phases and formed massive lens-shaped sulphide layers (Emsbo, 2009).

The ultimate sulphur source for Pb and Zn minerals is marine sulphate, which is found in sea- or porewater or in already existing phases containing sulphate, for example baryte. Furthermore, a reduction of sulphate to sulphide took place through biogenic and/or thermogenic processes. This is shown in the values of sulphur isotopy from galena and sphalerite ranging between -10 to 30 $\delta^{34}S$, but the bulk of values are within -5 to 15 $\delta^{34}S$ (Leach *et al.*, 2005). Moreover, some deposits show trends between lighter values from biogenic sulphate reduction and heavier values from thermogenic sulphate reduction, which can signify temperature changes from early to late stages, or progressive enrichments of heavier sulphur in an isotopically closed system, and also lateral, vertical as well as stratigraphic changes in isotopy were found at different deposits showing a complex history (Leach *et al.*, 2005).

As already mentioned, evaporitic fluids play a major role in transporting metals within SEDEX systems. Fluid inclusions from sphalerite in the Red Dog district in northern Alaska show that ore-forming fluids had probably temperatures below 200°C and moderate to high salinity, around 10–20 wt. % NaCl equivalent. Considering the salinity levels and the electrolyte composition it is assumed that original evaporative seawater had about 30 wt. % NaCl equivalent and got diluted on its flow path (Leach *et al.*, 2004). At the Century and Burketown mineral field deposits in northern Australia similar compositions of primary fluid inclusions in sphalerite were reported with 21.6 wt. % NaCl equivalent and homogenization temperatures range from 74°C to 125°C (Polito *et al.*, 2006). A slightly wider temperature range from 105°C to 261°C is given for fluid inclusions in sphalerite from the Mehdiabad SEDEX-type sub-seafloor replacement deposit in Iran, where variable salinity values between 0.03–19.44 wt% NaCl equivalent indicate fluid mixing (Maghfouri *et al.*, 2021). Although temperatures and salinities of mineralising fluids are relatively similar and obviously a relevant factor, also the chemical composition might have been of vital importance for the genesis of SEDEX deposits and might also give hints why there were certain periods in time when these deposits formed preferentially. Firstly, the emergence of these deposits in the Paleoproterozoic reflects major changes in the atmo-/hydrosphere when oxygenation at the Earth's surface was happening. Around 2.4 Ga the rise in oxygen began and was also accompanied by increasing marine sulphate levels from oxidative weathering of continental sulphides (Farquhar *et al.*, 2010). Secondly, there were secular variations of Ca^{2+}, Mg^{2+}, Na^{2+} and SO_4^{2-} in seawater (Fig.1), whereas at times higher concentrations of Ca^{2+} than of the other mentioned constituents were present. This chemical composition of marine water produced $CaCl_2$-rich brines through evaporation of seawater (Lowenstein *et al.*, 2003). Hardie (1996) suggested that reactions at greenschist and amphibolite facies conditions between seawater

and basalt at the MOR absorbed Na^+, Mg^{2+} and SO_4^{2-} from the water and released Ca^{2+} and K^+ into the sea and combined with high oceanic crust production rates would produce $CaCl_2$ enriched seawater. Moreover, brines enriched in Ca^{2+} compared to SO_4^{2-} would experience further depletion during the precipitation of gypsum, which in turn would produce very metalliferous solutions due to the increased solubility of metals in chloride-rich fluids especially in sediments without Ca or Mg silicates and/or carbonates, which would increase the pH of the fluid, and so an external source of sulphur would be needed to form ore phases due to very low sulphate concentrations in the mineralising brine (Wilkinson, 2014; Yardley, 2005).

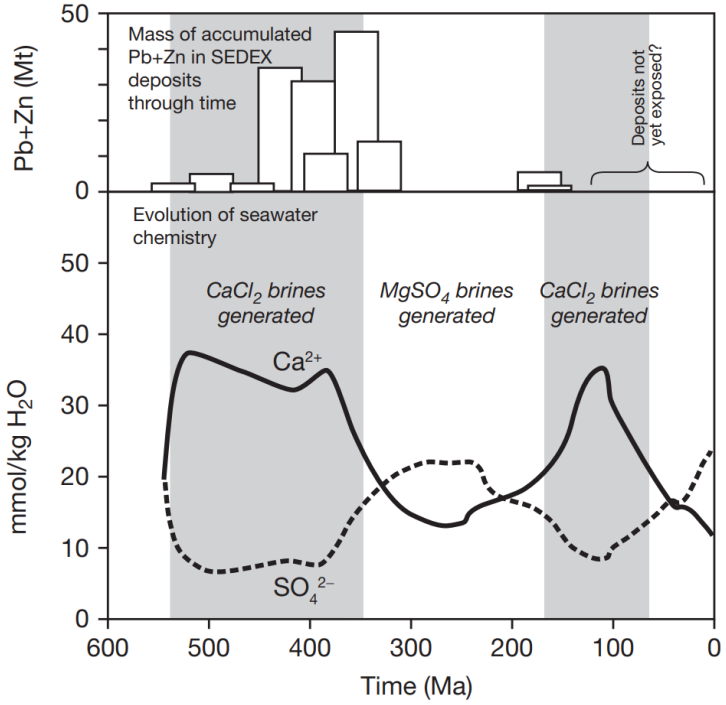

Figure 1: Comparison of Ca^{2+} and SO_4^{2-} concentrations in seawater with the temporal occurrence of SEDEX deposits (Wilkinson, 2014).

SEDEX deposits have characteristic orebody morphologies. They consist of different zones, are stratabound & stratiform, and reached initially hundreds of metres to 1.5 km in length. Vertically the ore body may encompass several ore lenses on top of each other for up to tens of metres, which represent several ore-forming events of the hydrothermal system (Emsbo, 2009). The area of the submarine vent field and just beneath it, where fluids flow up, is called the vent complex. It consists of hydrothermal products and hydrothermal fracturing, cementation, and replacement are common textures. In addition, it is here where the highest ore grades are usually found (Lydon, 2004a). Bedded ores are the next adjacent zone, which forms an asymmetric field around the vent complex. They are composed of laminated layers (millimetres to metres in thickness) of sulphide ore phases and sometimes they are interlayered with host rocks. Furthermore, debris flows and/or turbidites from the elevated vent complex may occur. With increasing distance from the exhalative centres bedded ores are termed distal hydrothermal products because they become thinner, uneconomic, and pinch out finally (Lydon, 2004a). Hydrothermal fluids flow to the vent complex via a zone of fractured rock called feeder zone. It is the product of hydrofracturing and/or tectonism by syn-sedimentary fault zones. Here, a stockwork and a replacement mineralisation is present. However, the feeder zone is missing at many deposits (Lydon, 2004a). These kinds of deposits are referred to as vent-distal and were formed after the discharge into the seawater by

bottom-hugging, relatively cool, and highly saline fluids migrating like turbiditic currents into local depressions. Their high densities and speeds inhibited cooling and mixing with marine water. Finally, when fluids come to rest, dilution, temperature reduction, and the reaction with H_2S leads to a precipitation of sulphides and/or the replacement of minerals by ore phases in highly permeable juvenile sediments through infiltration of dense metalliferous brines (Sangster, 2002).

SEDEX deposits display lateral thickness variations, mineralogical, and chemical zonation, such as a decreasing amount of hydrothermal products with greater distance from hydrothermal vents and an accompanied rise of sedimentary input, and zonal changes in the distribution of different hydrothermal phases (Fig.2) as a result of different chemical behaviour between constituents during dispersal from hydrothermal upflow zones (Lydon, 2004a). Firstly, there is a change from reduced mineral facies to more oxidized mineral facies from the discharge centre to more peripheral areas as well as vertically, shown in decreasing Zn:Ba and Zn:Mn values towards the deposit limits. Secondly, a decreasing temperature away from hydrothermal vents is indicated by the order chalcopyrite, pyrrhotite, galena and sphalerite. Additionally, pyrite increases towards the fringes of the system. Thirdly, in the vent complex arsenopyrite and sulfosalts are important carriers for Sb, Bi, As, Hg and Ag, which is also contained within galena. Furthermore, carbonates vary from Fe-rich in the venting centre to Ca-rich in the periphery (Lydon, 2004a).

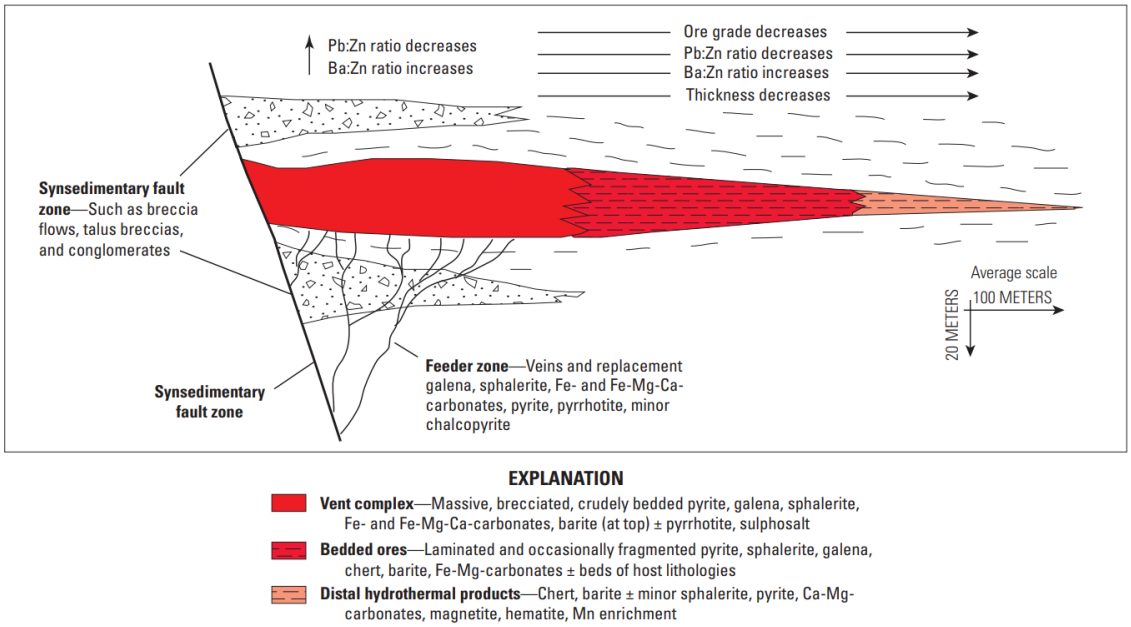

Figure 2: Profile through an idealized SEDEX deposit and indication of its zonal make-up (Emsbo, 2009).

Alteration patterns are manifold and have different manifestations for various deposits, but many ore bodies have partially consistent alteration mineralogy. The following is a compilation of mineralogical and chemical halos surrounding ore bodies of several deposits but does not represent the full scope of alteration phenomena but rather is supposed to give an idea of possible hydrothermal alteration characteristics.

Alteration zones can be very extensive and stretch for hundreds of metres to many kilometres; this is especially true for the McArthur River deposit (HYC) with a traceable halo for at least 23 km in strike, 250 m above as well as 50 m below the ore body (Large *et al.*, 2000). Also alteration zones of deposits in the Selwyn Basin, Canada, show similar extents (Goodfellow, 2004). In the case of deposits in the Proterozoic basins in northern Australia host rocks have large strata-bound

halos, which are expressed in gentle lithochemical variations such as Zn, Pb, and Tl. A common feature of the SEDEX mineralisation in Australia, like Century (Large *et al.*, 2005), George Fisher (Chapman, 2004), HYC (Large *et al.*, 2000), and Lady Loretta (Large & McGoldrick, 1998), are Mn enrichments in carbonates towards ore horizons as well as zones of Fe-rich carbonates, like siderite, ankerite, and ferroan dolomite. Additionally, sometimes pyritic envelopes and disseminated sulphides, especially sphalerite, occur. Deposits in the Selwyn Basin show different alteration styles. At the Tom deposit interlayered baryte, sphalerite and pyrite are found in cherty mudstones stratigraphically above the ore body (Goodfellow, 2004). Barium enrichment in the overlaying mudstone is present at the Howards Pass deposit, plus the elements Zn, Pb, Cu, Ni, Co, As, Sb, Cd, Hg as well as the amount of total S increase towards mineralised layers, which is attributed to pyrite and sphalerite in the halo (Goodfellow, 2004). High Ba values are not found at the Sullivan deposit, but the host sediment experienced pyrite, carbonate as well as muscovite alteration, and extensive albitization, chloritization, and tourmalinization (Freeze, 1966; Lydon, 2004b); the latter is also found to have happened at the amphibolite facies metamorphosed Schneeberg deposit, Italy, and similar to Australian deposits Mn contents in garnets increase towards ore layers. Moreover, there is a Zn substitution in biotite and staurolite, and an enrichment in K in host rocks (Niggli, 1987). The alteration mineralogy of the Schneeberg deposit is partly comparable to the highly metamorphosed Broken Hill Pb-Zn-Ag deposit (Australia), which forms a spectrum of clastic-sediment hosted base metal deposits with the genetically linked SEDEX-type (Emsbo, 2009). At Broken Hill the alteration zone consists of gahnite, quartz and pyrrhotite as well as abundant manganoan garnet, which is an indicator to sulphide ore (Plimer, 2006). At Rammelsberg, Germany, the situation is slightly different; there are also Mn-bearing siderite/ ankerite as well as ferroan dolomite present, but below the ore body is a silica-dominated alteration, called “Kniest” locally. Furthermore, chloritization took place and within the silicified sediments sulphides are common (Sperling & Walcher, 1990).

1.2 Graz Paleozoic

According to the tectonic interpretation of the Austroalpine by Schmid *et al.* (2004) the Graz Paleozoic is part of the larger Drauzug-Gurktal nappe system, which represents the tectonically highest part of the Upper Austroalpine basement nappes. It is underlain by the Koralpe-Wölz and the Silvretta-Seckau nappe systems (Fig.3) (Schmid *et al.*, 2004) and discordantly covered by sediments of the Mesozoic Gosau Basin in the west (Kröll & Heller, 1978), the Miocene Passail Basin in the centre (Weber, 1990), and the Miocene Styrian Basin towards the south (Ebner & Sachsenhofer, 1991). The metasedimentary lithologies of the Graz Paleozoic reflect different facies settings, contain fossils from the Silurian to the Carboniferous, and it was early recognised that they represent stacked nappes (Flügel, 1975; Ebner, 1976). Sedimentary records reveal a well differentiated basin structure with distinct topographic features controlling sediment deposition starting in the Silurian and lasting to the Early-Middle Devonian boundary when sediment accumulation compensated relief differences (Fritz & Neubauer, 1988). Different bathymetric situations are observed in the Schöckl and Laufnitzdorf nappes containing elevated deposition rates of clastics indicating greater water depths. Furthermore, there is an increase of pelagic sediments and corresponding water depths from the proximal Rannach to the intermediate Schöckl and distal Laufnitzdorf group lithologies, which highlights an extensional tectonic regime resulting in variations of sedimentary facies (Fritz & Neubauer, 1988). Additionally, Gasser *et al.*

(2010) suggested that the Kalkschiefer facies was located in a lagoonal-type depression adjacent to the Schöckl facies facing coastal areas as well as between the Schöckl carbonate platform and the pelagic Laufnitzdorf facies. These individual groups also show a distinct topography and different subsidence rates caused by block rotation, whereas sediment accumulation was highest in halfgrabens (Fritz & Neubauer, 1988). Over time, until the Early/Middle Devonian, a decrease of volcanic input and subsidence occurred, and a more homogenous sedimentation and carbonate production followed. Moreover, in the face of a missing substratum, heavy minerals of metamorphic provenance in sandstones as well as the geochemical composition of alkaline basalts indicate that the Graz Paleozoic represents a basin environment with an initial rifting sequence of an intra-continental setting (Fritz & Neubauer, 1988). From a paleogeographic point of view, this environment was located at the northern margin of Gondwana, part of the Balkan-Carpathian Ocean, has Devonian relationships to Variscan microcontinental pieces, and is part of the larger Noric domain, which encompasses the Noric group of the Greywacke Zone and the Gurktal Paleozoic additionally (Neubauer *et al.*, 2022).

Despite of divergent sedimentary facies, especially of the Schöckl-, Kalkschiefer-, and the Rannach & Hochlantsch groups, common stratigraphic trends occur (Fritz *et al.*, 1992). Up to the late Silurian alkaline mafic volcaniclastics are the principle lithologies of the basal units representing the rifting event. Until the early Devonian alternating carbonates and fine grained siliciclastics followed, whereas deposition took place in subbasins of variable water depths. Afterwards, in the lower to middle Devonian dolomites, sandstones, and fossil-rich limestones of a platform environment interlock with lagoonal coastal sediments (Fritz *et al.*, 1992). During the Givetian, another influx of alkaline mafic volcanism is recorded. In the Frasnian stage a facies change from a carbonate platform setting to a conodont-rich, pelagic environment with the deposition of flaser limestones and cherts is observed. In the Rannach and Hochlantsch groups the stratigraphy stretches up to the Bashkirian, the lowest stage of the Pennsylvanian (Carboniferous), albeit stratigraphic gaps with erosion and karstification as well as mixed conodont faunas occur (Fritz *et al.*, 1992). The Laufnitzdorf group has a different stratigraphic development displaying a consistent open-marine domain from the early Silurian to the late Devonian and a connection to the carbonate or clastic shelf and coastal areas from the Devonian to the Carboniferous (Fritz *et al.*, 1992). Besides, in the Rannach and Laufnitzdorf groups the sequence ends with Variscan flysch sediments (Gasser *et al.*, 2010; Neubauer *et al.*, 2007).

Gasser *et al.* (2010) split the complex in two main nappe systems. The Rannach and Hochlantsch coastal facies rocks belong to the upper nappe pile. The lower nappe stack consists of the Schöckl and Laufnitzdorf facies groups. These nappes are separated by the Rannach fault crosscutting the proximal portions of the Kalkschiefer facies, thus putting this unit within both systems of the Graz Paleozoic. Important features for the subdivision are the stronger, poly-phase, and differing deformation styles and higher-grade metamorphic imprints in the lower portion compared to the relatively undeformed upper one (Gasser *et al.*, 2010). Within the lower nappe system, ductile foliation, isoclinal folds, and an E–W trending lineation are the predominate deformation patterns. The deformation in the upper nappes encompasses large-scale open folds with various axis orientations, local imbrications, and steep brittle faults. Moreover, several strike slip faults dissect the whole complex (Gasser *et al.*, 2010). Evidence form the Schöckl nappe shows that deformation and metamorphism of the Graz Paleozoic commenced with the Permian event (Hollinetz *et al.*, 2024); this is supported by vitrinite reflectance of organic matter showing deep burial accompanied by enhanced heat flow between the Paleozoic and the Mesozoic (Rantitsch *et*

al., 2005). In addition, conodont faunas indicate ongoing sedimentation in the Carboniferous, meaning that the Graz Paleozoic was located in an external position to the Variscan orogeny leaving the nappe complex unaffected and that the deformational imprint took place afterwards (Ebner, 1976; Fritz, 1991). During the Permian, extensional tectonics resulting from the propagation of the Neotethys caused thinning of the lithosphere and the subsequent decompression melting of the lithospheric mantle resulting in mafic underplating and secondary crustal melting causing a high temperature (HT) low pressure (LP) metamorphic event (Schuster & Stüwe, 2008). In the Schöckl nappe this event (275-261Ma) is recorded as greenschist metamorphic imprint reaching 0.3-0.4 GPa and 520°C at the base and 475°C at higher structural levels indicating an upright metamorphic gradient (Hollinetz *et al.*, 2024). The Mesozoic Eo-Alpine event caused a second metamorphic overprint (~109 Ma) with a weaker metamorphic signature and structural influence on the Schöckl nappe and greenschist facies P/T conditions of ~440°C and 0.4-0.8 GPa (Hollinetz *et al.*, 2024). Furthermore, the metamorphic imprint varies for different nappes and ranges approximately between 200°C and 520°C in most parts of the complex (Hasenhüttl & Russegger, 1992; Russegger, 1996; Rantitsch *et al.*, 2005; Hollinetz *et al.*, 2024). Only in the most south eastern part of the Graz Paleozoic higher metamorphic conditions were computed with temperatures between 510-530°C using the garnet-chlorite as well as the garnet-amphibole thermometer, whereas garnet-biotite thermometer results in slightly higher temperatures of 550-580°C; however, these calculations use assumed pressures of 0.8 GPa (Schantl *et al.*, 2015).

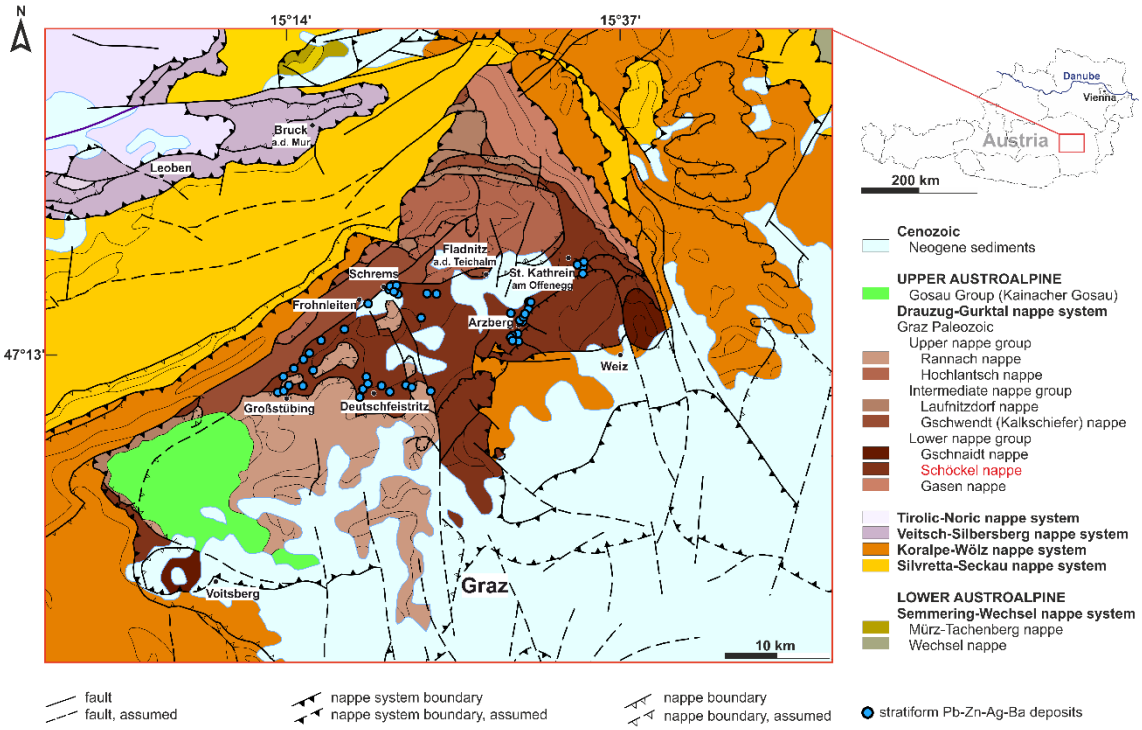

Figure 3: Geologic map of the Graz Paleozoic with Pb-Zn-Ag-Ba deposits and adjacent nappe systems (Rohrhofer *et al.*, 2024).

1.3 SEDEX deposits in the Graz Paleozoic

According to IRIS (Interactive Raw Material Information System), several different raw material occurrences are located within the Graz Paleozoic nappe system, and each of which is assigned to a deposit district. There is a stratabound As-Au mineralisation at Strassegg/Gasen and within a mercury ore district two deposits are bound to micritic carbonates. The magnesite district contains the Breitenau deposit, which is currently in production, and a second smaller occurrence. Both are stratiform and are hosted by metasediments. There are two iron ore districts; one containing seven stratiform magnetite occurrences in metabasalt and metatuffite and the other encompasses 15 lens-shaped manganoan iron carbonate bodies within phyllites. Lead-zinc-silver-barium deposits form the largest ore district encompassing 49 occurrences. The main mining sites were Arzberg, Haufenreith, and Kaltenberg-Burgstall in the east, and Deutschfeistritz, Rabenstein, and Großstübing west of the river Mur. They occur in an area of approximately 35 x 20 km and are located within the Schönberg formation, which is part of the larger "Peggauer-Gruppe" (Peggau group) (Flügel & Hubmann, 2000). The Peggau group makes up large parts of the lower nappe system, which can be subdivided in three parts containing a basal volcanogenic, an euxinic schist, and a carbonatic evolution. The group is presumably 1000 m thick and consists of mainly carbonates as well as shales and is generally poor in fossils, which makes a chronostratigraphic classification difficult, but it is considered to be of Upper Silurian (?) to Devonian age (Flügel & Hubmann, 2000). The Schönberg formation is around 300 m thick and is one of six partly contemporaneous units within the Peggau group (Flügel & Hubmann, 2000). Within this formation greenschists are present, which are interpreted as tuff layers. They have alternating layers dominated by bright carbonate & quartz and greenish chlorite & sericite. Additionally, there are greenschists/ metabasalts with magmatic textures, which occur as lenses mainly in tuffogene greenschists in various stratigraphic levels and reach several tens of metres in thickness (Weber, 1990). Furthermore, black shales are important marker horizons for mineralisation, grade continuously into carbonates, and in the carbonate-rich endmembers contain crinoid fragments (Weber, 1990). These rocks indicate euxinic conditions within the basin at certain times. However, they are not related to the exhalation of metalliferous fluids into the basin but are the result of increased sedimentary input accompanied by a spike in the production of organic matter and a decrease of oxygen in the water column up to anoxic conditions (Rantitsch *et al.*, 1998). Another important lithology in the Schönberg formation are carbonate phyllites, which sometimes have chlorite-rich layers indicative for tuffogene input. In these metapelites intercalations of banded carbonates occur, which partly bear echinoderm fossil fragments, and are called "Kalkrippen" that translates to "limestone ribs" due to their prominent topographical features (Weber, 1990). Besides, within these carbonates olistoliths of dolomitic rocks with a network of quartz veins are present and are several cubic metres in size (Weber, 1990). Further, conodonts revealed that the carbonates are Lochkovian (early Devonian) in age (Tschelaut, 1985). Intercalations of as well as interfingering of sericite phyllite in carbonate phyllite indicates a clay-rich sedimentary origin (Weber, 1990).

Weber (1990) showed in his comprehensive monography based on many years of research that lead-zinc-silver-barium deposits are bound to fine-grained metasedimentary units originally located in deeply subsided domains with limited water exchange. The ore bodies are stratiform, concordant and were formed within channel structures as 3rd order basins. In the western part of the deposit district, there are three known ore layers; in the stratigraphic lowest position mainly

baryte with fine bands of galena and rarely sphalerite is present. In the next higher level, the ore is dominated by galena and sphalerite, whereas baryte is only a minor constituent. The stratigraphically upper most ore horizon consists only of sulphides. (Weber, 1990) interpreted this zonation across the mineralised strata as evidence of progressive deepening of the basin. In the eastern part, only two mineralised layers are present, and they do not show the same trends as at those deposits west of the river Mur. At the important former mine of Arzberg, the stratigraphically lower ore layer contains only sulphides, whereas the upper layer is dominated by baryte (Weber, 1990). Moreover, at the Arzberg deposit secondary, discordant, mobilized galena bearing veins with quartz and Fe-rich carbonates as gangue phases exist (Weber, 2005).

The predominant sulphide phases in the deposits are galena, sphalerite, pyrite and pyrrhotite. Chalcopyrite, arsenopyrite, marcasite, cobaltite, ullmannite, breithauptite and others occur as minor ore phases. Apart from Ag bearing galena, discrete Ag minerals are freibergite, a Ag-rich (>40 wt.% Ag) variety of tetrahedrite, pyrargyrite, polybasite and Ag-Au-Hg alloys within remobilized galena were identified (Feichter, 2005; Weber, 1990). Furthermore, magnetite is a regular constituent of the ore paragenesis of some deposits, such as the baryte mineralisation of the Arzberg deposit and in larger quantities it formed within the mineralisation as well as the adjacent greenschists at the Arzwaldgraben deposit (Weber, 1990).

LA-ICP-MS analysis of sphalerite from SEDEX deposits of the Graz Paleozoic revealed that there is a strong variation of trace/critical metal contents. However, the data shows that the concentrations are generally low. Median values in sphalerite are 137µg/g Co, 8.7 µg/g Ga, 0.4 µg/g In, 0.3 µg/g Ge (Onuk, 2018). Furthermore, pyrite has higher Co over Ni and low As contents and chalcopyrite carries In and Ag (Melcher & Onuk, 2019).

Pb isotope analysis provides $^{207}Pb/^{206}Pb$ model ages of 460 Ma, which are significantly older than the metasediments themselves, pointing to an older crustal origin of lead (Feichter, 2005). The Pb isotope signature is typical for Pb deposits in the Austroalpine and signifies that the Pb source are metasediments with large quantities of Archean to Paleoproterozoic detritus (Schroll, 1997).

$\delta^{34}S$ values are different for various minerals; in sphalerites it ranges between -2 and +14 ‰, but the results make it possible to distinguish between primary (+6 to +12 ‰) and secondary remobilized (0 to +3 ‰) sphalerite formation at the Guggenbach deposit (Onuk, 2018). Pyrite from a tuffogene host rock has very low $\delta^{34}S$ values of -9 ‰ (Feichter, 2005). In addition, the S-isotopy of baryte corresponds to that of seawater in the Devonian period (Feichter, 2005; Schroll, 1997).

Besides, Tufar (1978) analysed fluid inclusions within barytes from Arzwaldgraben and found that they consist mainly of hydrogencarbonate and chloride plus $Ca^{2+}>Na^{+}>Mg^{2+}>K^{+}$ and cations of Fe, Mn, Ni & Zn. The calculated homogenisation temperatures are between 195°C and 250°C (Tufar, 1978) and might reflect formation temperatures (Weber, 2005), whereas temperatures computed using the chlorite thermometer of 290°C-340°C and the siderite-ankerite thermometer of 350°C-580°C for mineralisation and host rocks reflect changing conditions during retrograde metamorphism (Feichter, 2005). Additionally, the phengite components within micas indicate minimal metamorphic pressures of 2.8-5.2 kbar (Feichter, 2005).

2 Sampling and Methodology

Samples of ore and its host rocks were taken from locations that still provide accessible and intact mine workings from the long period of Pb/Zn extraction (Fig.4). At the Arzberg mine it is ore from the sulphide mineralisation within backfill of "Unterbau", from the in-situ upper ore body, as well as samples of the "ribbon chert", which is a 10 cm thick whitish banded layer, near the "Arzberg shaft". At the unnamed adit at Burgstall-Kaltenberg samples are from profiles across two ore horizons and its host rock. At the unnamed adit in the district Peggau-Taschen located near the "Moarbründl" creek west of mount "Draxlerkogel" samples are taken from black shale at the end of the adit, where the roof collapsed circa 230 m from the entrance, from weakly mineralised rocks next to the entrance to the underground mine workings and the hanging wall carbonate phyllite. Furthermore, un-/mineralized rock pieces of mine dumps at Arzwaldgraben and "Mitteregg" at Peggau-Taschen were collected. The Kalkrippe marble unit was sampled west of the "Hiedner Farm" in the municipal area of Großstübing.

In order to determine the spatial extent and development of the alteration halo and element zonation surrounding ore layers drill cores from the 1970s of the H1 drilling at Haufenreith (Fig.5) and G7 drilling at Guggenbach (Übelbach) (Fig.6), stored at the Styrian drill core repository in Ebersdorf near St. Radegund, were investigated. Samples were taken approximately up to 22 m below and above mineralisation (Fig.7). For further information on the drillings and its results see Weber (1990).

Hammer and chisel were used for sampling mainly, albeit at the Burgstall-Kaltenberg and Arzberg deposits samples from the mineralisation and its adjacent host rocks were extracted using an angle grinder due to its toughness.

Crushing of samples was done using a hammer and grinding was conducted with a vibratory disc mill with an agate grinding set in order to prevent metals contamination due to wear.

The ground rock samples were sent to Activation Laboratories Ltd. (ActLabs) in Canada to determine the whole-rock geochemical composition, whereas the analytical packages 4LITHO, 4F-S, and 8-4 Acid Total Digestion for metal concentrations above the detection limit of 10.000 ppm were used.

Moreover, polished thin or thick sections of the sampled lithologies were manufactured for microscopic analysis. Reflected and transmitted light microscopy was done using the digital microscope KEYENCE VHX 6000 to distinguish minerals, the relations between them, and textural features. However, the very small grain sizes of phyllites hindered an identification of individual phases. Hence, scanning electron microscopy (SEM) was necessary to assign mineral names to observed phases free of doubt and to determine their chemical composition in order to define alteration halos surrounding the Pb/Zn deposits. An SEM ZEISS Evo MA 10 at the Chair of Geology and Economic Geology of the Montanuniversität Leoben was used with distances to the samples of 10-11 mm and 15 kV acceleration voltage.

The timing of SEDEX ore formation in the Graz Paleozoic is poorly constrained and only based on fossil records of country rocks. Radiometric dating of REE phases was successfully performed determining intervals of ore deposition at other deposits (e.g. Abra, Western Australia, (Zi *et al.*, 2015)) Therefore, microprobe analysis was carried out on monazite and thorite in an attempt to do age dating at the Department of Earth Sciences of the University of Graz, Austria. The JEOL JXA-8530F Plus Hyper Probe was used. Only point measurements were done with 8 kV.

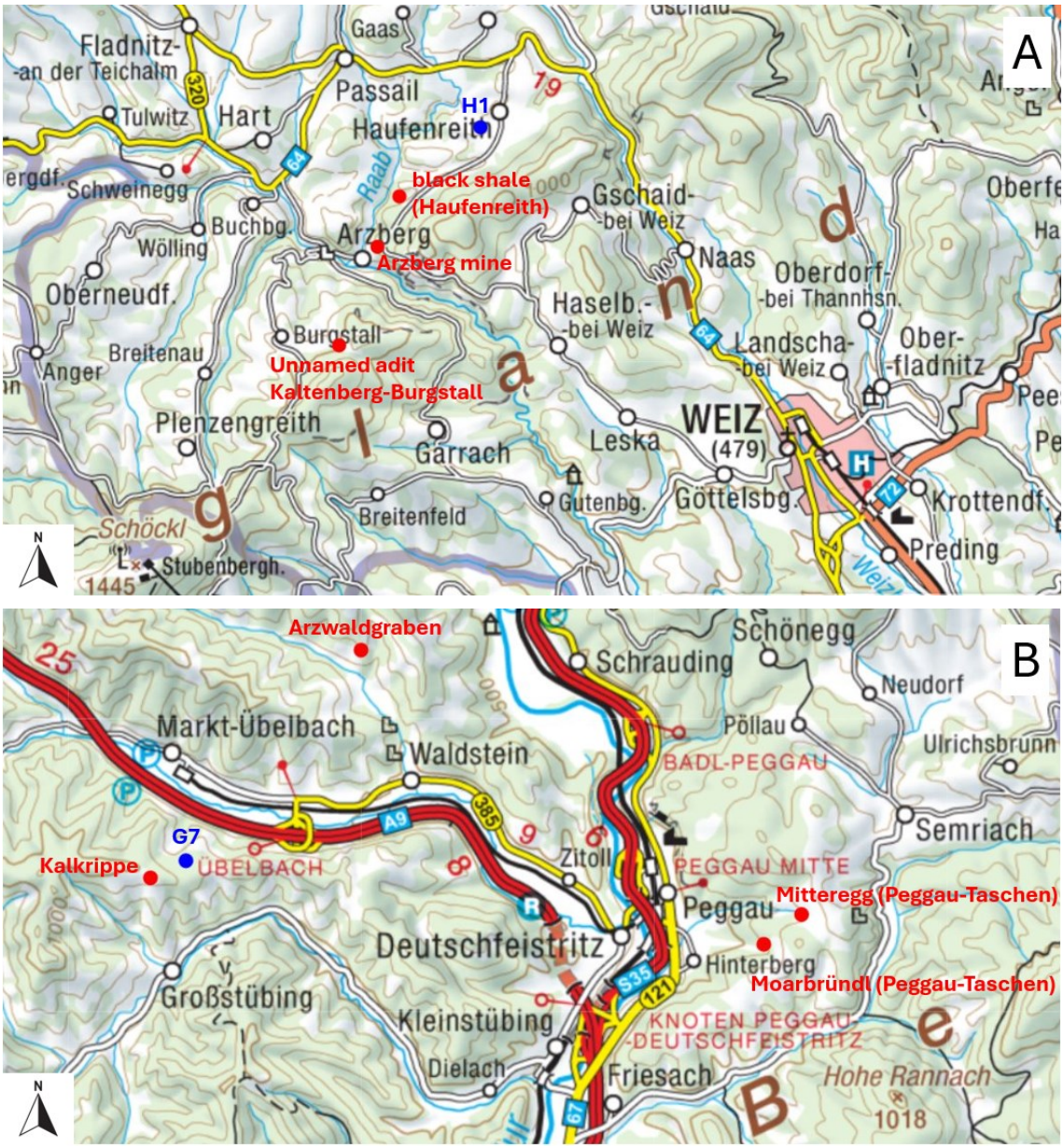

Figure 4: Geographic map of investigated sites of the eastern part (A) and the western part (B) of the deposit district in Styria (Austria); dots represent outcrops, mine workings as well as dumps (red) and drilling sites (blue); scale: 1:75.000; source: GIS Steiermark.

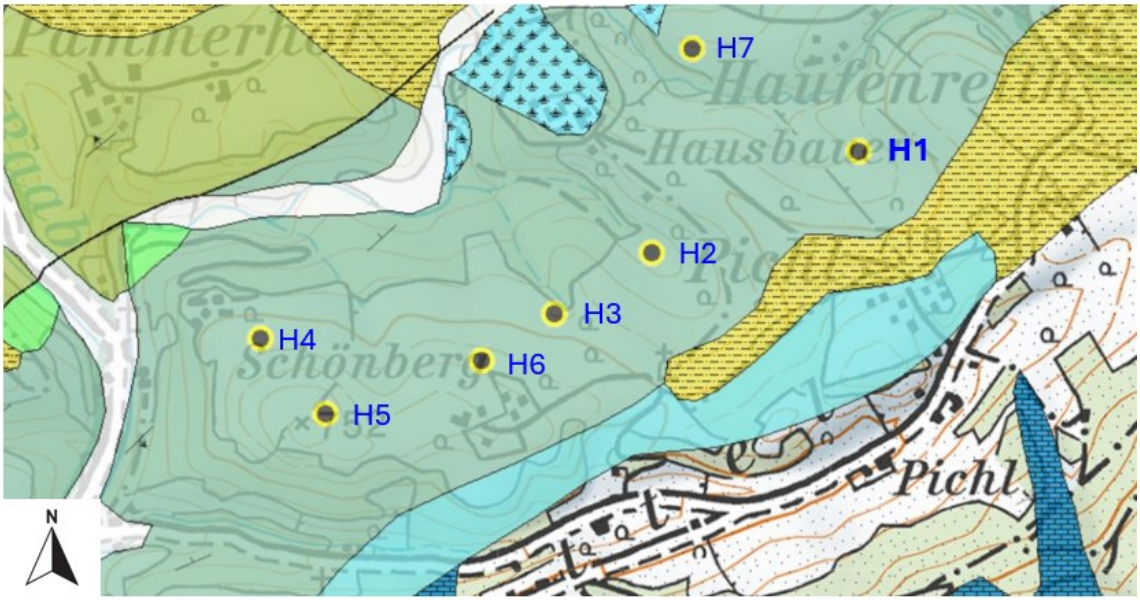

Legend

Drilling

Strike and dip, diping angles

>5° - 30°

>30° - 60°

Tectonics

Regional tectonic fault

Geology

Greenschist (tuff, lava)

Schönberg formation (black shale, carbonate phyllite, subordinate metavolcanics)

Striatopora marble (coral facies)

Schöckl marble (thick bedded to massive, grey to whitish grey banded rocks)

Sericite phyllites (Semriach formation)

Sand and clay

Travertine of Haufenreith

Rock debris (in parts from the Würm glaciation)

Alluvium

Figure 5: Geologic map of the surroundings of Haufenreith in the eastern part of the deposit district with drill sites of the 1970/80s exploration program; scale: 1:10.000; source: GIS Steiermark.

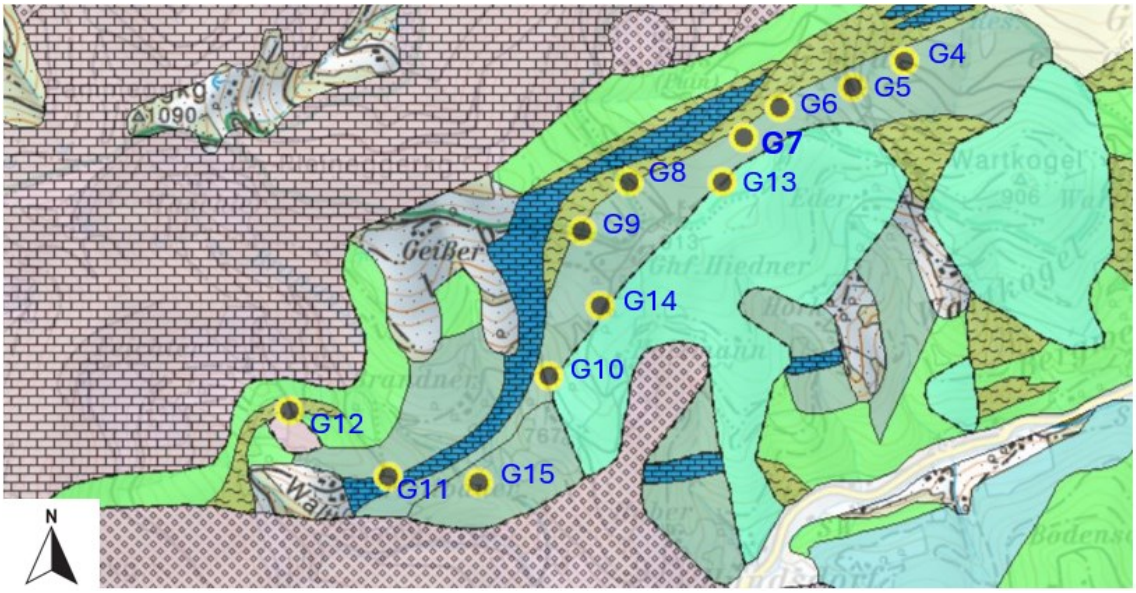

Legend

Drilling

Tectonics

Assumed tectonic fault

Geology

Parmasegg formation ("Kalkschiefer-Folge"): dolomite

Parmasegg formation ("Kalkschiefer-Folge") with clastic sediment dominance

Parmasegg formation ("Kalkschiefer-Folge") with carbonate dominance

Parmasegg formation ("Kalkschiefer-Folge"): alternating dark or massive carbonates, flaser limestones, carbonate schists (phyllites), dolomite, clay schists, silt and sand stones

Schönberg formation (black shale, carbonate phyllite, subordinate metavolcanics)

Schöckl marble (thick bedded to massive, grey to whitish grey banded rocks)

Parmasegg formation ("Crinoiden-Schichten"): crinoidal limestone/dolomite, sandy limestones, thick-bedded limestone, carbonate schists, clay schist

Dolomite, dolomitic sand- and siltstone, siltstone

Carbonate phyllite

Black shale, dark phyllite

Metavolcanics: Diabase (metabasalt), diabase tuff, greenschist

Fluvial sediments from glaciation

Rock debris (in parts from the Würm glaciation)

Alluvium

Figure 6: Geologic map of the surroundings of Guggenbach (Übelbach) in the western part of the deposit district with drill sites of the 1970/80s exploration program; scale: 1:20.000; source: GIS Steiermark.

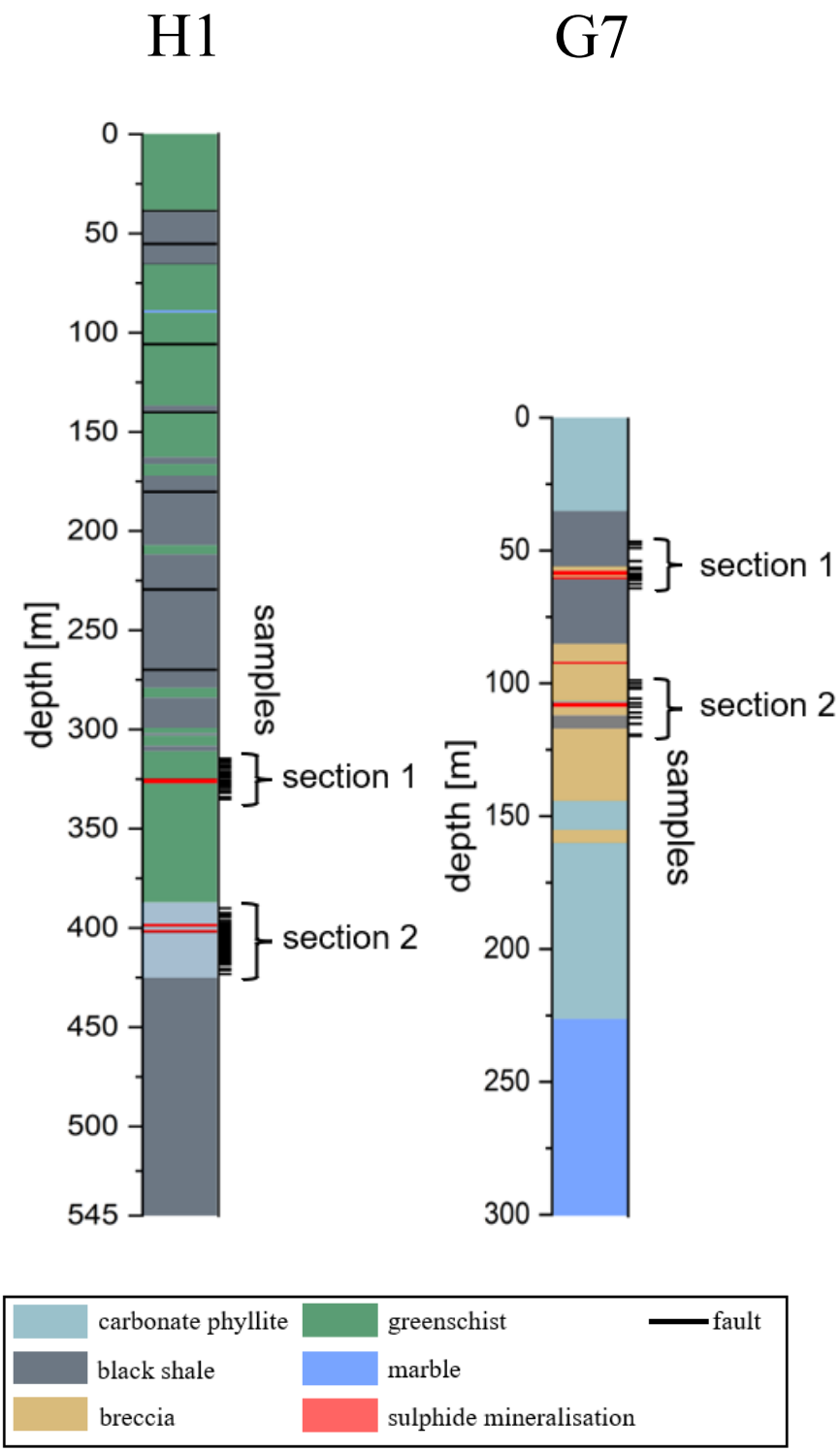

Figure 7: Schematic stratigraphy of the H1 (left) and G7 (right) drill cores based on the original drill core mapping from the 1970/80s exploration plus indication of investigated drill core sections and sampling points of this thesis (BBU, unpublished data).

3 Results

The following chapter describes analytical results of the whole rock geochemical data from drill cores as well as from samples taken at ore occurrences. Whole rock geochemical major, minor, and trace element data are not normalised and concentrations below the detection limit are either displayed as values equal zero for linear axes or as the value one for logarithmical axes. Furthermore, the mineralogical and petrological findings gathered from microscopic investigations are presented, whereas the focus lays on rock forming minerals as well as mineralisation and alteration related phases, whereas secondary minerals from weathering processes are not described in detail due to their low relevance in this thesis. The terms sulphide mineralisation and ore horizon as well as alteration zone and alteration halo are used synonymously.

3.1 Geochemistry

The geochemical composition of rocks can be used to discriminate lithologies. For sedimentary units the concentration of CaO + MgO versus SiO_2 help to visualize and distinguish carbonate dominated strata from other lithologies like siliciclastic, tuff or carbon rich sediments as well as mineralised rocks (Fig.8). For the sampled lithologies of the Graz Paleozoic a wide range of CaO + MgO values is observed ranging from 0.08 to 48.0%. The SiO_2 contents vary from 7.82 to 69.03%. Generally, both components have a broad and continuous spectrum from low to high values. High percentages of CaO + MgO (>38%) are found in samples of Kalkrippe marble, "Ribbon Chert" from Arzberg, Kaltenberg-Burgstall, as well as hanging wall marble of the second section of H1 section 2 drill core and the G7 section 1 drill core. Other rock samples from Kaltenberg-Burgstall were taken immediately next to ore layers and have much lower percentages of CaO + MgO and significantly higher SiO_2 concentrations. Other lithologies like the metatuffite from the first section of the H1 drilling has CaO + MgO contents between 19.35% and 22.33%, and SiO_2 ranges from 41.53% to 45.56%, or carbonate-phyllites from the drill cores of H1 and G7 have CaO + MgO from 7.16% to 42.26% and SiO_2 from 12.39% to 69.03%. Breccias from the two sequences of the G7 drilling have concentrations of CaO + MgO from 8.25% to 26.22% and SiO_2 from 26.51% to 62.61%. Black shales have very low CaO + MgO contents of 2.46% (Peggau-Taschen) and 3.16% (Haufenreith) and moderate SiO_2 values of 51.25% (Haufenreith) and 53.60% (Peggau-Taschen).

Ore samples have trends to low concentrations of CaO + MgO, and SiO_2 is often significantly lower than in unmineralized lithologies. This is especially true for samples from locations with known ore occurrences like Arzberg, Arzwaldgraben and Kaltenberg-Burgstall. Mineralised samples from Arzwaldgraben hosted by greenschists display very low CaO + MgO concentrations ranging between 0.08% to 1.26% and SiO_2 concentrations between 24,91% to 49,51%.

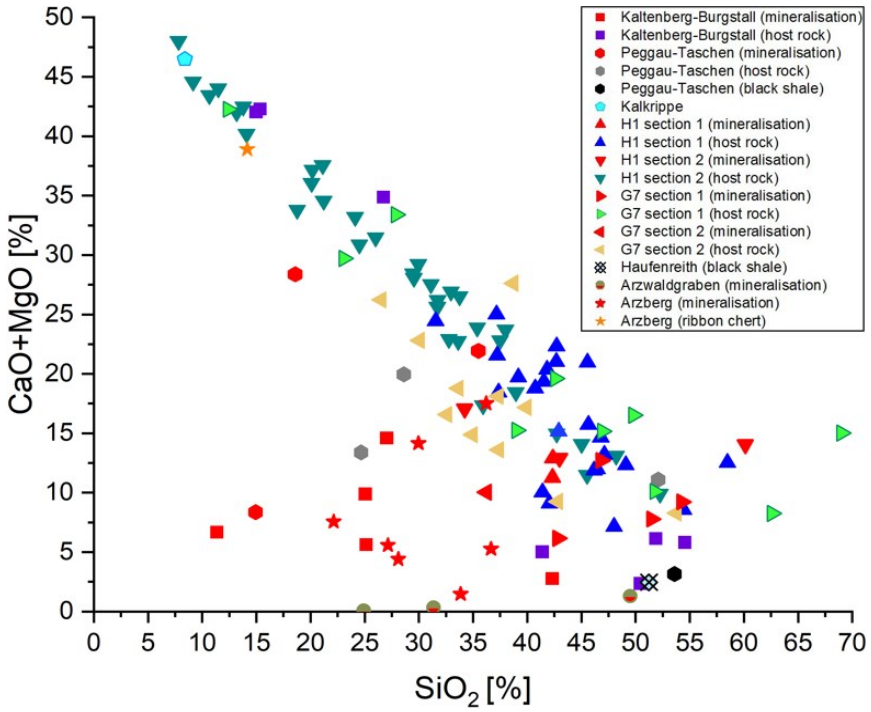

Figure 8: SiO_2 vs. CaO+MgO diagram using whole rock geochemical data.

Whole rock geochemical data of Al_2O_3 and SiO_2 show a trend from carbonate rich lithologies like the Kalkrippe marble unit with low concentrations to carbonate-poor black shales enriched in Al_2O_3 and SiO_2 (Fig.9). This trend follows the amount of silicates in analysed lithologies. Especially ore samples tend to have lower Al_2O_3 and SiO_2 concentrations due to high amounts of sulphides and/or sulphates.

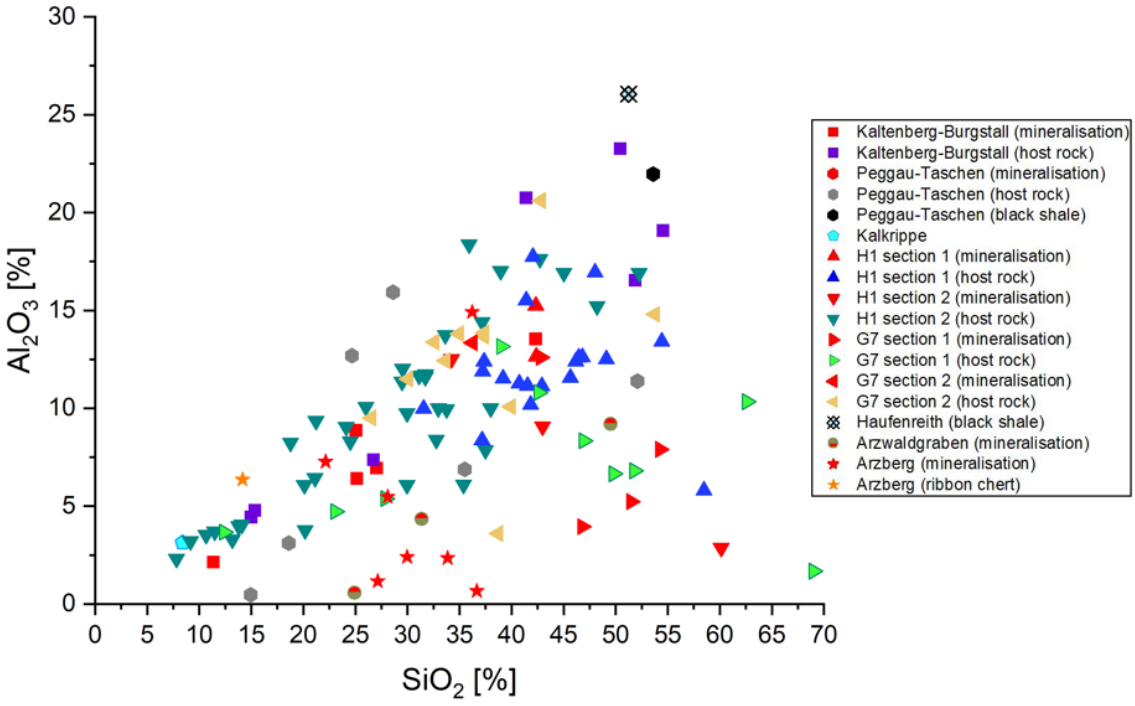

Figure 9: SiO_2 vs. Al_2O_3 diagram using whole rock geochemical data.

The distribution of $Na_2O + K_2O$ vs. SiO_2 is very similar to Al_2O_3 vs. SiO_2 highlighting that feldspars and micas are the driving factor for enrichment of these elements (Fig.10).

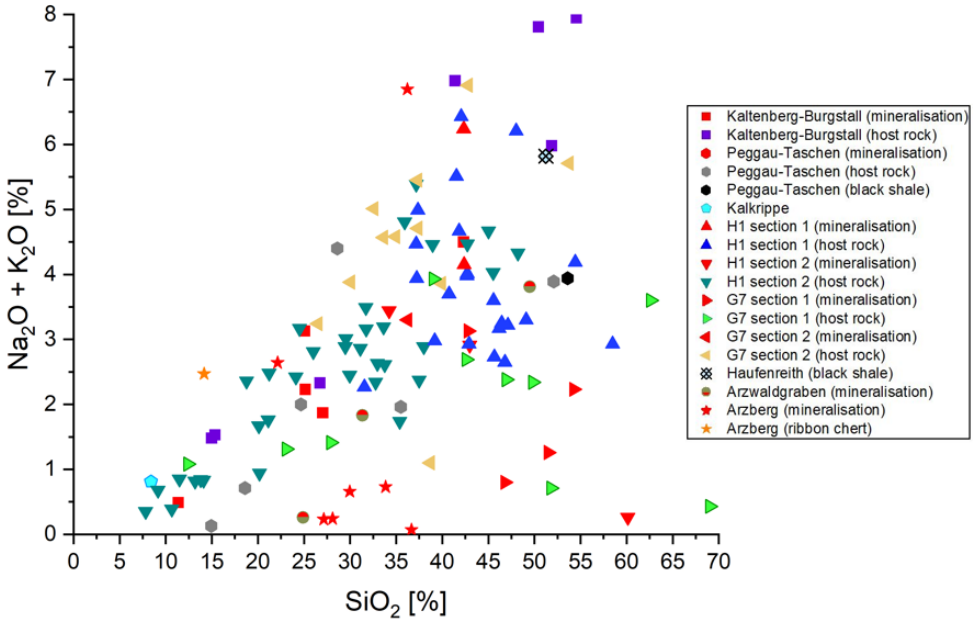

Figure 10: SiO_2 vs. Na_2O+K_2O diagram using whole rock geochemical data.

Plotting TiO_2 vs. SiO_2 shows two groups of samples (Fig.11). One group with TiO_2 concentrations below 1.5%, which consists of the bulk of samples, and the other one with values above it, which encompasses samples from the H1 section 1 drill core, where metatuffite is present, as well as from the G7 section 2 drill core and from Peggau-Taschen, plus one ore sample each from Arzwaldgraben as well as Arzberg, where high TiO_2 concentrations indicate an abundance of Ti-rich minerals. Generally, carbonates and ore samples tend to have low TiO_2 concentrations.

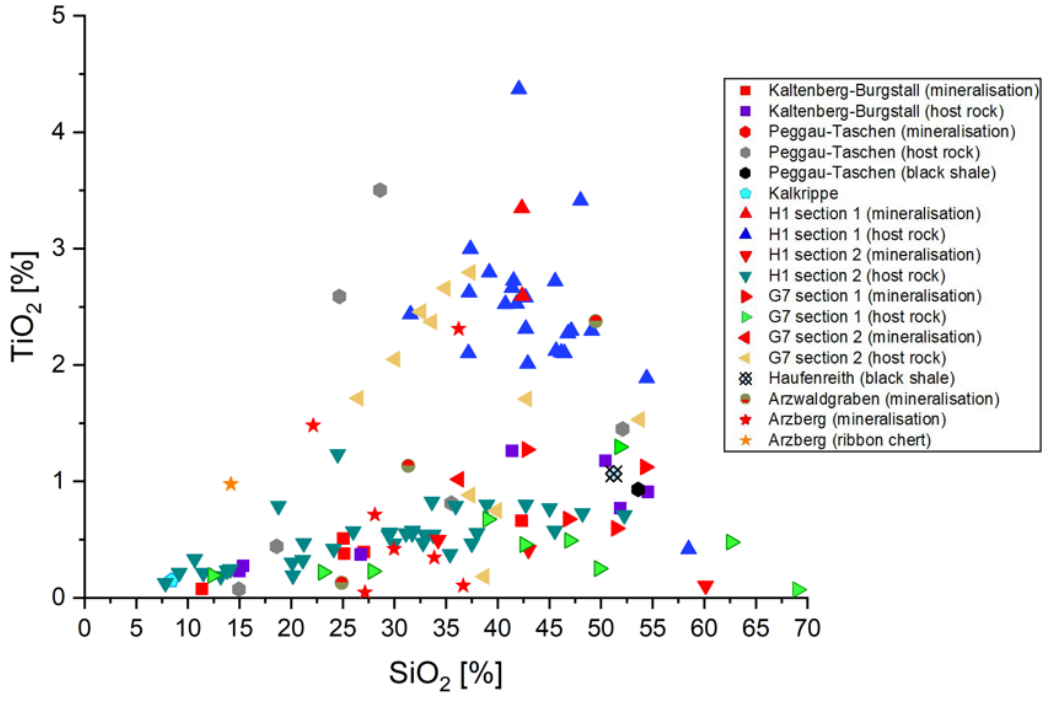

Figure 11: SiO_2 vs. TiO_2 diagram using whole rock geochemical data.

Naturally, ore samples have high Pb and Zn contents (Fig.12), but some samples show a clear dominance of one over the other, such as from the locations Arzberg (Pb>Zn), Kaltenberg-Burgstall (Pb>Zn), section 2 of the H1 drill core (Pb>Zn), section 1 of the H1 and G7 drillings (Zn>Pb). Moreover, ore from known Pb/Zn occurrences tends to be higher in metals than samples from the drill cores. Host rock lithologies and black shales, which are unrelated to sulphide or baryte ore (Rantitsch *et al.*, 1998), show relatively low concentrations of Pb, mostly below 100 ppm, and Zn below 500 ppm. Wider ranges of metal contents of host rocks are found at Kaltenberg-Burgstall, especially those immediately next to ore, and the section 1 of the H1 drilling.

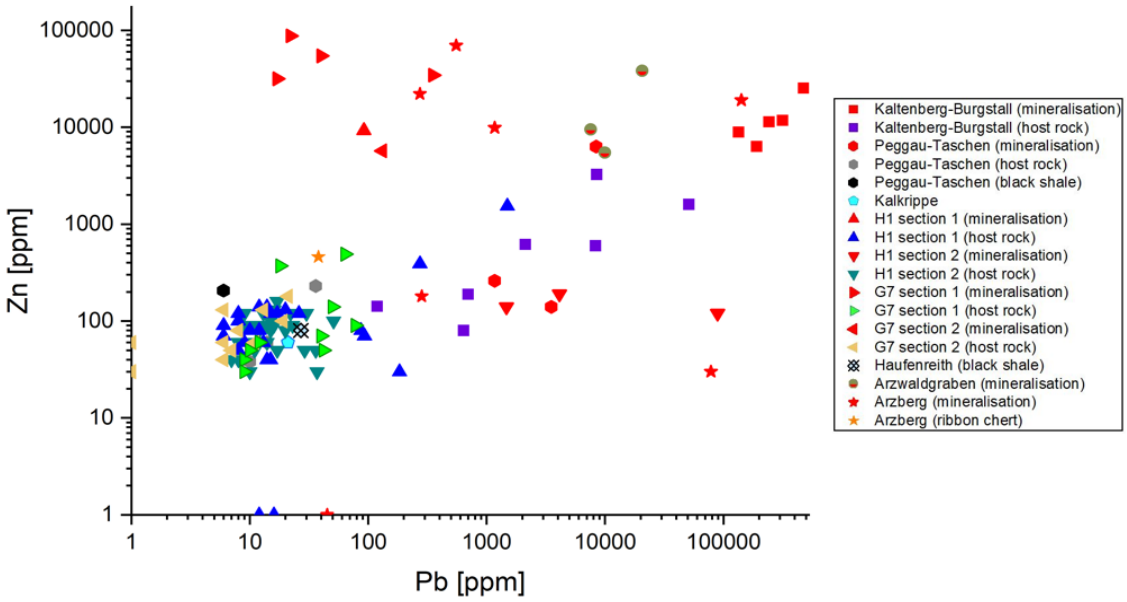

Figure 12: Pb vs. Zn diagram using whole rock geochemical data.

Metal enrichments in mineralisation compared to host/country rocks are evident not only for Pb and Zn but also for Ba, Co, Ni, Cu, As, Ag and Sb (Fig.13), whereas the median metal contents illustrate this well. Ore horizons have high median concentrations of Ba (5040 ppm), Zn (9230 ppm) and Pb (3520 ppm). However, wide ranges of Ba, Zn and Pb for ore samples are explained by both lower metal concentrations in mineralisations of drill cores compared to massive ore horizons like at Arzberg and metal deposition following a temperature gradient (Pb→Zn→Ba) (Lydon, 1995). Concentrations in host rocks seem to follow this depositional gradient as well having higher median Ba (437 ppm) concentrations over Zn (80 ppm) and Pb (14 ppm). Outliers of Ba, Zn and Pb occur in samples which are located close to mineralisation, such as host rocks of ore horizons in the unnamed adit at Kaltenberg-Burgstall. Median concentrations of Co (20 ppm), Cu (60 ppm), Ag (16 ppm), which is above the detection limit (>100 ppm) in some samples of Kaltenberg-Burgstall, and Sb (3 ppm) in mineralisation are higher than Co (12 ppm), Cu (30 ppm), Ag (1 ppm), which is below the detection limit (<0.5 ppm) in the majority of host rock samples, and Sb (1 ppm) in host rocks, whereas the ranges for host rocks tend to be wider than for ore samples. Only median values of Ni (40 ppm) in host rocks are slightly higher than Ni (38 ppm) in mineralisation, however, ranges for Ni are also wider in country rocks. Median As contents in host rocks (9 ppm) are lower than in mineralisation (11 ppm) but the ranges and outliers reach higher concentrations in host rocks.

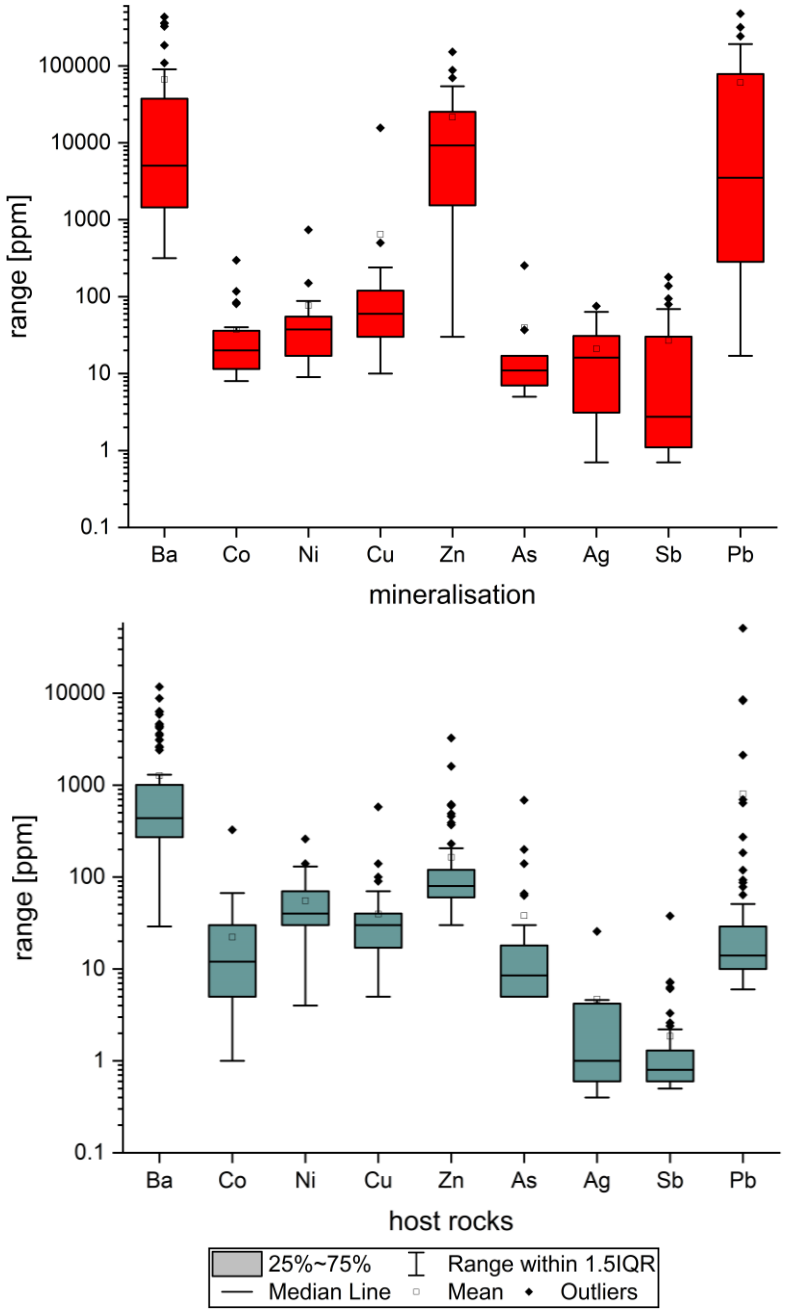

Figure 13: Ranges of selected metals in mineralisation (upper diagram) and host rocks (lower diagram) using whole rock geochemical data.

Plotting REE concentrations from whole rock samples of ore, host rock, and barren samples against the average European shale REE concentrations (Haskin & Haskin, 1966) reveals a distinct positive Eu anomaly in many samples relative to other rare earth elements, and compared to the average concentration in the European shale Eu is up to 2.45 times higher in host rock from Kaltenberg-Burgstall (Fig.15). High Eu values are often associated with host rocks of sulphide mineralisation. REE concentrations are lower than average European shale concentrations in most samples but some defy this trend showing an enrichment. Especially LREE (light rare earth elements) are more strongly enriched compared to average European shale REE concentrations than HREE (heavy rare earth elements) being depleted in most cases. The Kalkrippe marble unit and some individual samples from the H1 section 1 as well as the G7 section 1 & 2 drill cores have a different normalised REE distribution compared to all other samples since they show REE depletion, which is stronger for LREE than for HREE, whereas Gd has the highest value among

normalised rare earth elements of the Kalkrippe marble unit. For ore samples, REE contents are generally below average European shale concentrations, including very low normalised REE values are from baryte rich ore samples (Fig14).

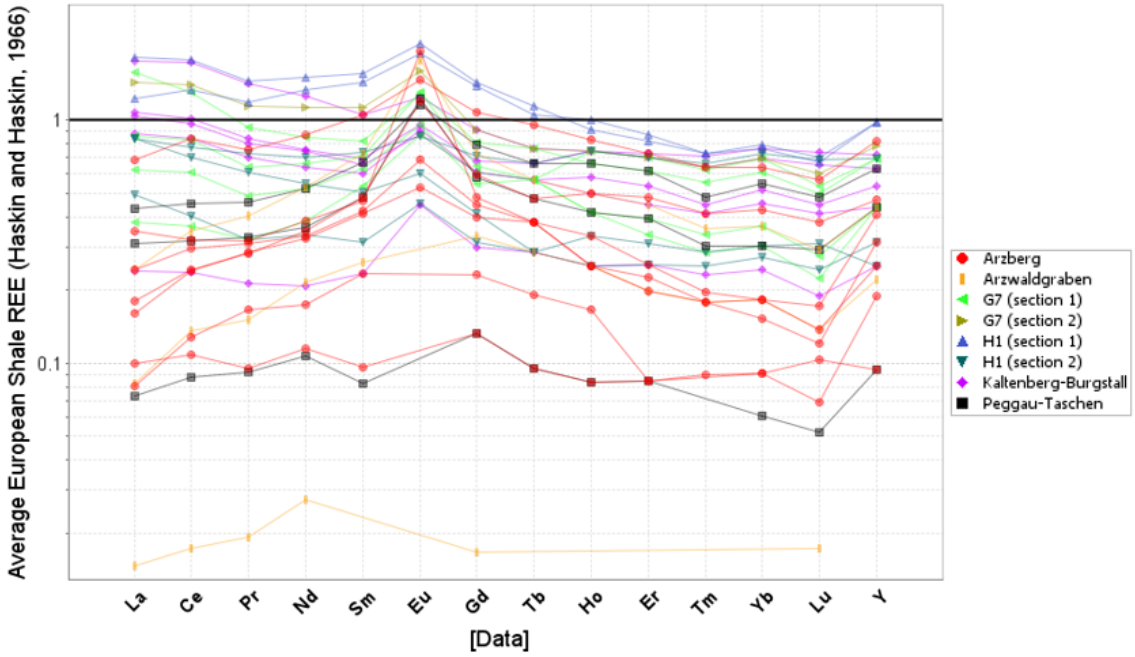

Figure 14: Diagram of whole rock geochemical data of ore samples normalised to average European shale REE (Haskin & Haskin, 1966).

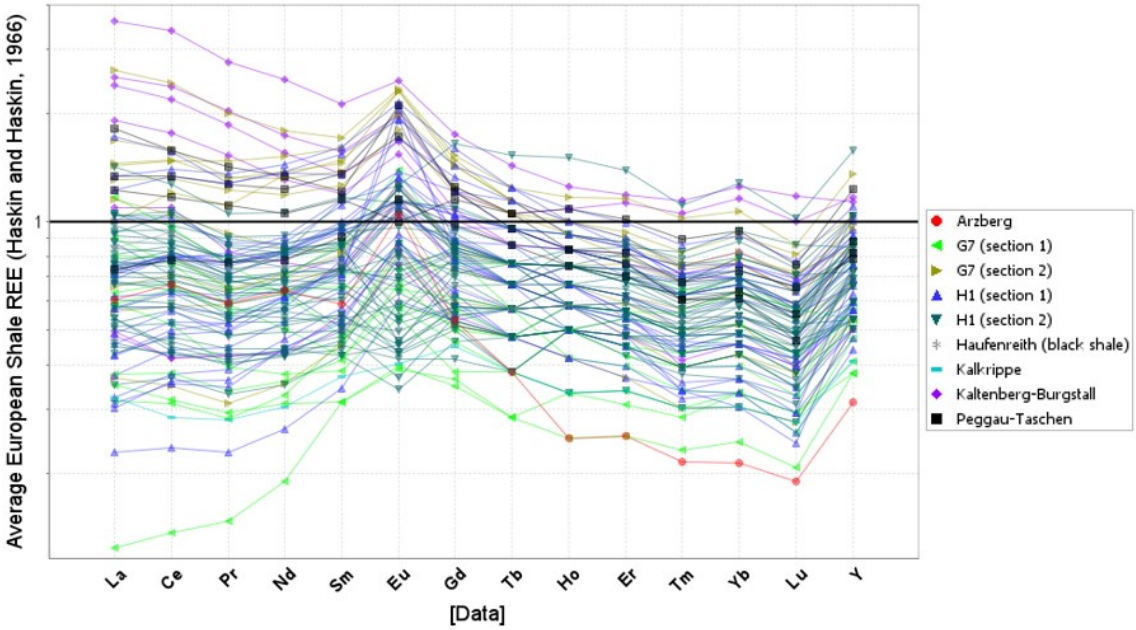

Figure 15: Diagram of whole rock geochemical data of host rock and barren samples normalised to average European shale REE (Haskin & Haskin, 1966).

Normalising REE concentrations from to chondrite concentrations (Nakamura, 1974) shows a strong LREE enrichment in host rock and barren samples (Fig. 17). HREE concentrations are elevated as well but do not reach levels of LREE. The europium anomaly is recognisable only in a few samples but less pronounced compared to average Europian shale REE normalisation, and shows a negative anomaly relative to other normalised REE data in the H1 section 2 drill core

and in unmineralised samples of the G7 section 1 drill core. Ore samples tend to be less enriched in both LREE and HREE compared to host rock or barren samples (Fig.16).

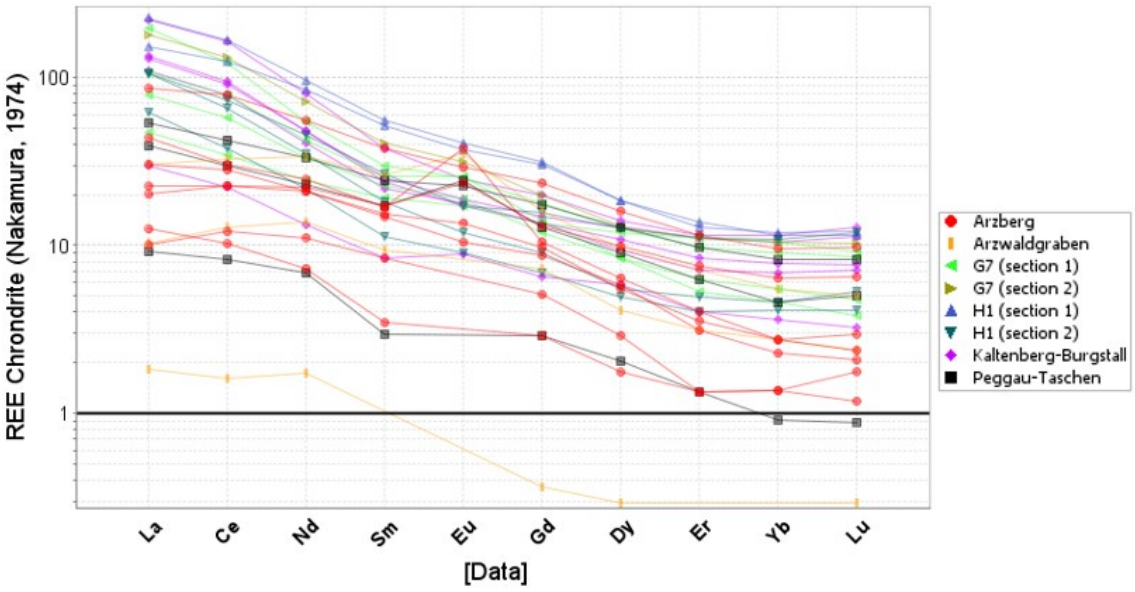

Figure 16: Diagram of whole rock geochemical data of ore samples normalised to REE chondrite (Nakamura, 1974).

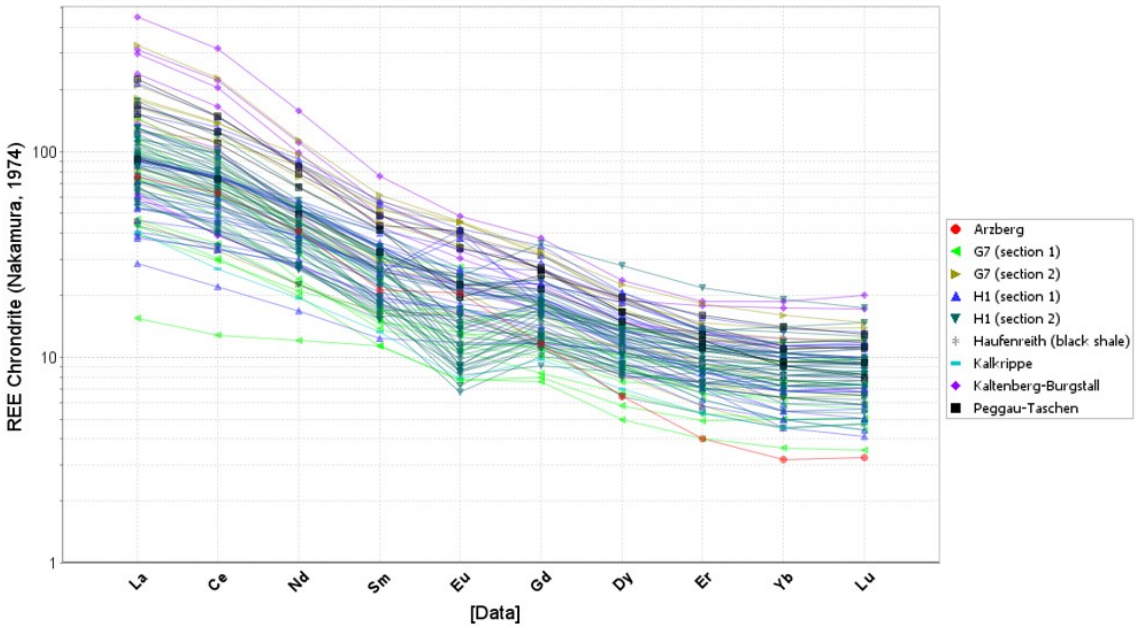

Figure 17: Diagram of whole rock geochemical data of host and barren rocks normalised to REE chondrite (Nakamura, 1974).

The correlation matrix of the main components from whole rock geochemistry of 29 ore samples from Arzberg, Arzwaldgraben, Kaltenberg-Burgstall, Peggau-Taschen and from both sections of H1 and G7 drill cores (Fig.18, upper diagram) shows a negative correlation of total S with all other components, which is strongest with SiO_2 and Al_2O_3 and weakest with Fe_2O_3(T) and MnO. Further, Al_2O_3, Na_2O, K_2O, TiO_2, and P_2O_5 correlate well likely because of an association of mineral phases containing these elements such as the combined occurrence of Al_2O_3, Na_2O, and K_2O in feldspars and/or sheet silicates. Carbonates are represented by two component groups

encompassing Fe_2O_3(T) & MnO and CaO & MgO showing a negative correlation with silicates, Ti-bearing phases, and phosphates due to different (sedimentary) origins as well as between these two groups indicating different formation processes. The correlation matrix of selected elements encompassing base metals, HFSE (and REE reveals a strong correlation among REE and HFSE as well as between both groups (lower diagram). Silver correlates well with Pb as well as REE and HFSE. Cobalt, Ni, Cu, and As correlate strongly. Furthermore, there is a pattern of Pb, Zn, and Ba not correlating with each other highlighting a depositional gradient of these base metals.

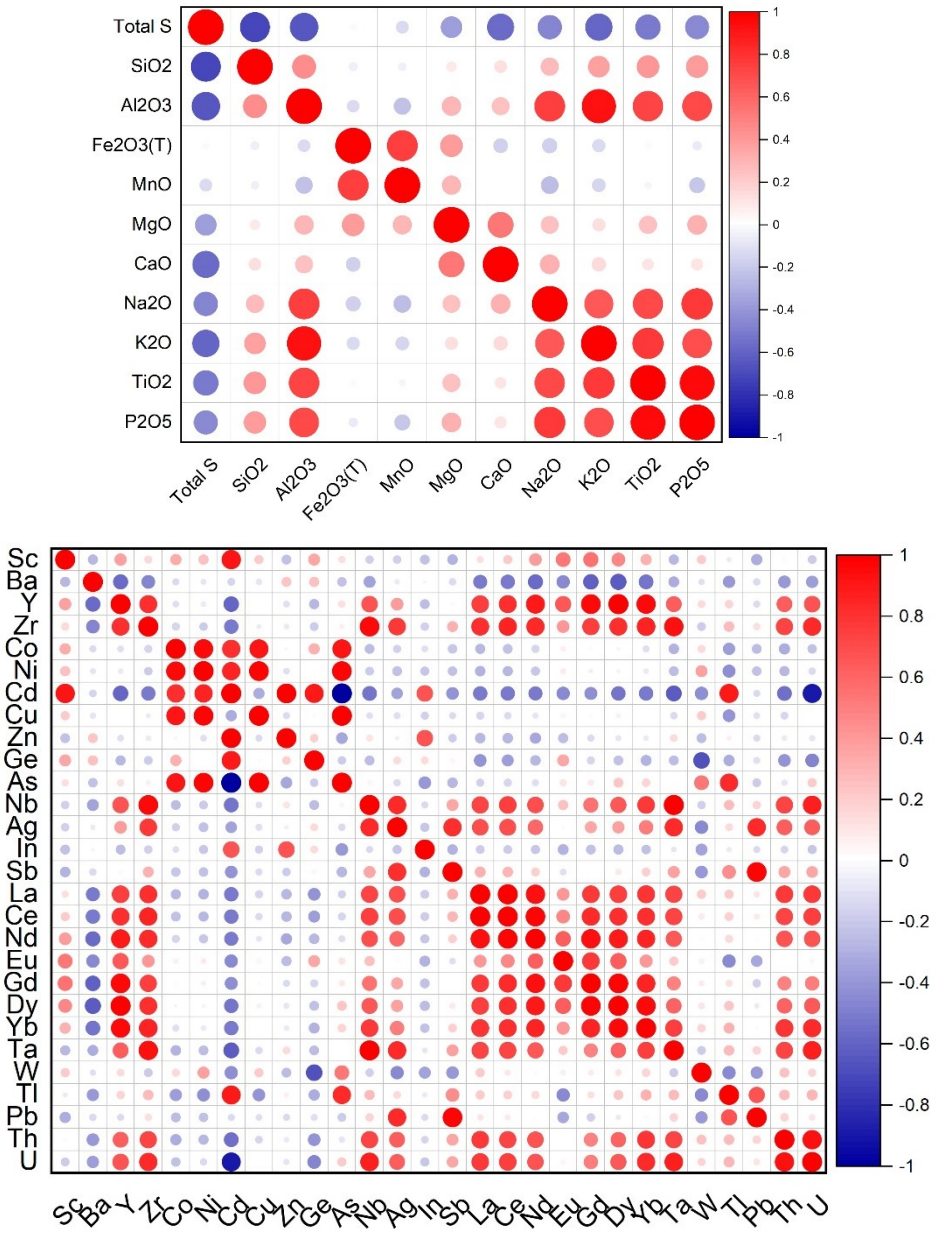

Figure 18: Correlation matrices of major (upper diagram), minor and trace elements (lower diagram) of ore samples using whole rock geochemical data.

The correlation matrix of 94 samples from host and barren rocks of all investigated locations and drill cores (Fig.19) shows that the main components (upper diagram) SiO_2, Al_2O_3, Na_2O, K_2O, plus TiO_2 and CaO have a strong negative correlation resulting probably from various sedimentary regimes of carbonates and clastics. The strong correlation between Al_2O_3 and K_2O

can be attributed to sheet silicates. Na_2O correlates best with TiO_2. Total sulphur tends to correlate weakly with clastics. MgO and MnO have the strongest correlation with Fe_2O_3(T). The correlation matrix for minor and trace elements (lower diagram) shows a correlation between REE and HFSE as well as Ag, whereas Ag also correlates with Ba, Cu, Sb and Pb. Other than in ore samples, there is a moderate correlation among Ba, Zn and Pb. Futhermore, cadmium correlates well with Co and Zn but negatively with As. Barium, Zn, and Pb show a weak to moderate correlation with REE and HFSE.

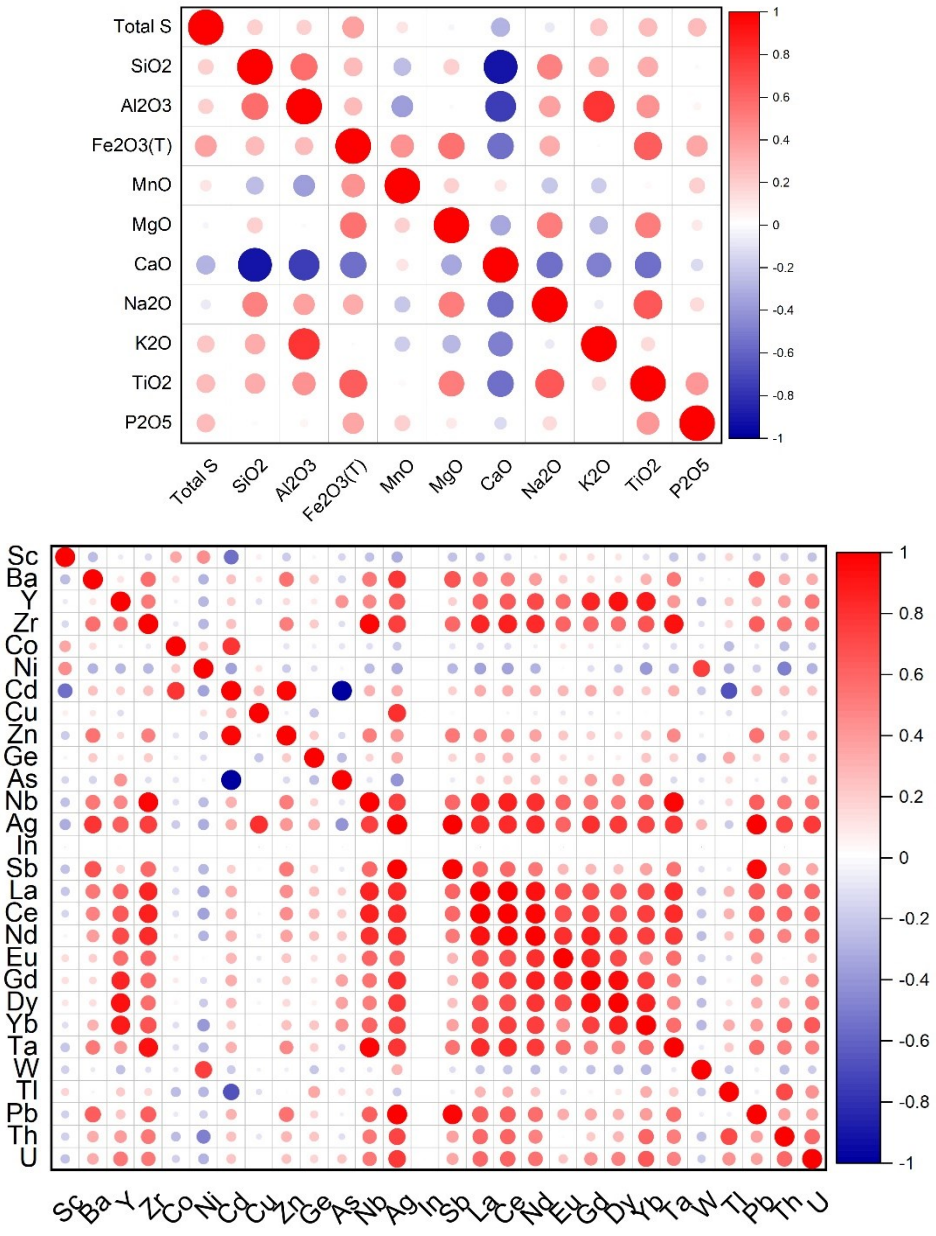

Figure 19: Correlation matrices of major (upper diagram), minor and trace elements (lower diagram) from whole rock geochemical data.

3.1.1 H1 section 1 drill core

The section 1 (25 samples) of the H1 drill core (see Figure 7 for overview) is made of a thin mineralised stratiform ore zone, carbonate-bearing phyllite close to and up from the mineralised zone, and metatuffite below the mineralised zone (Fig.20 & 21). The SiO_2 concentration along the profile does not show strong differences between the two lithologies but has its peak stratigraphically above and close to ore. Al_2O_3 and TiO_2 show a similar distribution along the section with the maxima next to the mineralisation. Apart from the maximum and minimum near the ore layer, TiO_2 has very similar concentrations stratigraphically above and below the ore horizon in both lithologies. Al_2O_3 has the highest and lowest value at the same positions as TiO_2 but there are slightly higher values above than below the sulphide mineralisation. CaO and MgO correlate, show higher concentrations stratigraphically below the mineralisation and low concentrations above. MnO behaves inverse to CaO and MgO and has high values at the ore horizon. Na_2O has two areas with high contents; firstly from 335,1 m to 326,6 m and secondly from 322.1 m to 317.7 m. K_2O shows three major peaks at the mineralisation and stratigraphically above it; below values vary at a lower level. P_2O_5 has the highest concentrations at the ore layer, is significantly lower in barren rocks, and has slightly higher values in metatuffite compared to carbonate phyllite. Fe_2O_3 (T) has overall similar values in both lithologies with some variations and does not show any enrichment at the mineralisation. The ore is dominated by Zn (9230 ppm) over Pb (92 ppm), whereas Zn has its maximum at 326.6 m in the lower part and Pb has the highest concentrations (1500 ppm) at the upper part of the mineralised zone at 325.9 m, whereas Zn is still enriched (1540 ppm). Obviously, total S has elevated values at the Zn & Pb maxima, but within the carbonate phyllite it has several zones of higher concentrations peaking stratigraphically above the mineralisation. Additionally, there is a small increase in total S in the metatuffite. Other elements important for the mineralisation are Cu, Ba, Co, Ni, and As. Apart from As, these elements have the highest concentrations below the ore layer where they are generally more elevated especially in metatuffite compared to carbonate phyllite. At the mineralisation only Ba has higher concentrations; all the other metals have decreasing concentrations, whereas Cu increases from below the detection limit (>10 ppm) in the lower part to 60 ppm in the upper part of the sulphide mineralisation. Furthermore, As seems to have a negative correlation with Co and Ni. It has its maximum (66 ppm As) well above the Pb/Zn ore at 316.42 m just beneath where Ba, Pb, total S and other elements have elevated concentrations. The Rare Earth Elements (REE), e.g. La, Ce, Nd, and Eu, as well as the High Field Strength Elements (HFSE), e.g. Y, Nb, Ta, Th, and U, have a very similar distribution with an anomaly at the ore and higher values above the mineralisation in carbonate phyllite than below, whereas there is a very slight increase in concentrations in metatuffite.

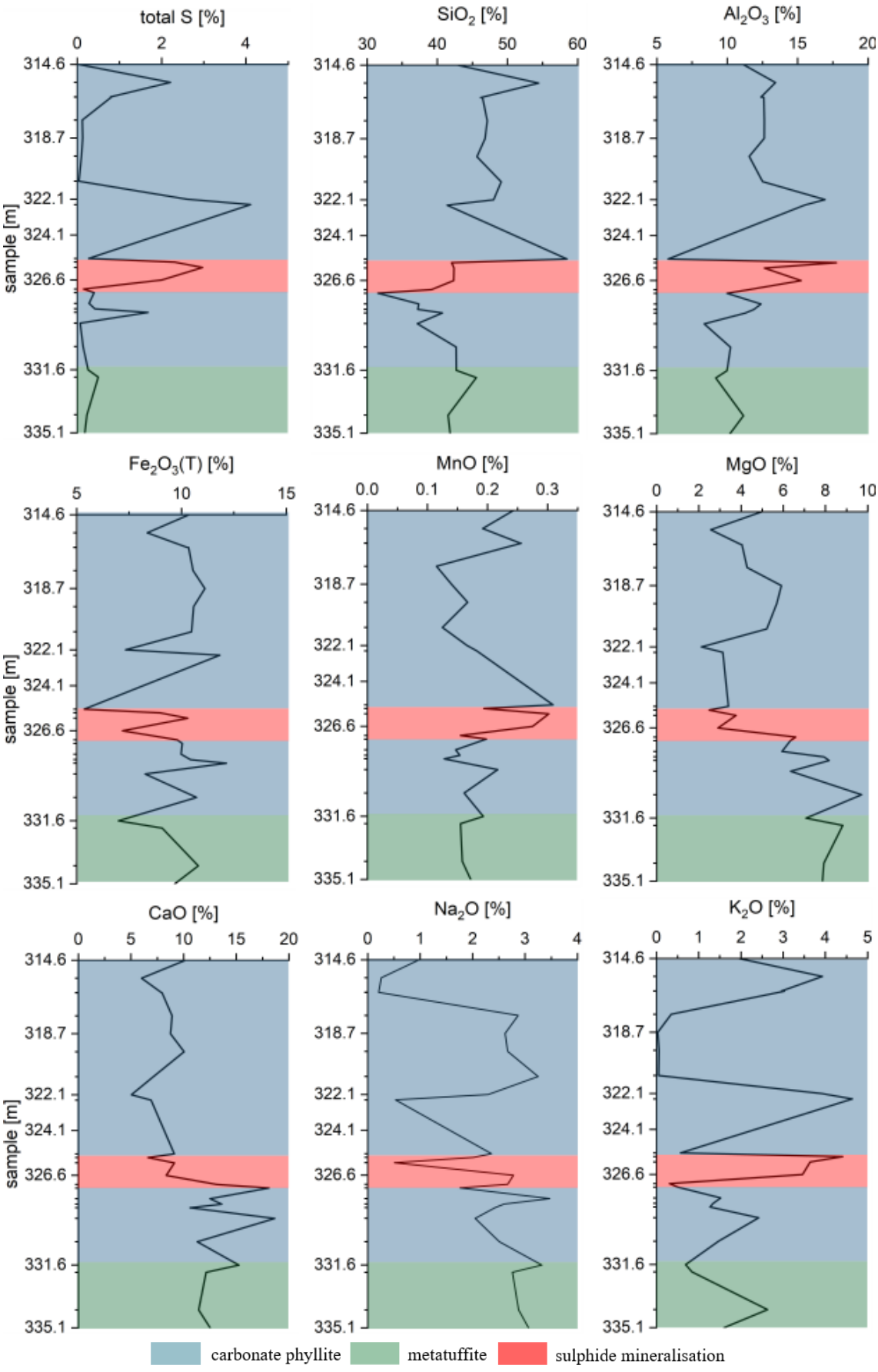

Figure 20: Distribution of main components along the H1 section 1 drill core.

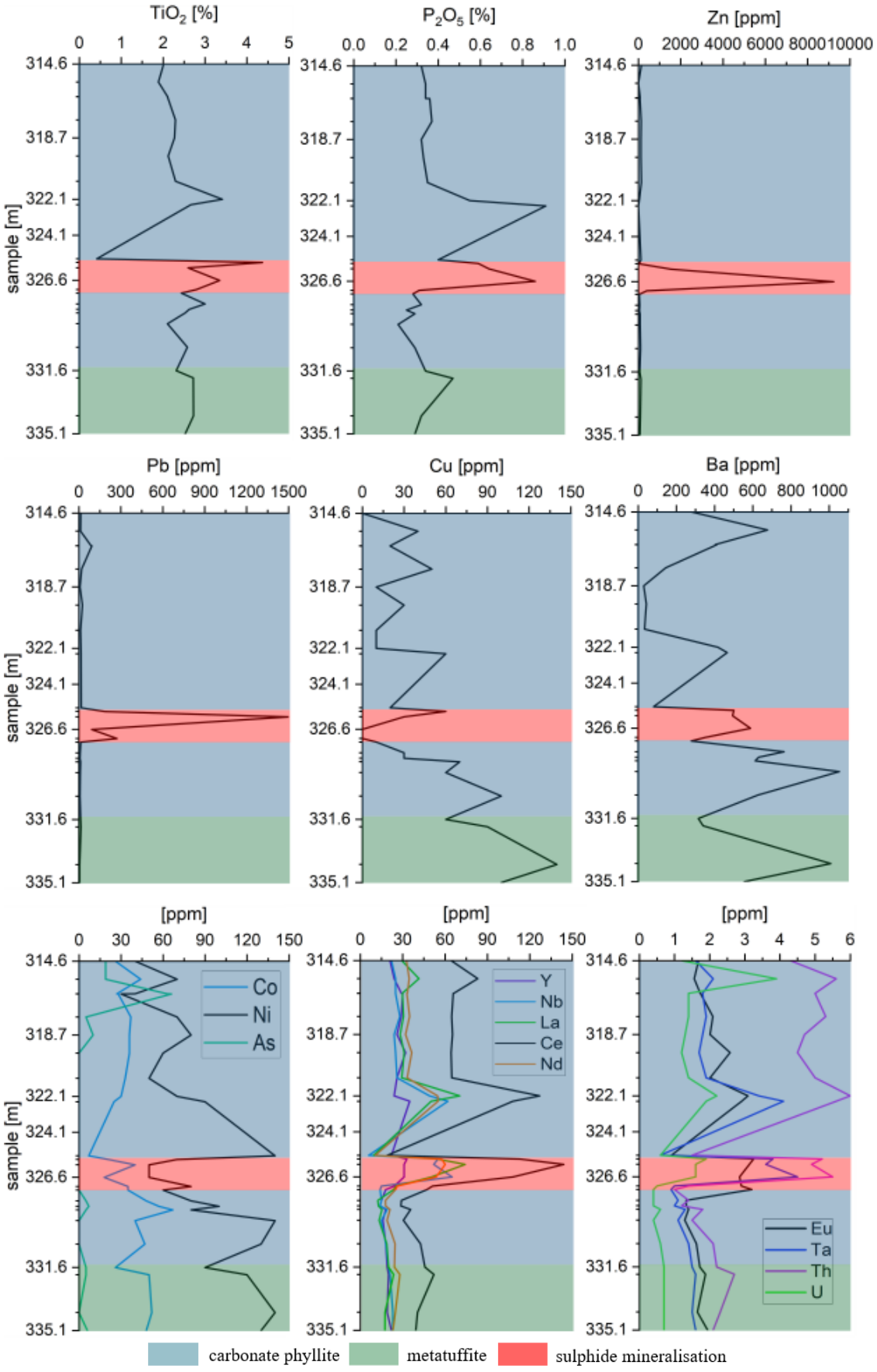

Figure 21: Distribution of main components and selected elements along the H1 section 1 drill core.

3.1.2 H1 section 2 drill core

The second mineralised section (39 samples) of the H1 drill core, ca 75 m below section 1 (see Figure 7), consists of carbonate phyllite, marble, and thin mineralised layers (Fig.22 & 23). SiO_2 concentrations are high near ore horizons, below it, and show clear differences between marble layers and carbonate phyllite, which is silica rich. The situation is very similar for Al_2O_3; high values are also connected to mineralisation, but are highest beneath ore horizons, and its distribution correlates with silica regarding lithologies having high concentrations in carbonate phyllite. CaO can be used to distinguish between phyllite and marble, since the concentrations are clearly elevated in marble over carbonate phyllite and are low at mineralised layers. MgO behaves differently to CaO and differences between marble and carbonate phyllite are less pronounced. It is especially enriched at ore and shows lower values at thin marble layers, but an enrichment in the marble stratigraphically above the mineralisation occurs with increasing distance from ore horizons. MnO has also higher concentration near the ore horizons, is generally slightly elevated above the mineralisation than below it and stretches across both lithologies. Na_2O shows stark concentration differences above and at or below sulphide mineralisation, where it reaches high contents in carbonate phyllite and marble equally. K_2O is enriched at the mineralisation and below in carbonate phyllite. In marble there are trends to lower concentrations. TiO_2 tends to have higher values in carbonate phyllite as well as mineralised strata, whereas in marble it is often decreased, however, the highest values are found in marble at the top end of the section. The concentrations of P_2O_5 are slightly lower at ore layers than in most other barren metasediments, whereas the differences are generally low, albeit P_2O_5 peaks in marble above the mineralisation. Fe_2O_3 (T) has its highest values at ore and varies across the section in both lithologies, which do not show big differences. Lead has a clear anomaly at the mineralised zone (up to > 1 %), whereas Zn does not exhibit a similar distribution since it is not only enriched at the ore horizons but instead shows a wider area of higher concentrations, which seems to be bound to carbonate phyllite, since there are trends to lower concentrations in marble. The concentration of total S peaks at the mineralisation but increases approximately 10 m in the hanging wall from the ore horizons. Copper peaks at the sulphide mineralisation but distribution variations occur along the section. Barium is strongly enriched in a zone between 2 to 5 m from ore, but concentrations are very similar outside of the enriched zone along the drill core section. The ore-related metals Co, Ni, and As have a rather complex distribution. Cobalt and Ni correlate with each other and tend to have concentrations below the detection limit in thin marble intercalations, although, in the thick marble sequence stratigraphically above the mineralisation elevated concentrations exist. Arsenic shows a different distribution than Co and Ni and is especially enriched from the ore into the overlaying marble layer where it has significantly more abundant. Lanthanum, Ce and Nd concentrations vary along the profile, whereas variations are strong near ore horizons and seem to have a tendency for lower concentrations compared to the rest of the section. The same is true for Y, Nb, Ta and U which ate depleted as well and show stronger variations at the mineralised zone. Furthermore, Th is clearly enriched at ore and below it, whereas marbles have generally lower Th concentrations.

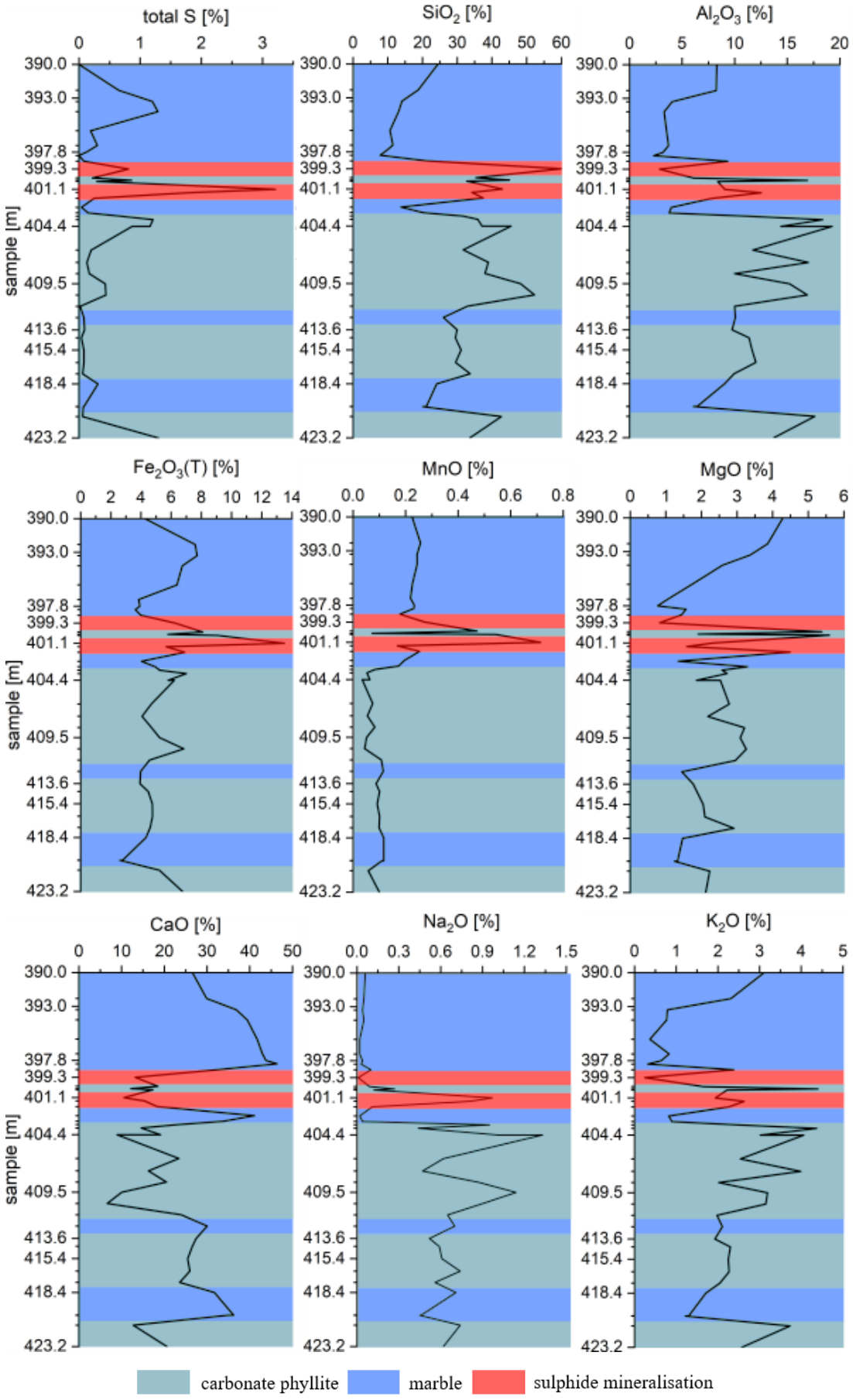

Figure 22: Distribution of main components along the H1 section 2 drill core.

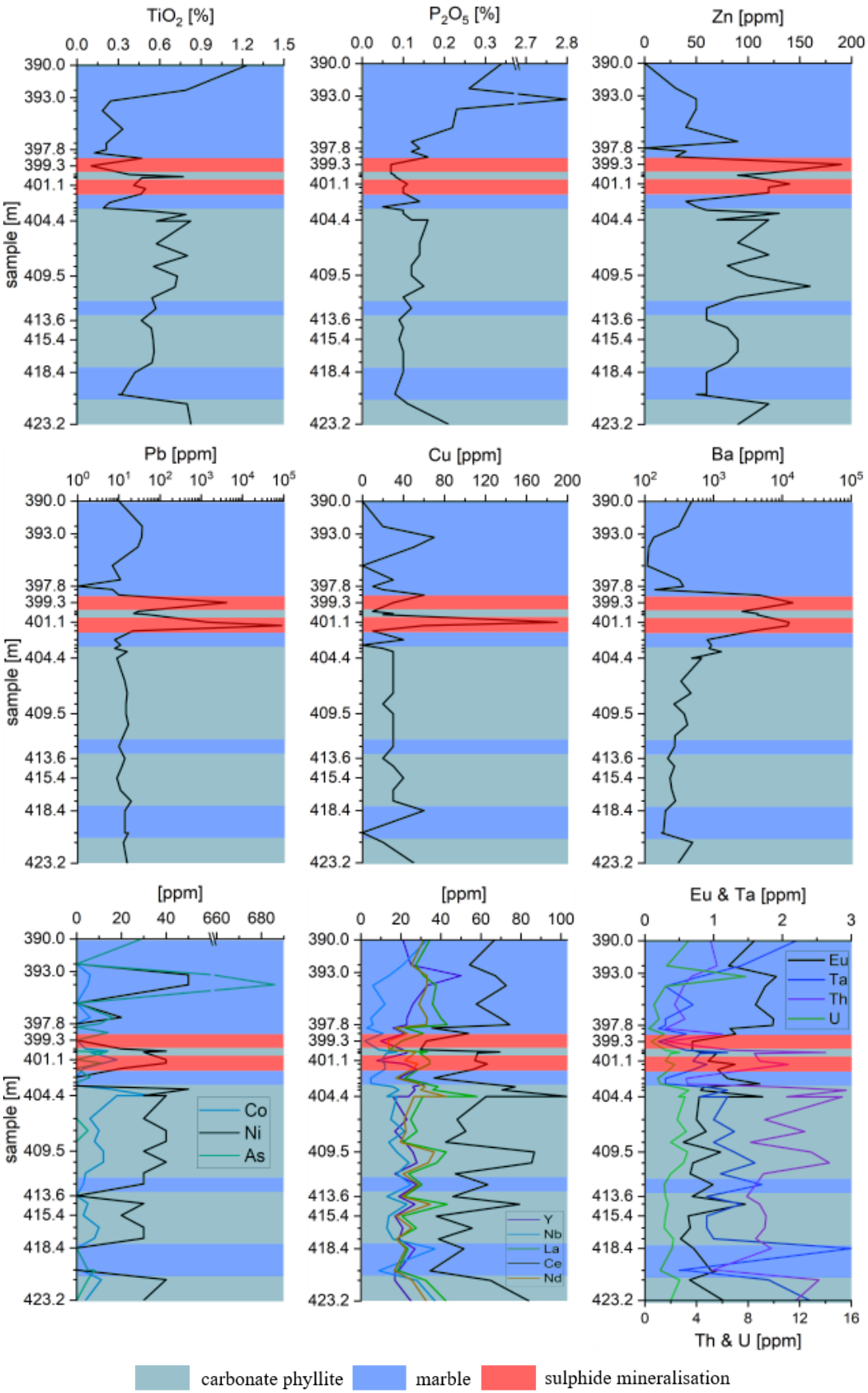

Figure 23: Distribution of main components and selected elements along the H1 section 2 drill core.

3.1.3 G7 section 1 drill core

The G7 drill core section 1 (14 samples) comprises carbonate phyllite mantling a breccia zone that hosts weak sulphide mineralisation (Fig.7, 24 & 25). The SiO_2 contents along the section tend to be higher in mineralised breccia than in carbonate phyllite. Al_2O_3 shows a similar pattern but less pronounced, whereas near ore greater variability of Al_2O_3 concentrations occurs. CaO concentrations are low in the vicinity of sulphide mineralisation and in its brecciated host rock compared to carbonate phyllite in the footwall as well as the hanging wall of the breccia, which is distinctly more enriched. MgO has similar concentrations in the footwall carbonate phyllite and breccia but shows a strong enrichment in the carbonate phyllite adjacent to the breccia in the hanging wall. However, values decrease continuously in the hanging wall reaching concentrations comparable to the carbonate phyllite in the footwall of the sulphide mineralisation. MnO peaks at the sulphide mineralisation but elevated concentrations are present in the carbonate phyllite immediately overlaying the breccia. Na_2O has its maximum just above the sulphide mineralisation in the breccia, but concentrations are generally similar throughout the section and are not affected by lithological changes. K_2O is similar to Al_2O_3 with a maximum in carbonate phyllite and stronger variations within breccia and sulphide mineralisation. Sulphide mineralisation shows a strong trend to significantly more elevated TiO_2 concentrations compared to barren breccia and carbonate phyllite in the upper and lower parts of the section. P_2O_5 peaks in between the sulphide mineralisation but values are distinctly lower in both lithologies as well as the mineralized breccia. Fe_2O_3 (T) has the highest concentrations in the vicinity of sulphide ore, whereas breccia has a stronger variation of Fe_2O_3 (T) concentrations than carbonate phyllite. The base metals Zn, Pb and Cu peak at different positions within breccia. Pb has its highest concentrations (353 ppm) at the lower sulphide mineralisation, whereas Zn has its maximum (8.77 %) at the upper mineralized zone and Cu reaches its maximum of 580 ppm in barren breccia in the hanging wall of the sulphide ore, which is richer in Cu compared to carbonate phyllite. Sulphide mineralisation is naturally rich in total sulphur, which generally correlates with base metals. Barium forms a wider halo of higher concentrations around the sulphide mineralisation stretching into carbonate phyllite with a trend to higher concentrations (<0.5 %) above the upper sulphide mineralisation. The elements Co, Ni, and As generally do not correlate with each other. Cobalt has its maximum in the upper sulphide mineralisation but has elevated concentrations in breccia and the lower adjacent carbonate phyllite. Arsenic was only detected in the breccia and the footwall carbonate phyllite but is low in sulphide mineralisation. Nickel shows low concentrations at sulphide mineralisation and tends to have lower values in breccia than in carbonate phyllite, whereas a strong enrichment occurs in the upper most part of the section in carbonate phyllite. REE, e.g. La, Ce, and Nd, correlate with each other and show varying concentrations like many other elements in breccia, whereas higher values tend to be found in the Pb bearing lower sulphide mineralisation. Europium behaves a little different and shows a general increase in the mineralisation. HFSE, e.g. Y, Nb, Ta, Th, and U, have varying concentrations in breccia near ore as well. Especially, Nb and Ta are enriched in the vicinity of sulphide ore. Thorium and U are enriched near ore but also show increasing values towards mineralisation in both lithologies. Yttrium does correlate negatively with REE in breccia but increases slightly at the sulphide mineralisation. Thorium is slightly enriched at the mineralized breccia and reaches its maximum in the footwall carbonate phyllite. Besides, carbonate phyllite at 46.2 m has the highest tungsten concentrations (155 ppm) of all samples and ore at 58.2 m the maximal In concentrations (2.7 ppm).

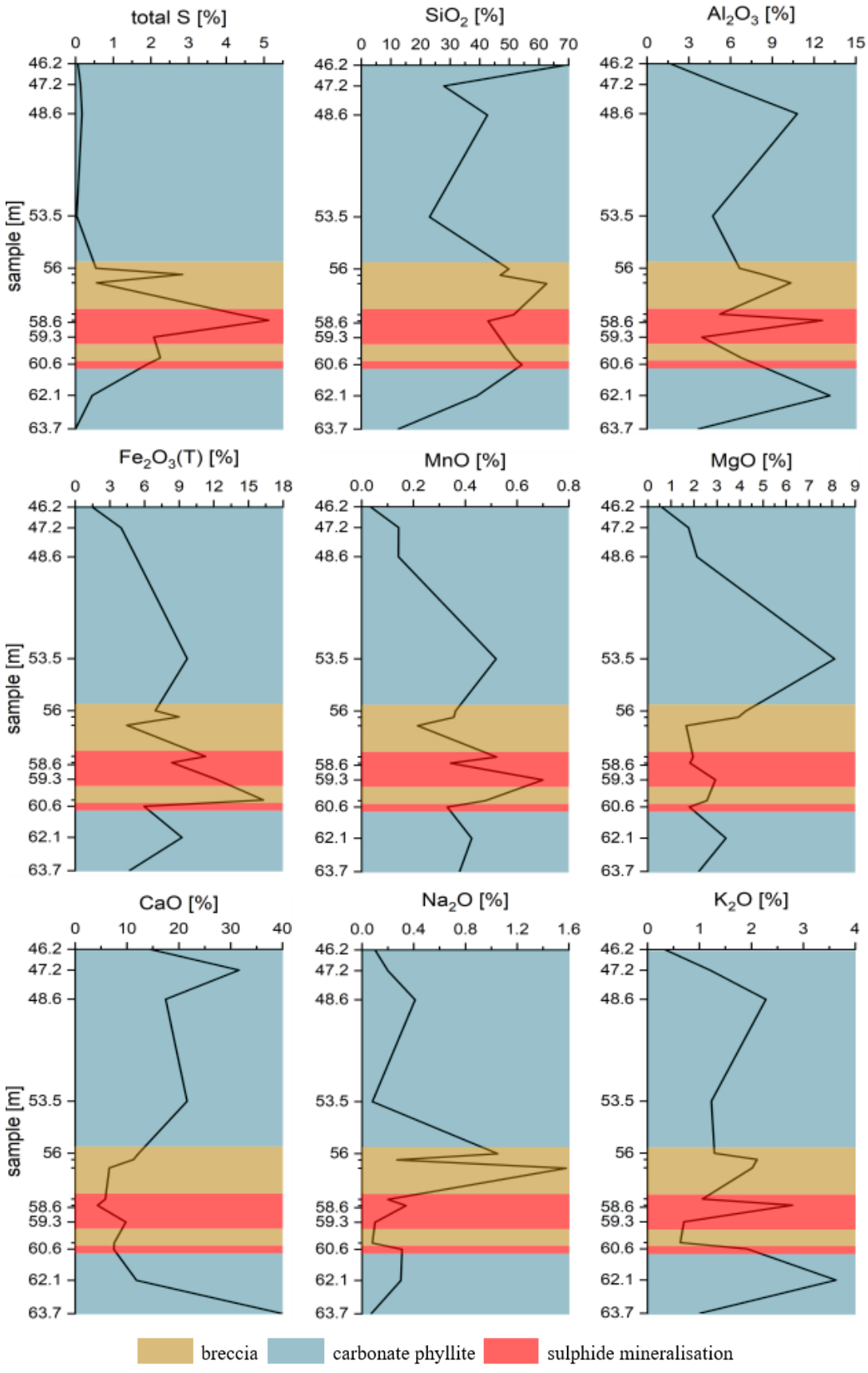

Figure 24: Distribution of main components along the G7 section 1 drill core.

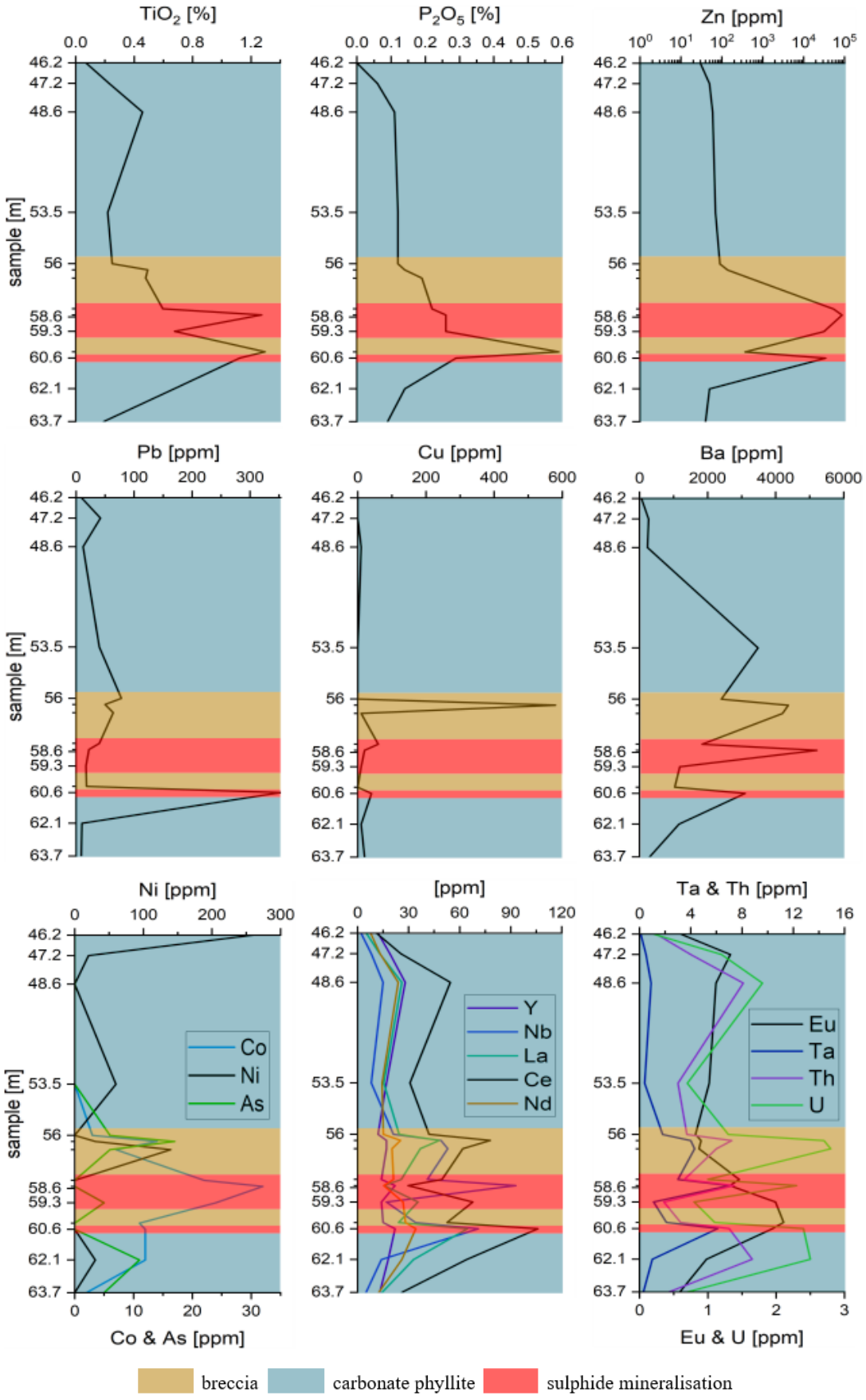

Figure 25: Distribution of main components and selected elements along the G7 section 1 drill core.

3.1.4 G7 section 2 drill core

The section 2 (12 samples), circa 35 m beneath section 1, of the G7 drill core comprises mainly of breccia and a thin sulphide mineralisation as well as a carbonate phyllite layer (Fig.7, 26 & 27). The SiO_2 content along the section are quite constant and only in the carbonate phyllite elevated concentrations occur. Al_2O_3 and K_2O do not show anomalies along the profile and have trends to lower concentrations from top to bottom. CaO is depleted at the sulphide mineralisation and has higher values beneath the mineralisation than stratigraphically above. The situation is similar for MgO, it is also decreased in the proximity of mineralisation, whereas stratigraphically below the ore horizon a negative correlation to CaO is present. MnO has elevated concentrations near ore and has generally lower values below mineralised zones. Fe_2O_3 (T) has a very similar trend as MnO with elevated concentrations from the ore layers up wards. TiO_2 and P_2O_5 correlate with each other and have a very similar distribution. Both constituents are depleted at the main mineralisation at 108.25 m and below, but concentrations increase towards the second minor mineralisation at 100.9 m. Zinc, Pb, Cu, as well as total S show a clear enrichment at the mineralisation at 108.25 m and to a lesser extent also at 100.9 m, whereas ore is Zn dominated - in historical data >5 % Zn and 1 % Pb are reported. Barium peaks in the immediate overlaying rock, although, compared to base metals, elevated concentrations span over a larger zone from the footwall of the mineralisation to the proximal hanging wall breccia of the main ore horizon. At the upper mineralised layer Ba increases, which also affects the rocks above ore. Nickel has three distinct anomalies along the section at both mineralisation and in the footwall of the main ore occurrence, but concentrations are still low and just above the detection limit (<20 ppm). Cobalt and As tend to have also increasing concentrations at ore. This is especially true for Co, which has elevated values from the mineralisation upwards. Higher As contents are bound to the main ore layers. REE, such as La, Ce, Nd, and Eu, have increasing concentrations from the proximal footwall of the mineralisation to the top of the section. The distribution of Y and Tl show a similar pattern but for Tl it is at a very low level. HFSE, i.e. Nb, Ta, Th, and U, have a clear anomaly at the mineralisation and stretches to the hanging wall, whereas values are significantly lower at the more distal footwall.

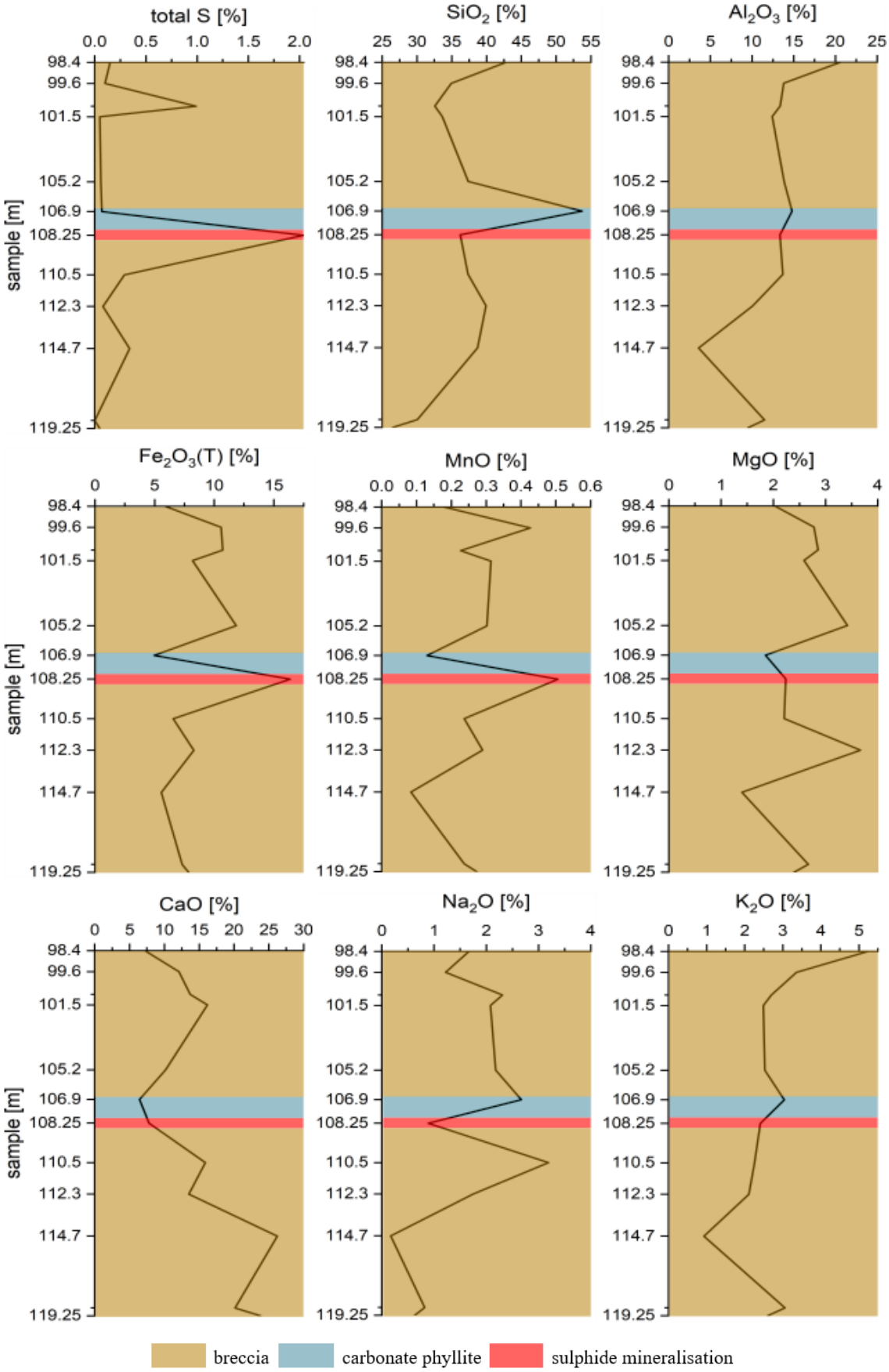

Figure 26: Distribution of main components along the G7 section 2 drill core.

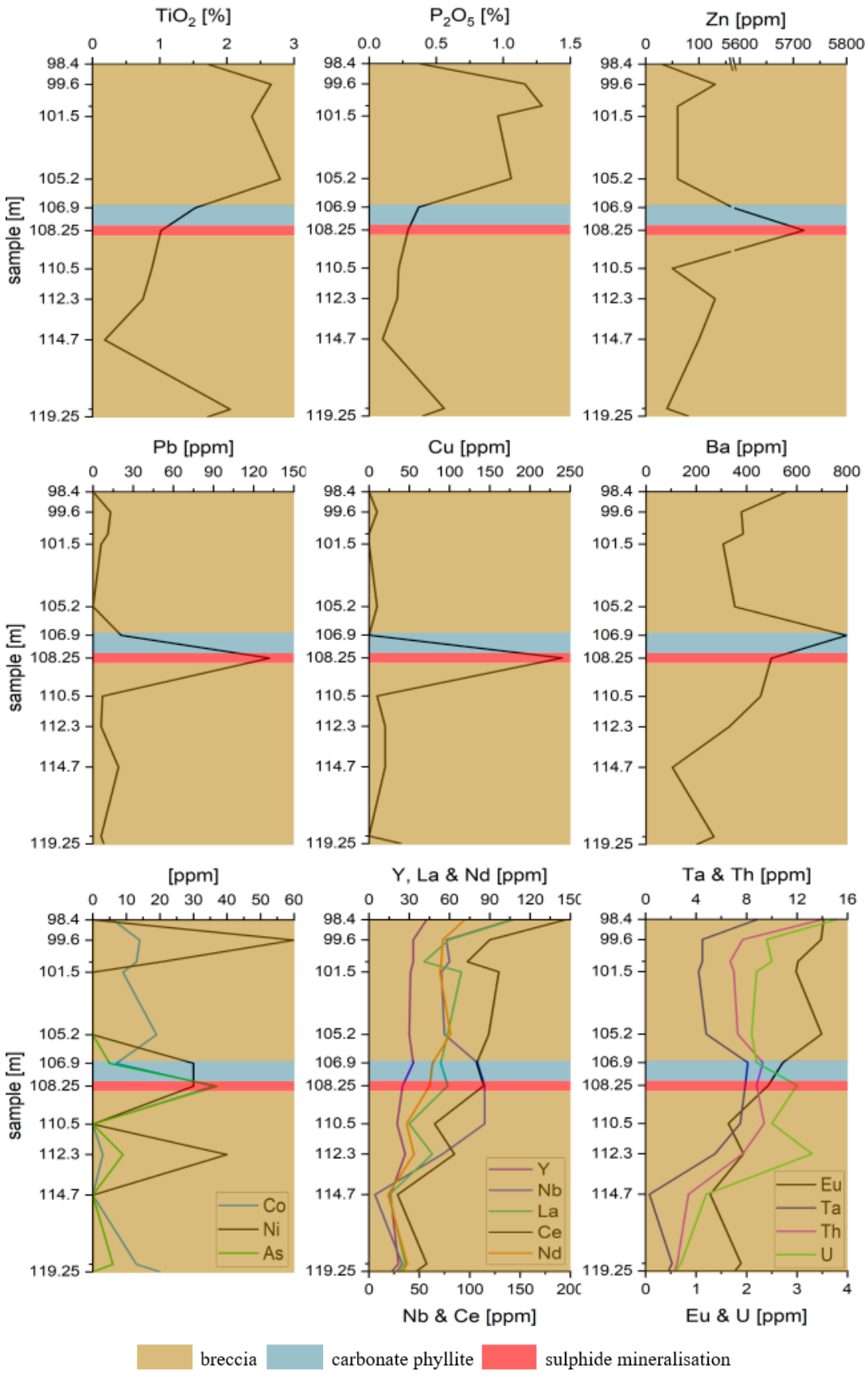

Figure 27: Distribution of main components and selected elements along the G7 section 2 drill core.

3.1.5 Unnamed Adit, Kaltenberg-Burgstall

At the unnamed adit in the Kaltenberg-Burgstall deposit two approximately 15 cm thick ore layers occur circa 30 cm from each other in a marble host rock with a carbonate phyllite interlayer between them. Five samples are taken along a profile with a length of approximately 1 m above, below, between, and from the ore horizons with a spacing of 15-20 cm (Fig.28, 29 & 30). SiO_2, Al_2O_3, K_2O, TiO_2, and P_2O_5 show similar distribution patterns. Their concentrations increase from the footwall, through the lower mineralisation to the marble interlayer and drop to a minimum at the upper ore zone. CaO is depleted in the carbonate phyllite interlayer. MgO has a trend to increasing concentration from bottom to top and has its maximum between the two ore horizons. MnO has its minimum in the lower ore horizon but its maximum in the upper one and has low concentrations in the interlayer. Na_2O peaks in carbonate phyllite. Fe_2O_3 (T) is clearly enriched in both ore horizons compared to barren host rock. Generally, the upper ore layer is richer in Pb and Zn compared to the lower one. On the other hand, Cu and Ba have higher concentrations in the lower mineralisation and are low in the upper one, whereas hanging wall concentrations are again higher. Cobalt and Ni correlate and are weakly enriched in both ore horizons, whereas As is depleted in the mineralisation and the carbonate phyllite interlayer. REE, e.g. La, Ce, and Nd, are enriched from the bottom of the section to the interlayer and concentrations drop at the upper ore layer, whereas HFSE, e.g. Nb, Ta, Y, Th, and U display the same trend. Besides, at Kaltenberg-Burgstall, the highest Mo concentration occurs in ore reaching 39 ppm which is at least 4 times higher than of all investigated locations and drill cores.

Figure 28: Two ore horizons in the unnamed adit at the Kaltenberg-Burgstall mining district.

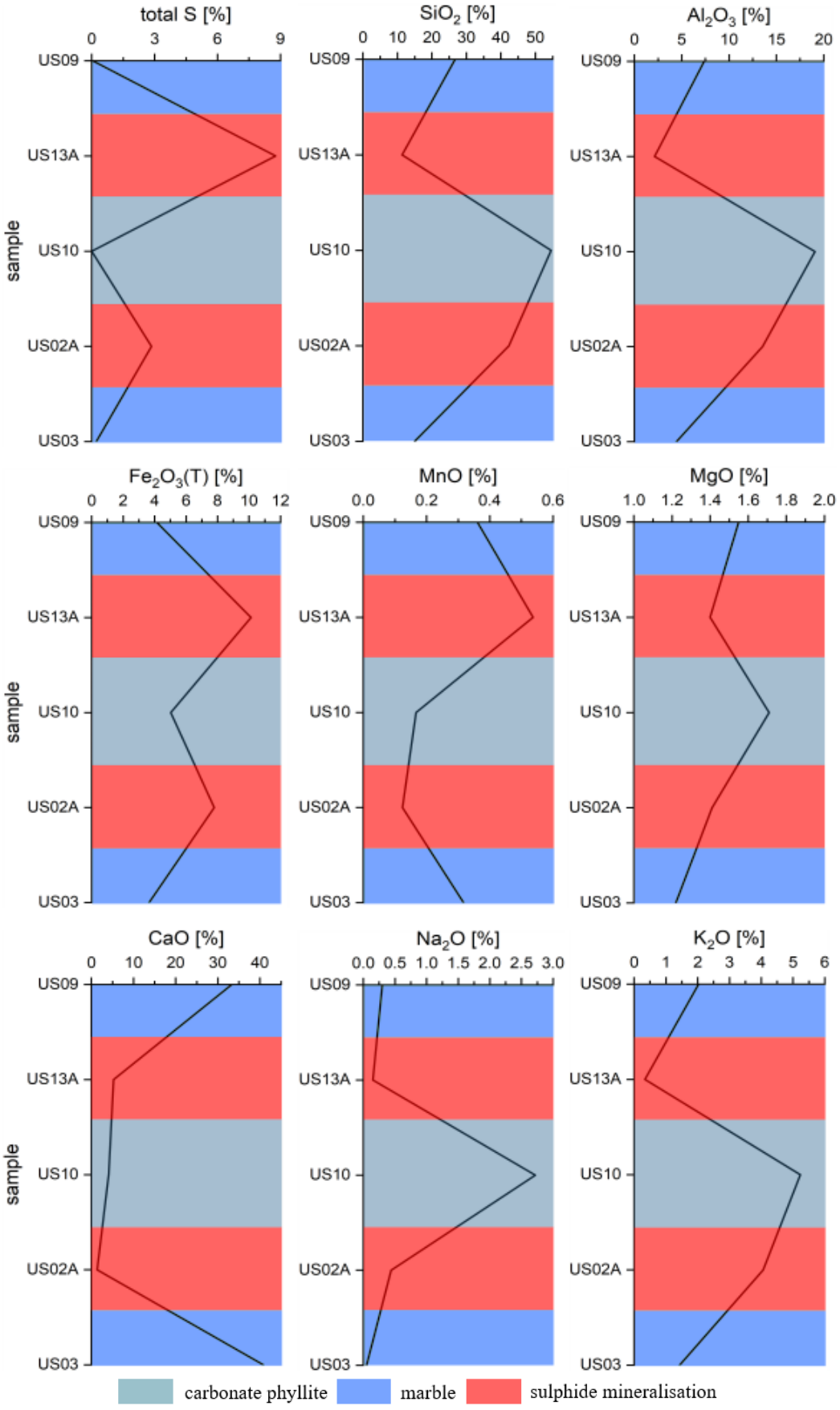

Figure 29: Distribution of main components across the two ore horizons in the unnamed adit at the Kaltenberg-Burgstall mining district.

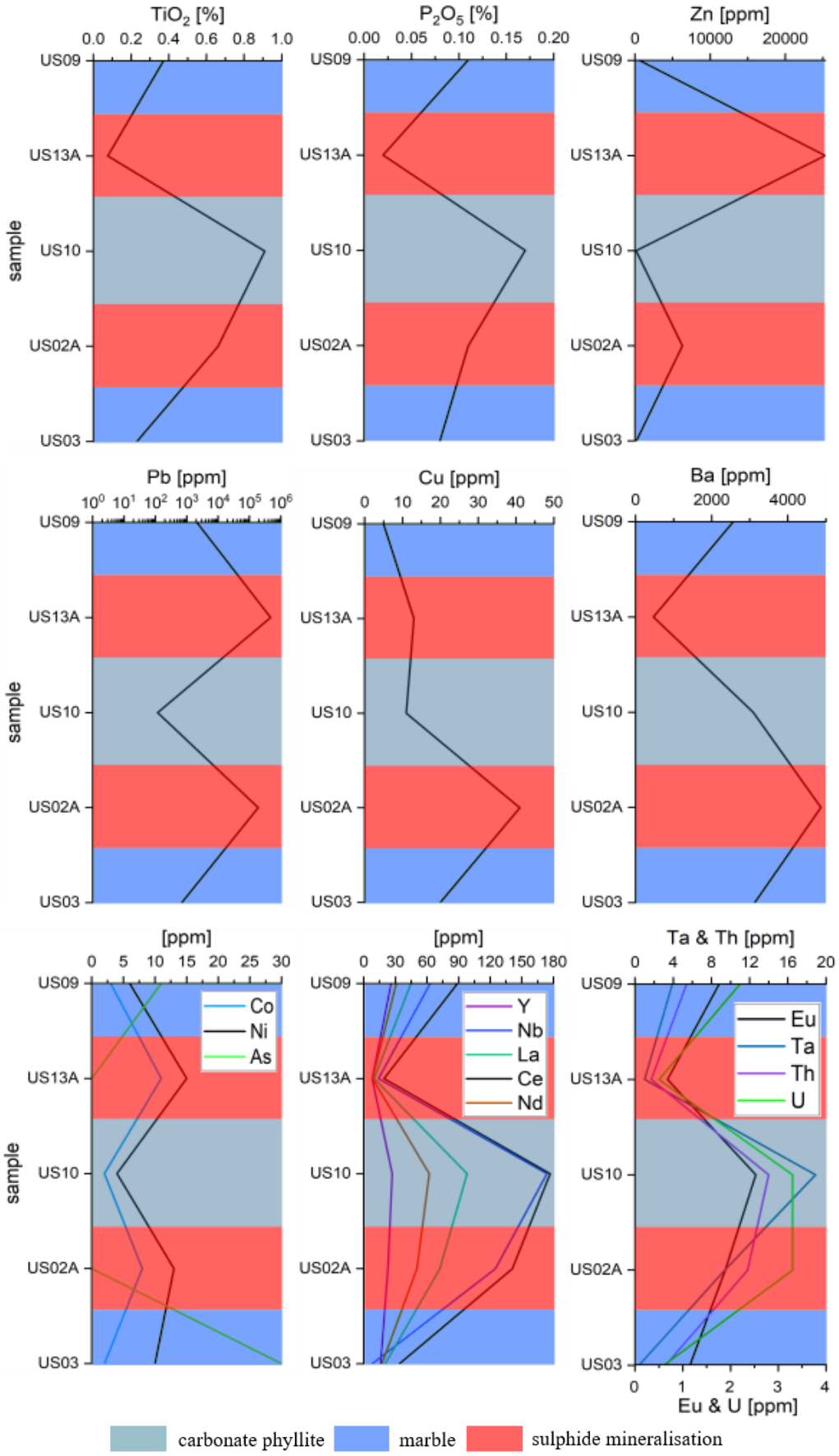

Figure 30: Distribution of main components and selected elements across the two ore horizons in the unnamed adit at the Kaltenberg-Burgstall mining district.

3.2 Mineralogy & Petrography

3.2.1 H1 section 1 drill core

From the H1 section 1 drill core 10 polished thin sections covering 315.6 m to 335.1 m depth were studied: two from metatuffite in the stratigraphic lowest position from the section, two from the sulphide mineralisation at 325.9 to 326.6 m, and 7 from carbonate phyllite (1 footwall and 6 hanging wall samples). The metatuffite in the lower parts of the section has a greenish colour with thin alternating dark green and bright whitish layers, which display strong deformation and mm-scale folding. Dark layers consist of tremolite and chlorite, whereas biotite occurs only in the lower parts and phengite is only present in the upper parts of the metatuffite layer. Additionally, albite is abundant, and the quantity of quartz increases from bottom to top. Generally, crystal sizes of dark layers are distinctly smaller than those of bright layers, which consist of mainly calcite with little interspersed silicates. Ilmenite porphyroblasts rich in mineral inclusions are bound to silicate-dominated layers (Fig.31A & B), are partly surrounded by titanite, and sometimes contain sulphides, like chalcopyrite. Titanite is not only found with ilmenite but also interspersed as fine-grained crystals in silicate-rich layers. Additional phases are frequently occurring fluorapatite as well as rare allanite-(Ce) and zircon, which are all associated with Ti minerals in the silicate rich layers. The quantity and diversity of disseminated sulphides increase from bottom to top. In the lower metatuffite only pyrite, which forms large subhedral crystals, and chalcopyrite were observed, whereas in the upper part additional galena and sphalerite, as well as rare Ni sulphides such as millerite and pentlandite occur.

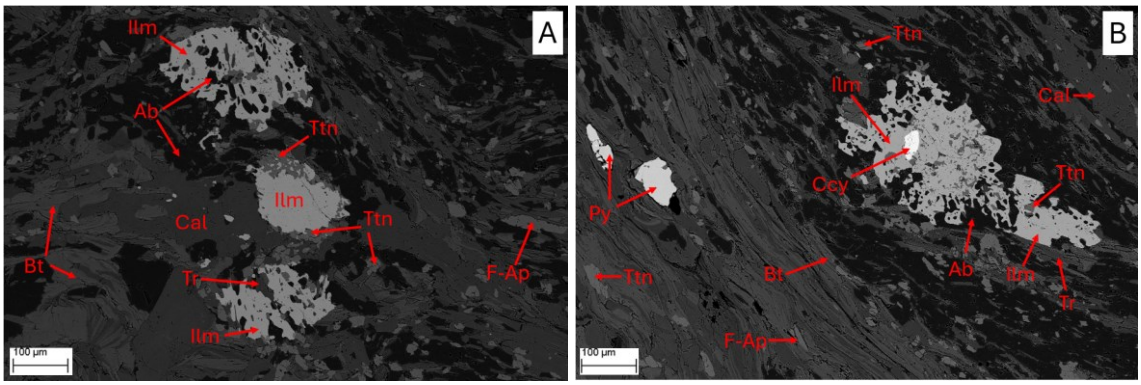

Figure 31: A & B: BSE images of ilmenite porphyroblasts in silica rich layers within metatuffite, depth 335.1 m; mineral abbreviations: Ab=albite, Bt=biotite, Cal=calcite, Ccy=chalcopyrite, F-Ap=fluorapatite, Ilm=ilmenite, Py=pyrite, Tr=tremolite, Ttn=titanite.

Carbonate phyllite is a major rock type of this section and hosts the Pb-Zn ore. In the foot wall of the sulphide mineralisation, it is relatively poor in sulphides. It has a greenish and sometimes slightly brownish colour and alternating carbonate-rich and silicate-rich layers, which are deformed and folded. Carbonate-layers consist mainly of calcite and little interspersed silicates. Silicates are abundant biotite and albite as well as accessory quartz. Pyrite is the main sulphide mineral and sometimes has inclusions of rare villamaninite [$(Cu,Ni,Co,Fe)S_2$], and of galena, which also occurs as inclusions in chalcopyrite. Furthermore, accessory chalcopyrite and sphalerite are associated with pyrite. Additionally, rare pentlandite was observed. Titanium phases encompass fine-grained titanite and significantly larger ilmenite. In general, sulphides and Ti bearing minerals occur within the silicate-dominated layers.

Drastic colour changes to dark yellow, orange and brownish or greyish tones occur in sulphide-rich carbonate phyllite. The sulphide mineralisation itself occurs mainly as thin, concordant, and sometimes diffuse vein-like structures, which are strongly deformed and folded, or to a lesser extent as disseminated phases in the host rock (Fig.32). The veins exhibit slightly larger crystal sizes compared to the host rock, whereas gangue minerals are quartz, dolomite plus rare ankerite, albite and orthoclase. Pyrrhotite is the most abundant sulphide mineral, but sphalerite and galena are common constituents, whereas only minor pyrite and accessory chalcopyrite are present. These vein-structures continue to 322.1 m in the hanging wall of the sulphide mineralisation; however, above the sulphide ore to 322.1 m galena decreases to only being an accessory phase, sphalerite as well as chalcopyrite disappear completely outside of the sulphide mineralisation, but pyrrhotite remains the dominant sulphide phase and the amount of pyrite increases slightly up to 322.1 m. Furthermore, a single, large, euhedral, twinned arsenopyrite crystal (Fig.33A) with rutile, pyrrhotite, and vein-like galena inclusions was observed within a vein-structure in the hanging wall of the sulphide mineralisation. Additionally, little cobaltite was found next to the arsenopyrite. Carbonate phyllite host rock of the vein-structures consists of mainly phengite with minor chlorite. Contrary to the carbonate phyllite below the sulphide mineralisation, Ti phases are only fine-grained rutile, which is associated with fluorapatite as well as rare zircon and sometimes forms chain-like successions (Fig.33D). Monazite occurs mainly as individual crystals, as clusters, or even as a thin vein at the vein-structure host rock boundary (Fig.33B) and is associated with rutile and fluorapatite. It is also present together with pyrrhotite and chlorite within larger disseminated infrequent aggregates (pseudomorphs) (Fig.33C), which are clearly relics of degraded minerals. Rare xenotime and thorite are mainly associated with monazite. Very rare allanite-(Ce) exists as inclusions in pyrrhotite. Besides, gangue phases of the vein-structures are present disseminated within the carbonate phyllite. Apart from carbonates of the dolomite-ankerite series, also rare siderite occurs as either individual minerals or as a discordant vein within a sulphide-bearing vein-structure.

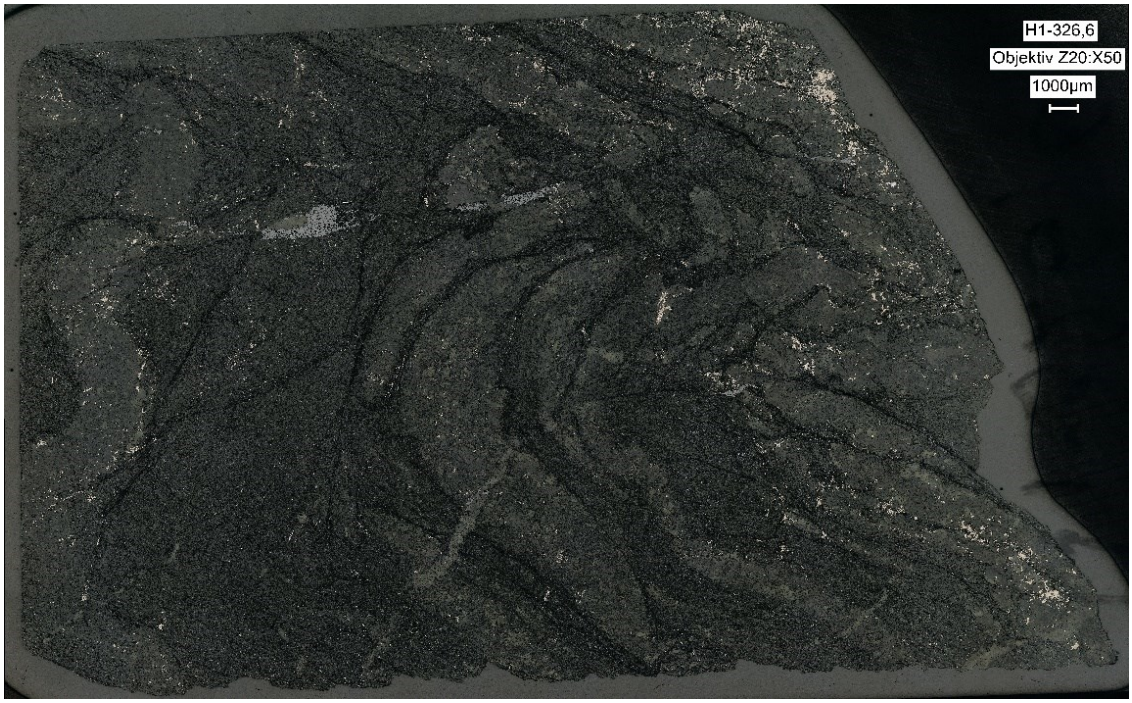

Figure 32: Reflected light microscopy image of the sulphide mineralisation of the H1 section 1 drill core at 326.6 m containing brighter sulphide bearing vein-structures.

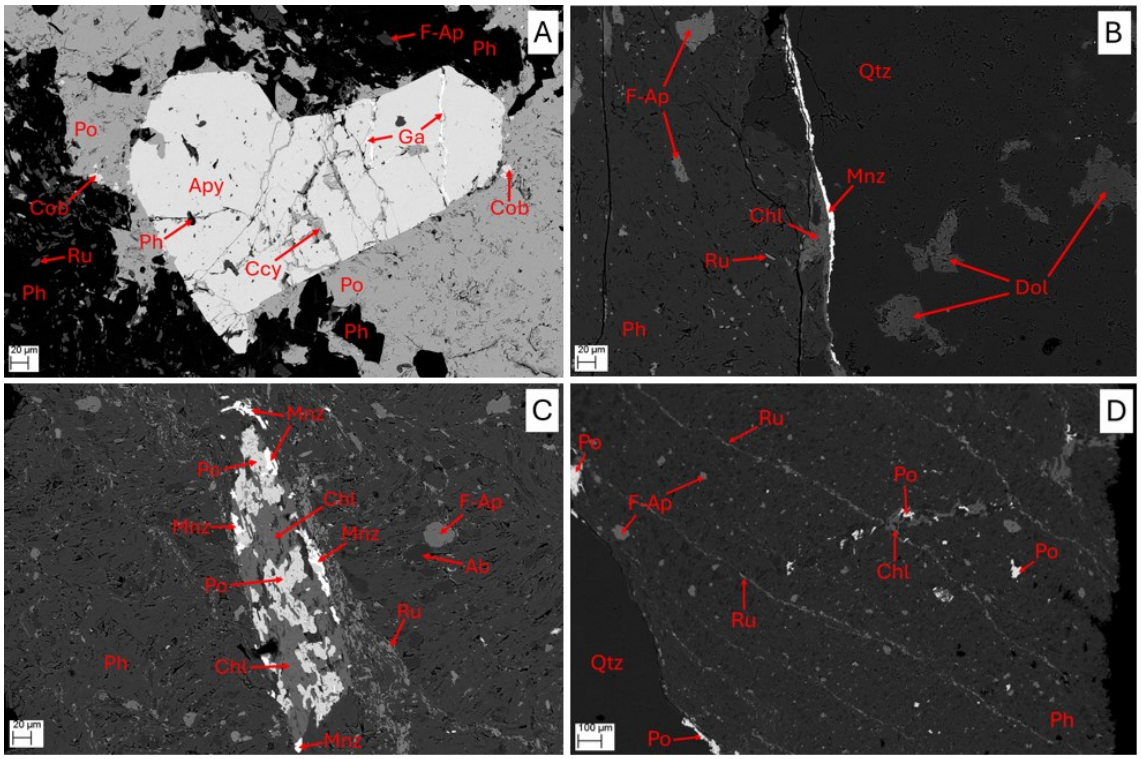

Figure 33: BSE images from the H1 section 1 drill core at 324.1 m; A: Twinned arsenopyrite crystal; B: Monazite vein at the boundary between a vein-structure and the host rock; C: mineral aggregate (pseudomorph); D: chain-like successions of rutile; Mineral abbreviations: Ab=albite, Apy=arsenopyrite, Ccy=chalcopyrite, Chl=chlorite, Cob=cobaltite, Dol=dolomite, F-Ap=fluorapatite, Ga=galena, Mnz=monazite, Ph=phengite, Po=pyrrhotite, Qtz=quartz, Ru=rutile.

Above the sulphide-rich carbonate phyllite, a greenish sulphide-poor carbonate phyllite occurs as a layer at 318.7 m. It is rich in chlorite and quartz as well as albite. Titanium phases are fine-grained rutile and significantly larger ilmenite. Furthermore, minor fluorapatite and accessory monazite as well as rare thorite occur. Sulphides are mainly pyrite, which occasionally has galena inclusions, accessory chalcopyrite and sphalerite, which both are associated with pyrite. Besides, silicates, Ti phases and sulphides are associated with chlorite. Moreover, carbonates are a major component and encompass calcite as well as rare dolomite.

At the top of the section at 315.6 m a sulphide-rich carbonate phyllite like that in the hanging wall of the sulphide mineralisation with orange, brownish to bright greyish colouring is present and it also shows strong deformation and folding. It contains sulphide-bearing concordant vein-structures as well. Sulphides are predominantly present within vein structures but are also disseminated in the host rock, and encompass mainly pyrrhotite, accessory pyrite with galena inclusions, and rare cobaltite. The gangue phases of the vein-structures are only quartz and dolomite, whereas feldspars are missing unlike vein-structures in the carbonate phyllite from 326.6 m to 322.1 m. The host rock itself consists primarily of phengite as well as chlorite and rutile, F-apatite, and monazite are minor constituents. Moreover, quartz and dolomite are also present in the host rock as disseminated phases. Besides, late discordant veins exist throughout the carbonate phyllite consisting of either pyrite with rare euhedral calcite crystals or of pure calcite.

3.2.2 H1 section 2 drill core

Section 2 comprises 19 polished thin sections from 390 to 423,2 m depth: nine from footwall rocks, 7 from hanging wall rock and 3 from the mineralized zone at 399-401 m. This section consists of two thin sulphide ore horizons, carbonate phyllite with marble interlayers in the footwall and marble in the hanging wall. The carbonate phyllite in the footwall has a medium to dark greyish colour with a layered texture and is strongly deformed and folded. It is streaked by brighter layers, which resemble concordant vein-structures, containing calcite, quartz, and partly albite. Sulphides are common within these structures but also exist as disseminated phases throughout the rock and their quantity increases towards the sulphide mineralisation. Pyrrhotite is the main sulphide phase followed by pyrite, which occurs often as large euhedral crystals. Other accessory sulphides are chalcopyrite, sphalerite and galena, which sometimes are also present as inclusions in pyrrhotite and pyrite, cobaltite, and pentlandite as well as rare ullmannite, and unspecified tiny Fe-Ni-Cu sulphides. The host rock is rich in phengite as well as chlorite and very rarely biotite occurs. Carbonates are dominated by calcite, but also little dolomite is present and occurs mainly within concordant vein structures. Other minor and accessory disseminated HFSE and REE phases exist especially in phengite and chlorite rich parts of the carbonate phyllite. The frequency of fluorapatite and monazite increases approaching the sulphide mineralisation. Monazite occurs accessorily within vein-structures but mainly as clusters within oval shaped or elongated larger aggregates (pseudomorphs) (Fig.34A & B), which are obviously similar to those in the H1 section 1 drill core, relics of degraded minerals. Additional phases in these relics are (urano-)thorite, calcite, REE fluorocarbonates, as well as rare galena, allanite-(Ce), and orthoclase. Furthermore, accessory zircon and rare baddeleyite with a zircon rim as well as rare xenotime, uraninite and brannerite are associated with phengite and chlorite. Apart from brannerite, rutile is the only common Ti bearing mineral, which like other REE and HFSE minerals is bound to layer silicate-dominated parts of the rock where it occurs as interspersed phases. Besides, there are deformed fissure fractures with calcite infill, which are partly also sulphide bearing, as well as late discordant calcite veins with rare thin monazite veins at the boundary to mica-rich parts of the host rock, as well as late rare discordant pyrite veins.

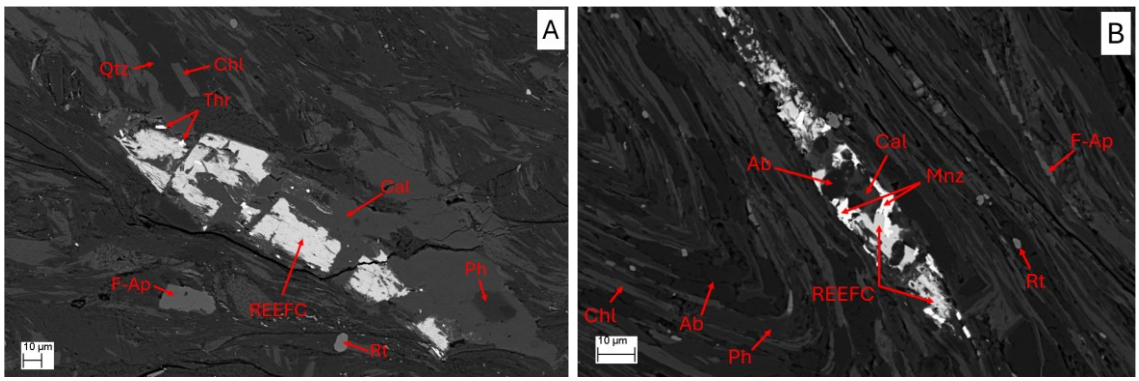

Figure 34: A & B: BSE image of deformed aggregates(pseudomorphs), depth 423.3 m (A) and 405.5 m (B); mineral abbreviations: Ab=albite, Cal=calcite, Chl=chlorite, F-Ap=fluorapatite, Mnz=monazite, Ph=phengite, Qtz=quartz, REEFC=REE-fluorocarbonate, Rt=rutile, Thr=thorite.

The marble interlayer at 418.4 m in the footwall has a dark blueish to greyish colour and a layered, deformed, and folded texture. In this sample two domains with slightly different mineralogical composition are present. One is calcite rich, and the other one is albite rich. Disseminated minor and accessory phases are identical comprising minor quartz, phengite as well as chlorite and accessory zircon, rutile, fluorapatite, and rare dolomite. Monazite, REE-fluorocarbonates, and thorite occur mainly together with calcite within disseminated aggregates, which are like those in the carbonate phyllite, but also exist to a lesser extent as individual phases disseminated in the

rock. Sulphides occur often layered as accessory phases and encompass mainly pyrrhotite and euhedral pyrite, plus galena, sphalerite, chalcopyrite, as well as rare cobaltite, pentlandite, and cubanite. A striking difference between the two domains of the sample are larger crystal sizes and a higher frequency of accessory phases and sulphides within the albite rich part compared to the calcite dominated one (Fig.35). Although in the albite rich part, calcite is still present as a major constituent.

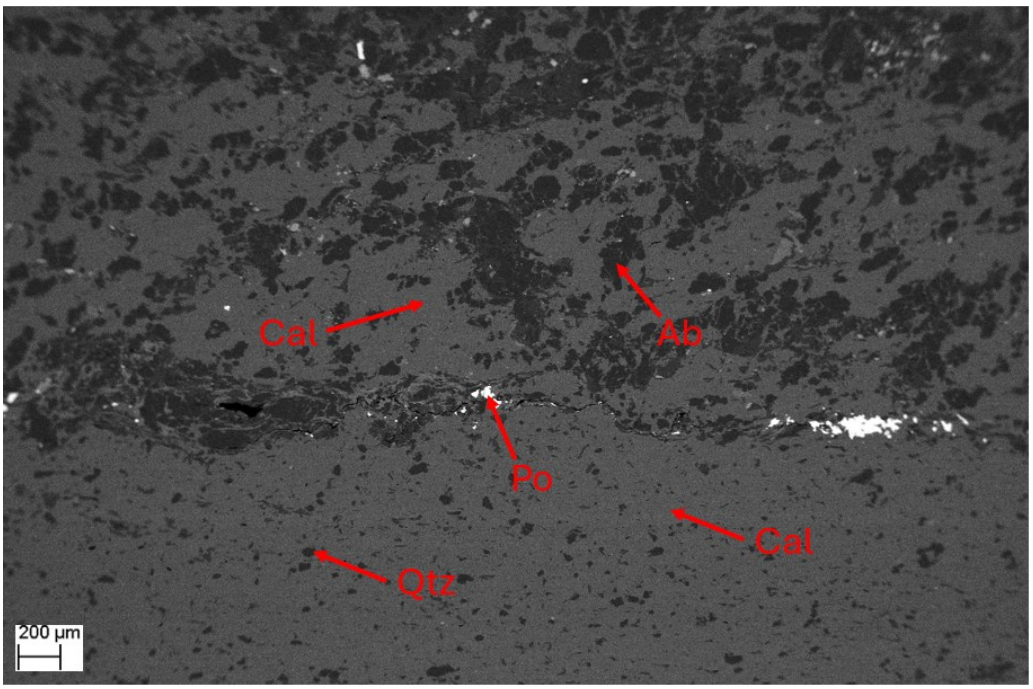

Figure 35: BSE image; Boundary of the albitization front in the marble interlayer at 418.4 m; Upper part of the image albite rich layer with sulphides and accessory phases in calcite matrix; Lower part of the image calcite plus minor quartz; Mineral abbreviations: Ab=albite, Cal=calcite, Po=pyrrhotite, Qtz=quartz.

The host rocks of the two sulphide mineralisations have a bright grey to beige and brownish colour, are layered, deformed and folded. The sulphide ore occurs as concordant layers. The lower mineralisation at 401.1 m is more abundant in galena than in sphalerite, whereas at the upper one at 399.3 m it is vice versa. Apart from Pb or Zn bearing sulphides, ferrous sulphides such as pyrrhotite and pyrite are common. Additional accessory phases are chalcopyrite and cobaltite as well as argentopentlandite, which only occurs in the lower sulphide mineralisation at 401.1 m. The sulphide ore is accompanied by layers of celsian with orthoclase as well as little hyalophane (Fig.36A & B). Carbonates are ubiquitous and are dominated by calcite, whereas minor ankerite and rare siderite as well as dolomite, which is only present in the ore horizon at 399.3 m, are associated with sulphide ore. Other components of the host rock are quartz and minor phengite as well as chlorite. Furthermore, monazite is present within the celsian layer as minor constituent but also occurs disseminated. Titanium-bearing minerals are ilmenite and rutile. Ilmenite is significantly larger than rutile, both are present disseminated and rutile forms rims surrounding ilmenite within the celsian layers. The accessory disseminated phases zircon, (urano-)thorite, monazite and Ti phases are mainly associated with phengite and chlorite. Moreover, fluorapatite occurs as layers but is often disseminated. Besides, late discordant pyrite veins and calcite veins, which host little galena and baryte, exist at the upper sulphide mineralisation at 399.3 m.

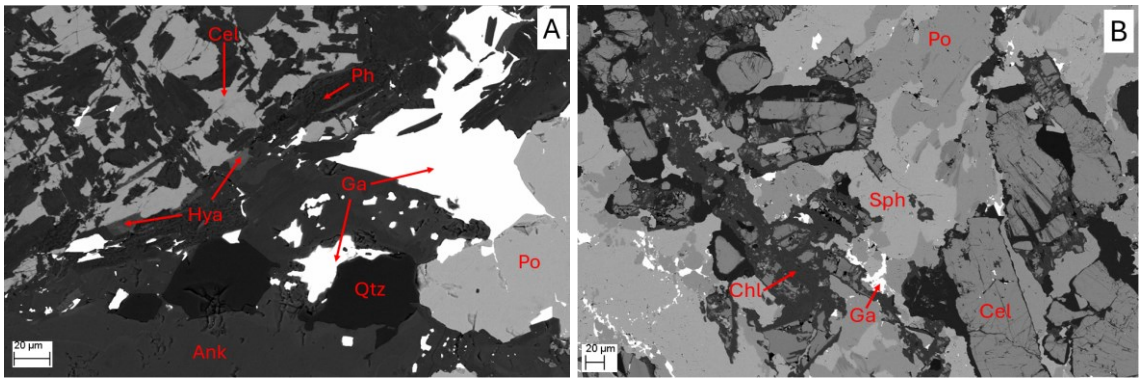

Figure 36: BSE image of Ba feldspar associated with sulphide mineralisation at 401.1 m (A) and 399.3 m (B) in the H1 section 2 drill core; Mineral abbreviations: Ank=ankerite, Cel=celsian, Chl=chlorite, Ga=galena, Hya=hyalophane, Ph=phengite, Po=pyrrhotite, Qtz=quartz, Sph=sphalerite.

The carbonate phyllite interlayer between the two sulphide mineralisations has a dark grey colour and a deformation texture. It consists mainly of phengite, chlorite and quartz plus minor calcite. Rutile is the only Ti phase and occurs as skeletal porphyroblasts (Fig.37) which are partly intergrown by pyrrhotite, monazite, fluorapatite and quartz. Other accessory and disseminated phases are zircon and thorite. Additional sulphides are pyrite and some galena, sphalerite and chalcopyrite plus rare, partly euhedral cobaltite, which is associated with pyrrhotite. Moreover, fissure fractures containing calcite are present.

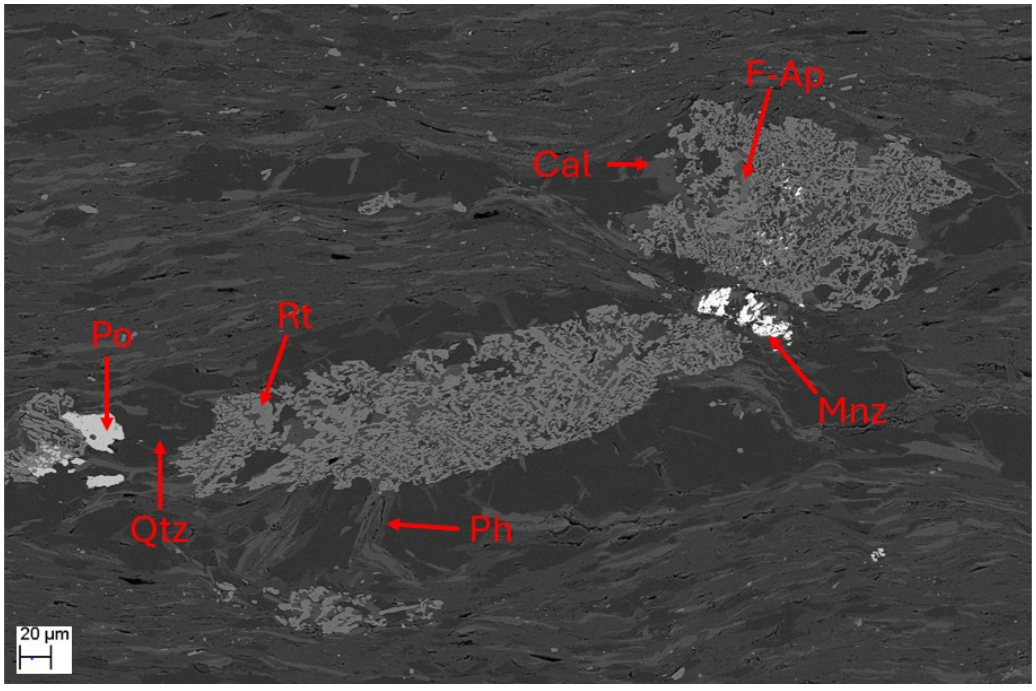

Figure 37: BSE image; skeletal rutile porphyroblast with intergrown fluorapatite, pyrrhotite and monazite, depth 400.3 m; Mineral abbreviations: Cal=calcite, F-Ap=fluorapatite, Mnz=monazite, Ph=phengite, Po=pyrrhotite, Qtz=quartz, Rt=rutile.

The marble in the hanging wall of the sulphide mineralisation has a bright grey colour with a blueish tint in the lower parts of the lithology and beige to brownish tones in the upper parts. The marble is dominated by calcite, whereas phengite, chlorite as well as quartz are minor constituents. Dolomite and less frequent ankerite are associated with sulphides and their abundance increases from bottom to top, whereas dolomite was found to form halos around concordant sulphide bearing vein structures (Fig.38A & B). The most common sulphide phase is pyrrhotite. Galena, which also forms infills of fractures in pyrite, sphalerite, chalcopyrite, and pyrite occurs accessorily. Additionally, arsenopyrite, which is associated with pyrrhotite, cobaltite, gersdorffite, and ullmannite is only present in small quantities, whereas glaucodot is rare. Sulphides are mainly present as layers, exist also in concordant vein structures in the upper parts, but generally are also present disseminated throughout this marble unit, whereas their abundance increases towards the top. Furthermore, hessite was found in phengite and chlorite dominated stylolite structures in the lower parts, which also show a notable frequency of As-rich sulphides. Moreover, ilmenite, rutile, monazite, (urano-)thorite, zircon, and rare allanite-(Ce) occur disseminated, are associated with phengite and chlorite, and are also present within stylolite structures. Ilmenite exists predominantly as porphyroblasts with a rim of rutile. Furthermore, there is an increase of HFSE and REE phases from bottom to top. Fluorapatite is associated with these phases, is present within the dolomite-rich halo of concordant vein structures (Fig.38B) and sometimes forms rich layers (Fig.38C). Besides, late pyrite veins with euhedral calcite crystals exist (Fig.38D). Late discordant crosscutting calcite veins are also present.

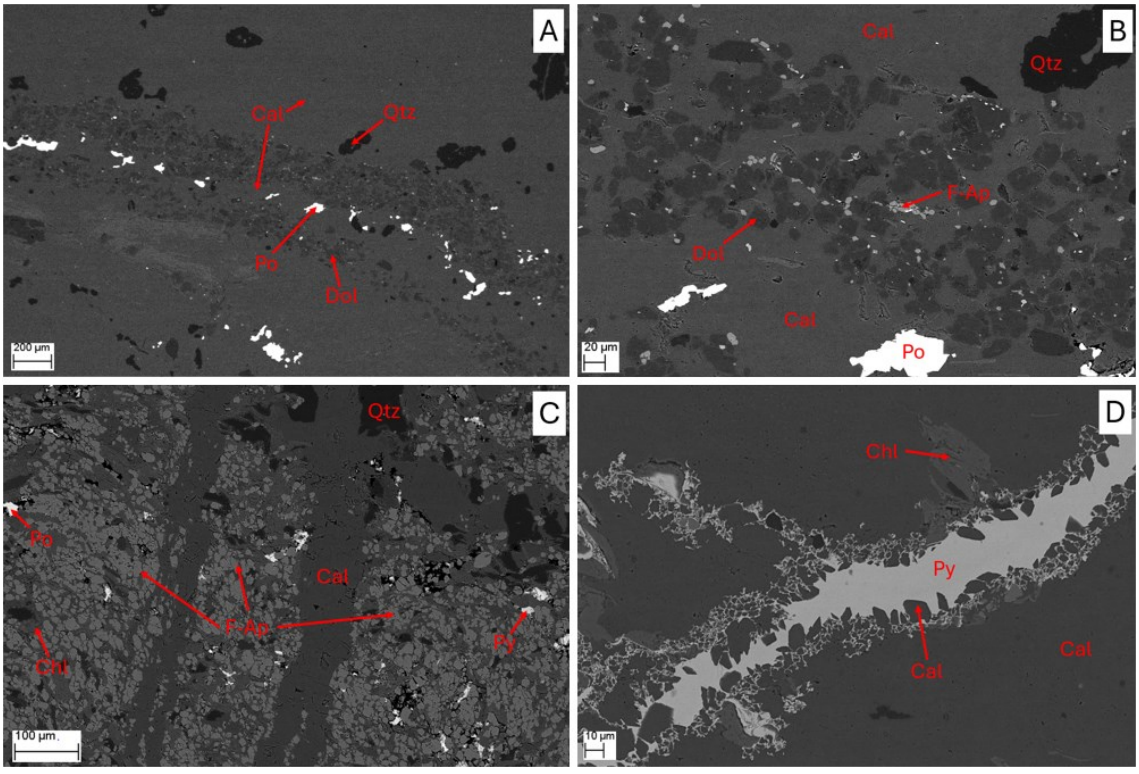

Figure 38: BSE images from the H1 section 2 drill core; A & B: Sulphide bearing calcite vein with a halo of dolomite and fluorapatite in marble, depth 393.3 m (A, B & C) and 393.0 m (D); C: Fluorapatite layer with sulphides dissected by late calcite veins in marble; D: Late pyrite vein with euhedral calcite crystals in marble; Mineral abbreviations: Cal=calcite, Chl=chlorite, Dol=dolomite, F-Ap=fluorapatite, Po=pyrrhotite, Py=pyrite, Qtz=quartz.

3.2.3 G7 section 1 drill core

The section 1 of the G7 drill core contains carbonate phyllite in the footwall and hanging wall of a breccia, which hosts sulphide mineralisation. A total of 17 polished thin sections cover the interval from 48.6 to 62.1 m depth, with 5 from sulphide mineralisation, 4 from breccia, and 2 from carbonate phyllite (1 each from footwall and hanging wall rock). The carbonate phyllite in the footwall is dark grey to bluish in colour and has a deformed and layered texture with darker and brighter, sometimes even brownish thin layers. The most abundant minerals are ankerite as well as phengite and minor quartz. Accessory disseminated phases are framboidal pyrite, zircon, fluorapatite, rutile, monazite and rare dolomite. A discordant thin (<1mm) vein is present having larger crystal sizes compared to the carbonate phyllite itself. The vein consists of mainly calcite and quartz plus little sulphides such as pyrite, sphalerite, galena, chalcopyrite, pentlandite and millerite. Additionally, xenotime was only found within this vein and siderite occurs immediately next to sphalerite and chalcopyrite. Besides, thin late discordant crosscutting calcite veins exist.

The breccia is greyish to brownish in colour and has a chaotic texture. Clasts, matrix and cement are often hardly distinguishable due to a very similar mineralogical composition. The clasts are either carbonate-rich, containing dolomite in the hanging wall of the mineralisation and ankerite in the interlayer between ore horizons, with minor phengite plus little calcite and quartz, or are composed of pure quartz. Additionally, there is accessory disseminated monazite, rutile, zircon, and fluorapatite within clasts. However, these phases tend to be especially abundant in phengite-rich stylolites, which are also sulphide-bearing. The cement phases, which have generally larger crystal sizes compared to clasts, are zoned and consist of an outer ankerite rim in contact to clasts and a quartz core. Additionally, patches of phengite and chlorite rich in fluorapatite, rutile as well as monazite occur. Sulphides are predominantly present in the matrix or late veins; only small framboidal pyrite is also present as layers and disseminated within clasts. Sphalerite is the main sulphide phase in the mineralisation. It forms a rich layer at 58.5 m, is present in the mineralisation as vein-like structures or as infill in between clasts but is also present accessorily in the host breccia and occurs as thin (~200µm) late discordant veins at 58.2 m. Iron sulphides are primarily pyrite, which forms partly euhedral and broken crystals in the breccia and the mineralisation, where it is interspersed in and associated with sphalerite but is also present as late discordant veins in phengite rich matrix at 60.6 m, and represents the dominant sulphide phase in the host breccia, while pyrrhotite is generally rare. Galena is only an accessory phase, has distinct smaller crystal sizes compared to sphalerite in the mineralisation, exists as inclusions in sphalerite as well as pyrite, in which it also forms fracture infills. Chalcopyrite occurs predominantly in the hanging wall host breccia associated with pyrite but is rare in the sulphide mineralisation, where it occurs as inclusions in pyrite. Apart from sulphides, carbonates are major constituents of the mineralisation. Ankerite is frequent, not only in clasts and as cement, but together with quartz also as part of the diffuse sulphide ore-bearing vein structures. Additionally, sometimes it is present as zoned and euhedral crystals, which often show signs of degradation with a skeletal habit and a replacement by quartz (Fig. 39A). Further, siderite is common and closely associated with sulphides (Fig. 39D), but it exists as late discordant veins too. Dolomite is rare. Furthermore, the sulphide mineralisation is characterized by a higher abundance of quartz compared to the host breccia. Feldspar is present as infrequent albite, which occurs with ankerite or within phengite and chlorite rich patches (Fig.39B & C). Apart from these patches and stylolites, monazite and fluorapatite exist as inclusions in the sphalerite rich layer, and rare rutile and xenotime are present. Besides, calcite is exclusively present as late discordant veins.

The carbonate phyllite in the hanging wall of the breccia has a dark grey colour with brownish tones and a layered deformed texture. Quartz, phengite, chlorite plus carbonates such as calcite, ankerite, siderite, and rare dolomite make up a groundmass in which minor fluorapatite and monazite as well as accessory rutile, zircon, and xenotime are disseminated. Sulphides are mainly framboidal pyrites having variable small crystal sizes, which form layers but are also present disseminated and show an association with quartz. Furthermore, larger pyrite with partly attached chalcopyrite occurs as porphyroblasts with pressure shadows containing quartz. Moreover, mobilized larger calcite and quartz with sphalerite and chalcopyrite is present. Besides, late thin discordant calcite veins crosscutting the carbonate phyllite exist.

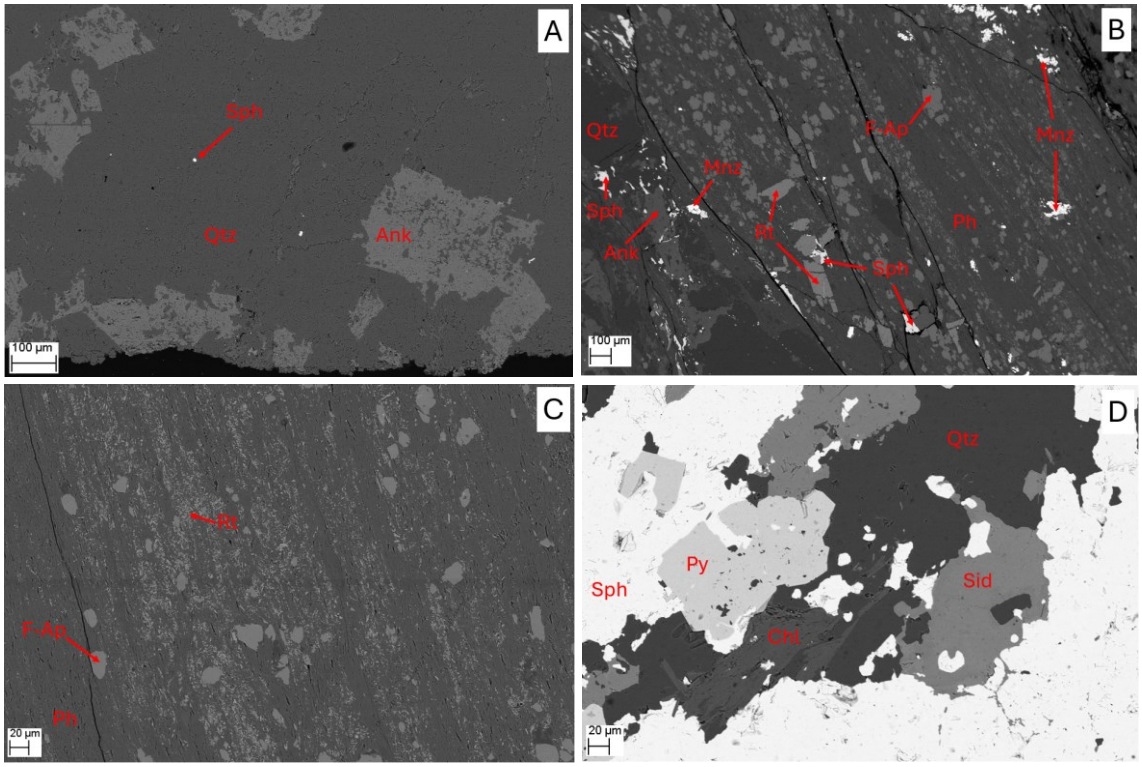

Figure 39: BSE images from the G7 section 1 drill core, depth 58.5 m (A & D) and 60.6 m (B & C); A: Degraded euhedral ankerite crystals in quartz; B & C: Typical mineralogy within the alteration zone; D: Alteration mineralogy at sulphide mineralisation; Mineral abbreviations: Ank=ankerite, Chl=chlorite, F-Ap=fluorapatite, Mnz=monazite, Ph=phengite, Py=pyrite, Qtz=quartz, Rt=rutile, Sid=siderite, Sph=sphalerite.

3.2.4 G7 section 2 drill core

For the section 2 of the G7 drilling only optical microscopy data is available, hence only general descriptions of the lithology are possible, whereas the section comprises 7 polished thin sections from 100.9 to 118.8 m depth, with 1 from sulphide mineralisation, and 3 each from footwall and hanging wall breccia. The section consists of predominately a breccia with a thin (<2 cm) sulphide mineralisation and a carbonate phyllite layer. The breccia has a bright grey to beige and brownish colour and a deformed layered texture. In the footwall of the sulphide mineralisation clasts are mainly carbonate rich or to a lesser extent pure quartz. The matrix is mainly carbonate and minor quartz. White mica occurs as layers in the breccia, whereas small but frequent Ti phases, probably rutile, are bound to these layers. Furthermore, accessory sulphides occur disseminated and as thin

layers as well as part of larger clasts and are mainly pyrite as well as rare sphalerite. Additionally, large euhedral pyrites have pressure shadows containing quartz.

Sulphides in the weakly mineralized sulphide ore horizon are mainly pyrite plus sphalerite and equally abundant chalcopyrite. The mineralisation has larger crystals of carbonate and quartz, which is also more abundant than in barren breccia. Mica is a minor constituent and occurs as layers, which are also rich in Ti phases, probably rutile.

The hanging wall breccia has a bright grey to beige and brownish colour and also a deformed layered texture. It is comparable with the footwall breccia regarding carbonate content and to a lesser extent pure quartz clasts and a matrix of the same mineralogy, albeit partly alternating mm scale mica rich layers and breccia exist. Furthermore, small and abundant Ti phases, probably rutile, are associated with mica. Additionally, pyrite occurs in layers as mainly small crystals.

3.2.5 Unnamed Adit, Kaltenberg-Burgstall

The investigation of the unnamed adit in the Kaltenberg-Burgstall deposit district encompasses 9 polished thin sections (8 from marble, 1 from carbonate phyllite) and 5 polished thick sections from ore horizons. In the unnamed adit two circa 15 cm thick massive sulphide ore horizons with a carbonate phyllite interlayer in a marble host rock occur. The only difference of carbonate phyllite to marble in the footwall and hanging wall of the sulphide mineralisation is a greater abundance of silicates compared to carbonates, whereas the same texture as well as crystal sizes exist. The sulphide mineralisation is Pb dominated, with galena as the major ore phase. Sphalerite is a minor constituent, pyrite as well as pyrrhotite are only accessory, and ullmannite is rare. Cerussite is common and is often present at the boundary between galena and gangue, which encompasses Fe-rich carbonates, such as ankerite and siderite, plus rare dolomite and quartz. Furthermore, phengitic mica and chlorite are frequent in the host rock, and feldspars are present as albite plus little orthoclase, and both are associated with sulphide ore. Titanium phases are mainly larger ilmenite laths containing sphalerite inclusions and accessory small rutile. Weathering products include coronadite, hetaerolite and plumbojarosite,

The marble host rock as well as the carbonate phyllite are bright grey to beige and brownish in colour and show a deformed layered texture. The host rock shows distinct mineralogical variations from the footwall to the hanging wall of the sulphide mineralisation. Carbonates are the most abundant minerals in marble. In the footwall calcite and accessory siderite are almost exclusively present. In the sulphide ore horizons, ankerite becomes the principal carbonate phase and calcite is only an accessory constituent. However, in the hanging wall of the sulphide mineralisation calcite and ankerite are equally abundant. Feldspars have also varying distributions. Albite occurs from the sulphide mineralisation to the hanging wall marble and orthoclase is found in the carbonate phyllite interlayer in between the two ore horizons. Chlorite is only present from the sulphide mineralisation into the hanging wall. Furthermore, the frequency of disseminated monazite increases from the footwall to the interlayer or the hanging wall host rock. Other REE phases are Ce rich fluorocarbonates (Fig.40C), which are present in the interlayer between the two sulphide ore horizons. Extraordinary findings are niobium rich columbite-(Fe) (Fig.40A) and euxenite-(Y) (Fig.40B), which are present disseminated in the carbonate phyllite interlayer and the hanging wall marble. Other HFSE bearing minerals are accessory, large, skeletal, and euhedral rutile or commonly occurring ilmenite and rare tiny zircon. Disseminated fluorapatite is associated with HFSE bearing phases and its frequency increases from being an

accessory constituent in the footwall to a minor component in the hanging wall host rock. Phengitic mica is an abundant phase throughout the marble, but quartz occurs only accessorily. Sulphides exist in small quantities disseminated in both marble and carbonate phyllite and encompass galena, sphalerite, pyrite, chalcopyrite, which occurs only in the host rock but is absent in ore horizons, as well as rare pyrrhotite, gersdorffite, and ullmannite.

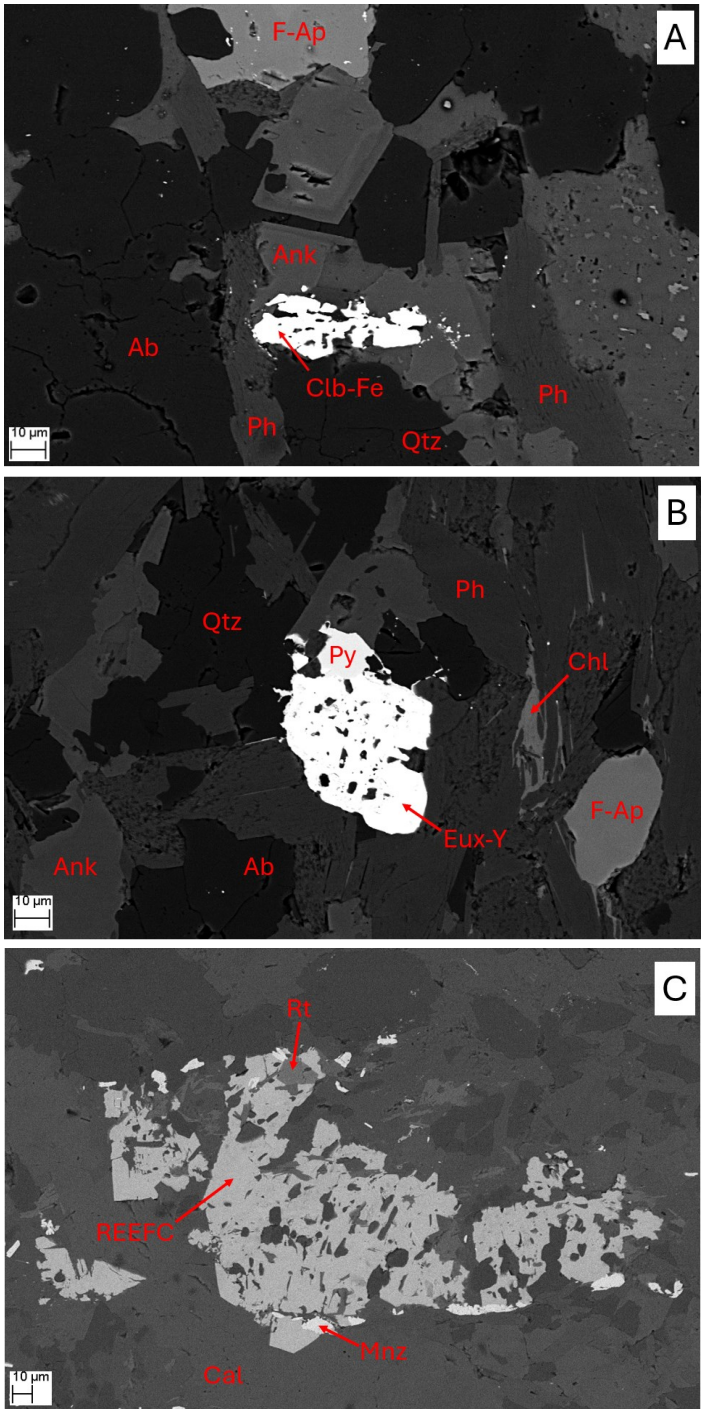

Figure 40: BSE images from the unnamed adit at Kaltenberg-Burgstall district; A: Columbite-(Fe) with typical alteration minerals; B: Euxenite-(Y) with typical alteration mineralogy; C: REE-fluorocarbonates in the alteration zone; Mineral abbreviations: Ab=albite, Ank=ankerite, Cal=calcite, Chl=chlorite, Clb-Fe=columbite-(Fe), Eux-Y=euxenite-(Y), F-Ap=fluorapatite, Mnz=monazite, Ph=phengite, Py=pyrite, Qtz=quartz, REEFC=REE-fluorocarbonate, Rt=rutile.

3.2.6 Unnamed Adit (near Moarbründl creek), Peggau-Taschen

The unnamed adit near the Moarbründl creek at Peggau-Taschen exposes a mineralisation next to the entrance to the mine workings. It is overlain by carbonate phyllite as well as black shale, which is present as interlayer and stratigraphically above carbonate phyllite at the end of the adit (where the roof collapsed, ~230 m from the entrance). Additionally, two faults containing a ca. 5 cm thick graphitic infill occur: one fault (Clar value: 157/30) around 170 m and a second fault (Clar value: 183/78) circa 180 m from the entrance. Samples comprise 8 polished thin sections: 2 from carbonate phyllite (from 0,5 m above the mineralisation and from ~193 m in the adit), and 5 from the mineralisation.

The mineralisation is made up of larger dolomite-rich brecciated clasts. The matrix in between clasts is rich in quartz, sulphides and ankerite (Fig.41B). Occasionally, minor layer-like phengite occurs in the matrix plus associated accessory albite, rutile and fluorapatite. Additionally, predominantly in the quartz-ankerite matrix individual disseminated accessory celsian crystals are present (Fig.41A). The main sulphide phase of the mineralisation is frequent subhedral pyrite. It regularly contains inclusions of galena, which also forms fracture infills, of chalcopyrite, and of barytocalcite as well as witherite (Fig.41E). Sphalerite and pyrrhotite are rare and are exclusively present in pyrite. Galena and minor chalcopyrite (Fig.41C) are not only limited to pyrite inclusions but are common sulphide phases, whereas galena (Fig.10D) shows a stronger association with pyrite than chalcopyrite. Additional rare phases are monazite bordering pyrite (Fig.41F), baryte within the quartz-ankerite matrix as well as cerussite and covellite in fractured pyrite. Towards the hanging wall the mineralisation becomes poorer in sulphides containing minor pyrite plus rare galena and baryte. Associated with pyrite accessory ankerite and albite occur. Larger brecciated clasts as well as matrix consist of calcite and/or quartz. Furthermore, phengite and chlorite are present mainly as patches containing broken limonite (pyrite pseudomorphs) and are rich in layers of accessory monazite, fluorapatite, xenotime and rutile. Moreover, monazite forms thin veins between individual phengite and chlorite crystals.

Optical light microscopy of layered and deformed carbonate phyllite at 0.5 m above the sulphide mineralisation comprises layers of carbonate and/or quartz clasts as well as matrix and of phengite, relatively coarse-grained chlorite, disseminated carbonate clasts and minor interspersed fine-grained quartz and carbonate. Abundant titanium phases, probably rutile, occur in layers associated with sheet silicates. Accessory sulphides are present in the carbonate-quartz matrix and disseminated within mica and chlorite dominated layer, whereas they encompass subhedral larger pyrite and rare chalcopyrite bordering pyrite. Carbonate phyllite ca. 193 m from the entrance to the mine workings is similar in composition but in contrast shows a higher ratio of phengite and chlorite to carbonate and quartz with distinctly smaller grain sizes for all minerals compared to carbonate phyllite 0,5 m above the mineralisation. Sulphides are disseminated and include tiny accessory pyrite, which also forms thin (<0,2mm) discordant late veins, and chalcopyrite. Titanium phases, probably rutile, occur as tiny crystals layer-like between sheet silicates regularly.

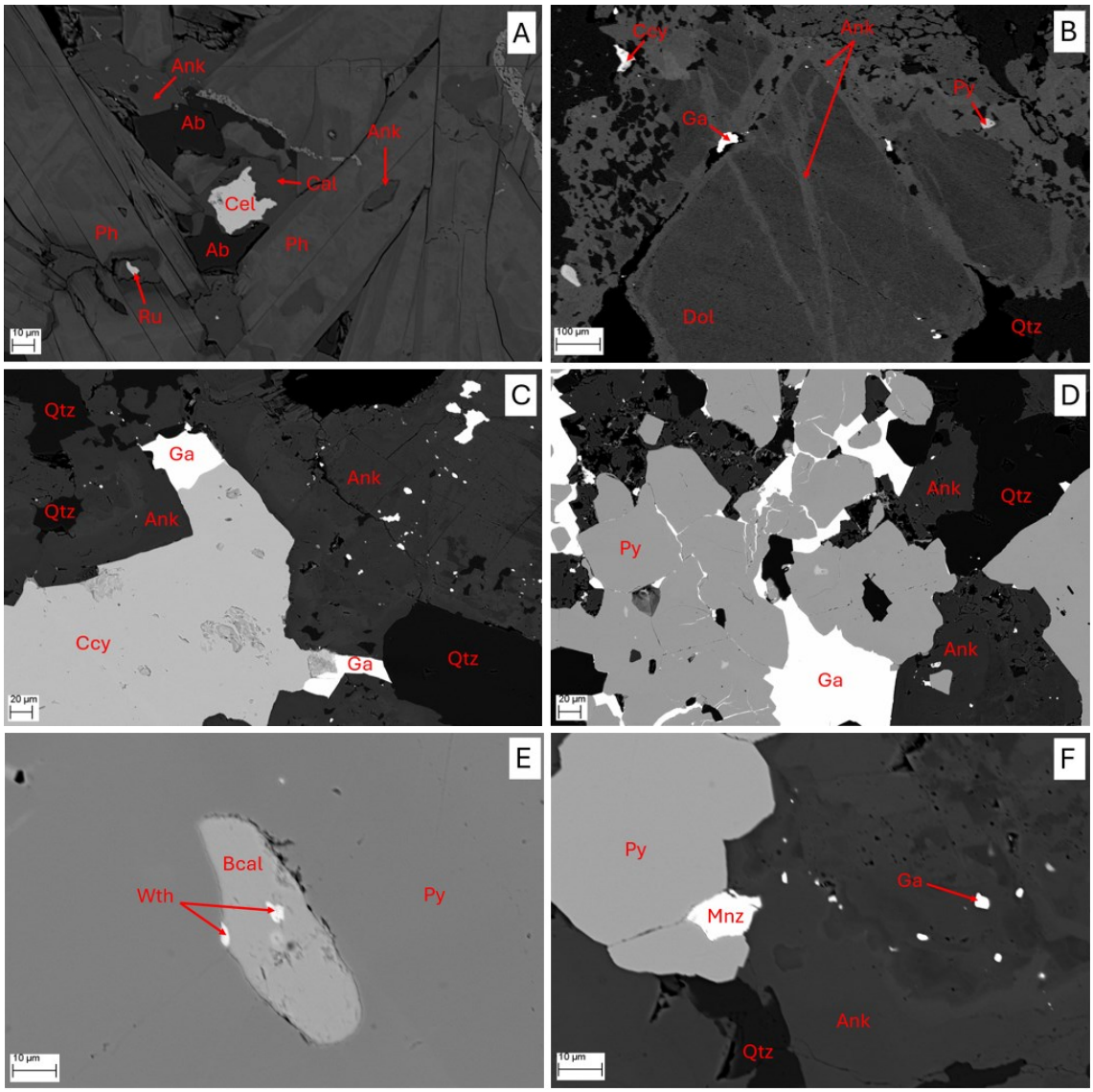

Figure 41: BSE images of the mineralisation in the unnamed adit near Moarbründl creek at Peggau-Taschen; A: Celsian within a layer of phengite in the matrix in between brecciated clasts; B: dolomite clasts surrounded by ankerite with sulphides and quartz within the matrix; C & D: typical sulphide mineral assemblage; E: Barium-rich carbonate inclusions in pyrite; F: Monazite in the sulphide rich ankerite-quartz matrix; Mineral abbreviations: Ab=albite, Ank=ankerite, Bcal=barytocalcite, Ccy=chalcopyrite, Cel=celsian, Dol=dolomite, Ga=galena, Mnz=monazite, Ph=phengite, Py=pyrite, Qtz=quartz, Ru=rutile, Wth=witherite.

3.2.7 Arzwaldgraben

At Arzwaldgraben mine workings are not accessible anymore; hence sampling was performed on dumps. In total four polished thin sections were analysed, one each of baryte and sulphide ore and two of magnetite rich host rock. Optical microscopy was performed on samples of both sulphate and sulphide mineralisation, whereas additional SEM analysis of host rock samples was carried out.

Baryte ore contains predominantly massive baryte with thin mm-scale layers of sulphides, which to a lesser extent are also disseminated in between baryte. Sulphides are mainly galena and sphalerite, which partly has inclusions of chalcopyrite, and subhedral to euhedral pyrite. Sulphides are accompanied by magnetite, which has a xenomorphic decomposed fragmented habit and has partly inclusions of sulphides. Additionally, accessory phengite occurs in very thin layers.

In the sulphide ore sample, sulphides are mainly sphalerite plus minor pyrite. Subhedral magnetite occurs as diffuse layers and within sphalerite in association with pyrite. Quartz is common and chlorite is associated with magnetite. Additional phases are phengite and carbonate.

Host rock samples have a dark green to brownish colour and are rich in subhedral to euhedral magnetite layers, whereas sometimes magnetite exhibits a chromite core. In the first sample sulphides are associated with magnetite, which are mainly pyrite occurring both as layers of crystals overgrowing magnetite and as inclusions in magnetite (Fig.42). This sample consists of quartz, hyalophane, phengite, and chlorite, which is associated with magnetite, plus minor calcite and dolomite. Accessory phases are monazite, ilmenite, rutile and fluorapatite. The second host rock sample has a similar composition with abundant quartz layers, hyalophane, and phengite. Minor carbonates are exclusively siderite. Accessory phases are monazite, rutile, and fluorapatite. Magnetite is accompanied by layers of accessory and disseminated smaller sulphides, such as pyrite, sphalerite, galena being also present as inclusions in pyrite, as well as chalcopyrite. Additionally, baryte is present. In both samples cerussite and coronadite occur as weathering products.

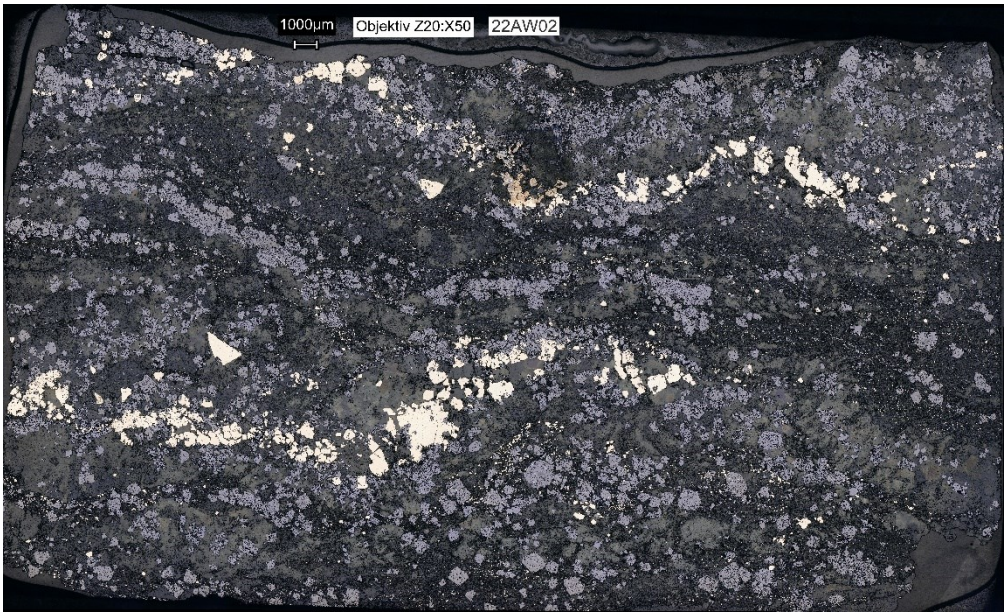

Figure 42: Reflected light microscopical image of the first host rock sample containing magnetite layers with associated pyrite.

3.3 Mineral Chemistry

3.3.1 Carbonates

This mineral group is ubiquitous and encompasses calcite, members of the dolomite-ankerite series, and siderite. Secondary Pb bearing carbonates (cerussite) and Ba rich carbonates from Peggau-Taschen are excluded in this chapter. The distinction between ankerite and dolomite is made by Fe>Mg (atom %) for ankerite and Mg>Fe (atom %) for dolomite.

Calcite has relatively low Mg, Mn, and Fe concentrations compared to other carbonate minerals. Elevated Fe concentrations (1.1 to 2.2 at.%) in calcite occur especially in euhedral calcite crystals, which have very low Mg and Mn concentrations, within late pyrite veins or in those bordering pyrites or late siderite veins. Increasing Fe concentrations are often accompanied by an enhanced incorporation of Mg into calcite. Mn is generally below 0.7 at.% but two measurements at the unnamed edit in the Kaltenberg-Burgstall deposit district give 2.9 at.% and 4.3 at.% Mn, which are both calcites associated with Mn-rich weathering products.

Dolomite occurs at all locations but is especially frequent at H1 drill core sections, at G7 section 1 drill core also as brecciated clast, and in the “ribbon chert” at Arzberg. Compared to the siderite as well as ankerite its median Mn content is distinctly lower.

Ankerite is a common carbonate mineral associated with mineralisation where it is more abundant than dolomite, which is present more frequently in the alteration zone. Manganese and Fe correlate positively in ankerite (Fig.43). Highest Mn concentrations up to 2.9 at.% are found in ankerite in the hanging wall mineralisation at Arzberg and up to 2.0 at.% at Arzwaldgraben. Besides, ankerite of the baryte-rich sulphide mineralisation in the Arzberg mine has detectable Sr concentrations ranging between 0.1 at.% to 0.3 at.% with a median of 0.2 at.% (N = 13).

Siderite has the highest median Mn concentrations (Tab.1). At locations where sulphide mineralisation exists and mining took place, Mn incorporation into siderite is strongest but Mg contents tend to be lower such as at Arzberg (up to 3.3 at.% Mn and 5.5 at.% Mg), Arzwaldgraben (up to 2.9 at.% Mn and 4.6 at.% Mg), and Kaltenberg-Burgstall (up to 2.5 at.% Mn and 5.2 at.% Mg) compared to the drill cores H1 (up to 1.9 at.% and 5.3 at.% Mg) and G7 (up to 1.8 at% Mn and 6.8 at.% Mg).

carbonates	element	siderite	ankerite	dolomite	calcite
range	Mg [apfu]	0.00 - 0.22	0.08 - 0.23	0.18 - 0.39	0.00 - 0.10
	Ca [apfu]	0.00 - 0.21	0.48 - 0.64	0.50 - 0.67	0.81 - 0.99
	Mn [apfu]	0.00 - 0.09	0.00 - 0.10	0.00 - 0.14	0.00 - 0.03
	Fe [apfu]	0.70 - 0.99	0.17 - 0.38	0.10 - 0.25	0.00 - 0.11
median	Mg [apfu]	0.12	0.16	0.27	0.00
	Ca [apfu]	0.02	0.54	0.55	0.97
	Mn [apfu]	0.04	0.02	0.01	0.00
	Fe [apfu]	0.81	0.27	0.17	0.02
number of measurements		124	239	182	393

Table 1: Range and median number of atoms per formula unit (apfu) of Mg, Ca, Mn and Fe in carbonates plus the number of measurements of individual carbonate minerals.

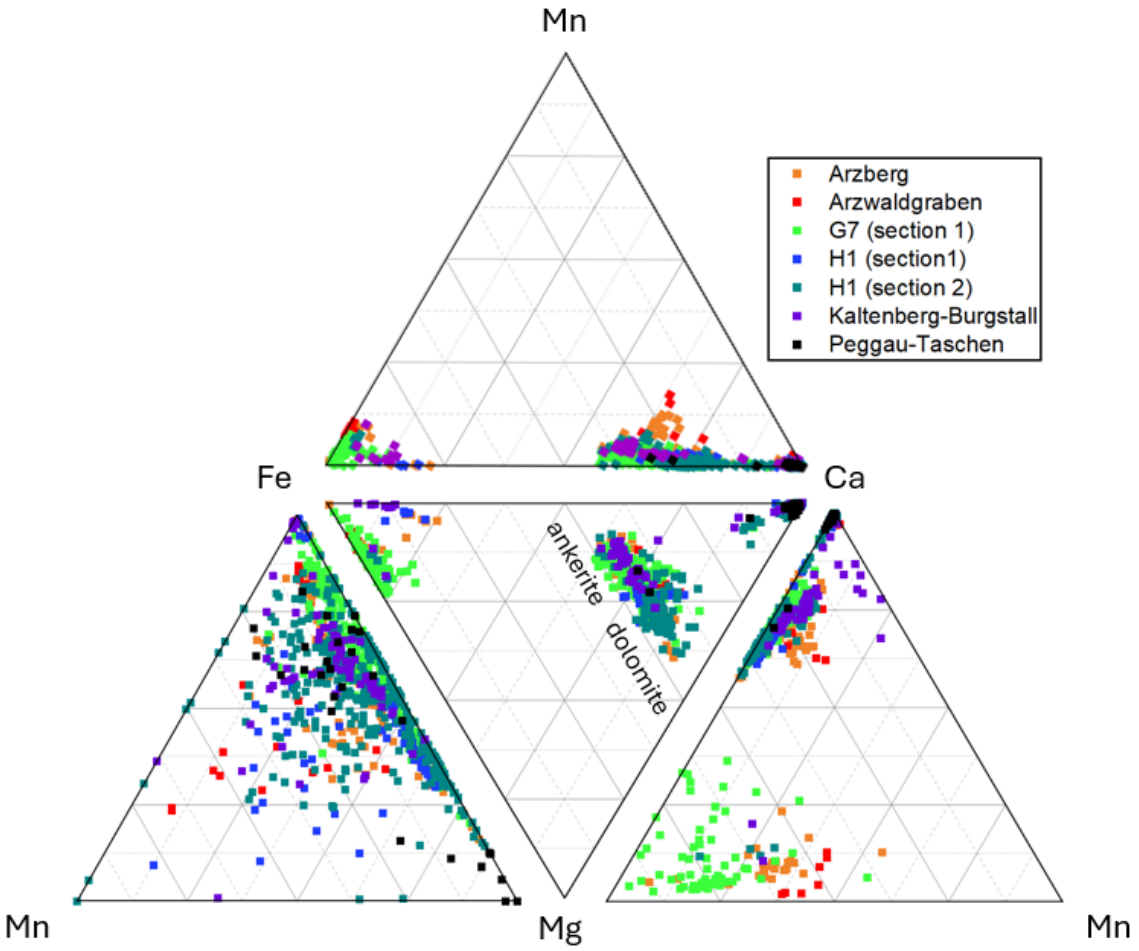

Figure 43: Ternary diagrams showing compositional variations regarding Mg, Ca, Mn and Fe (at.%) in carbonates.

3.3.2 Feldspar

SEM results show that feldspar occurs as albite with negligible Ca and K contents, and as orthoclase. Barium rich varieties are celsian, which is present at the H1 section 2 drill core and at Peggau-Taschen, and hyalophane, which exists in the H1 section 2 drill core and at Arzwaldgraben, whereas it consists of 6.6-14.9 wt.% K_2O and 3.0-11.3 wt.% BaO.

3.3.3 Chlorite

In total 333 chlorite analyses were performed. The maximum FeO concentrations are 44.0 wt.% and the maximum MgO concentrations are 18.7 wt.%. These minerals fall into different subclasses in the classification diagram for chlorites after Hey (1954) (Fig.44). Chlorites in samples of the drill cores from H1 section 1 & 2 are mainly brunsvigite and diabantite or to a lesser extent pycnochlorite and ripidolite, whereas the range of compositions is much greater than of chlorites from the drill core G7 section 1 as well as from localities with Pb/Zn ore occurrences like Arzberg, Kaltenberg-Burgstall, Peggau-Taschen and Arzwaldgraben. Chlorites from the mentioned localities and the drill core G7 section 1 have a trend to slightly lower Si concentrations and are generally richer in Fe as well as lower in Mg than most chlorites of the samples from the H1 drill cores. They are mainly brunsvigite, and daphnite, or in the unclassified field above

brunsvigite, and ripidolite. One chlorite falls into the pseudothuringite field, which is probably an outlier from samples of the H1 section 1 drill core. Chlorites from Arzwaldgraben have slightly higher Mg and lower Fe concentrations than those from other localities with known sulphide mineralisation. However, these chlorite compositions are from a single host rock sample from Arzwaldgraben.

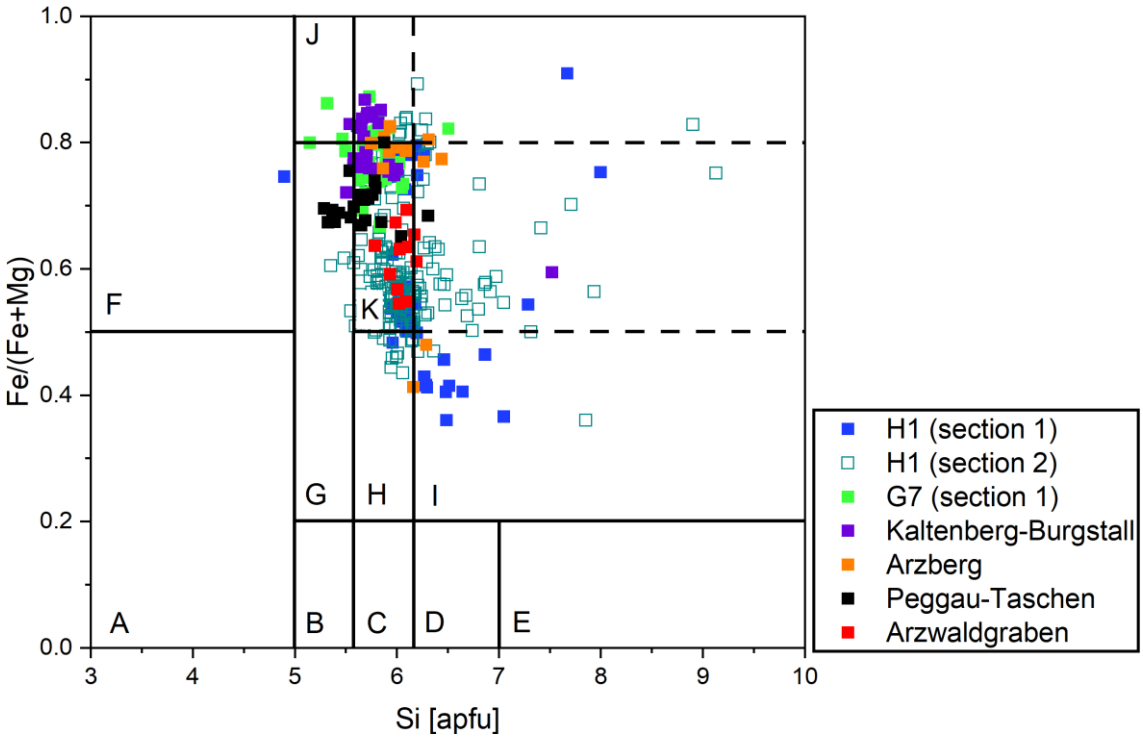

Figure 44: Chlorite classification after Hey (1954) shows compositional variations of analysed chlorite crystals; A=corundophilite, B=sheridanite, C=clinochlore, D=pennine, E=talc-chlorite, F=pseudothuringite, G=ripidolite, H=pycnochlorite, I=diabantite, J=daphnite, K=brunsvigite

3.3.4 White Mica

Data from 538 white mica group minerals show that the bulk of crystals have more than 7 atoms per formula unit (apfu) Si, whereas some are just below 7 apfu Si (Fig.45). According to Deer *et al.* (2013) stoichiometric muscovite has 6 apfu Si and stochiometric phengite 7 apfu Si, whereas there is a continuous spectrum of Si enrichment between both. Consequently, analysed white mica minerals can be categorised as phengite. Furthermore, Fe concentrations are generally higher than Mg concentrations in white mica at Arzberg, Arzwaldgraben, Peggau-Taschen, and Kaltenberg-Burgstall but Fe and Mg concentrations are similar from drill core samples that show lower Fe/(Fe+Mg) ratios. SEM data show detectable Ba contents in white mica at all locations reaching 7.8 wt.% BaO at Peggau-Taschen with a simultaneous depletion of K_2O. Additionally, Na_2O incorporation into white mica is especially present at drill cores from H1 section 1 & 2 as well as G7 section 1 reaching 4.8 wt.% Na_2O, whereas locations with known ore occurrences have lower maximum Na_2O concentrations compared to drill cores of up to 1.5 wt.% at Kaltenberg-Burgstall. At Arzwaldgraben Na_2O incorporation into white mica is generally missing, however once 0.2 wt.% Na_2O was measured.

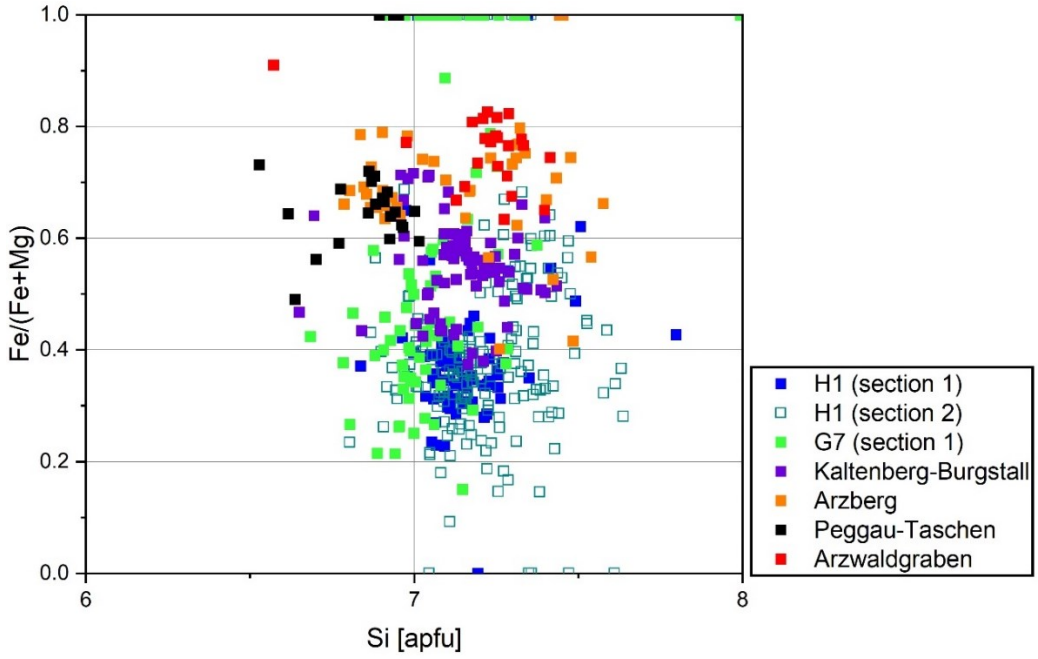

Figure 45: Diagram showing compositional variations of Si and Fe/(Fe+Mg) in white mica and phengite.

3.3.5 REE Phases

Results of microprobe analysis of 43 monazites from Arzberg and 30 from Peggau-Taschen indicate an enrichment of Ce_2O_3 compared to La_2O_3 and Nd_2O_3 (Fig.46). However, monazite from Arzberg has higher Nd_2O_3 than La_2O_3 concentrations, whereas at Peggau-Taschen it is vice versa. SEM analysis supports this observation and shows that the REE composition of monazite from Arzberg seems to be slightly different from other investigated samples such as from Arzwaldgraben, Kaltenberg-Burgstall, Kalkrippe unit as well as from drill cores of H1 section 1 & 2 and G7 section 1, which all have higher La_2O_3 over Nd_2O_3 concentrations. Furthermore, microprobe analysis revealed that ThO_2 concentrations are low and range between 0.2-3.6 wt.% and a median of 1.0 wt.% at Arzberg and between 0.1-4.0 wt.% and a median of 0.9 wt.% at Peggau-Taschen. PbO was not detected in any crystals by microprobe, so that an age determination of monazite by electron microprobe was not possible.

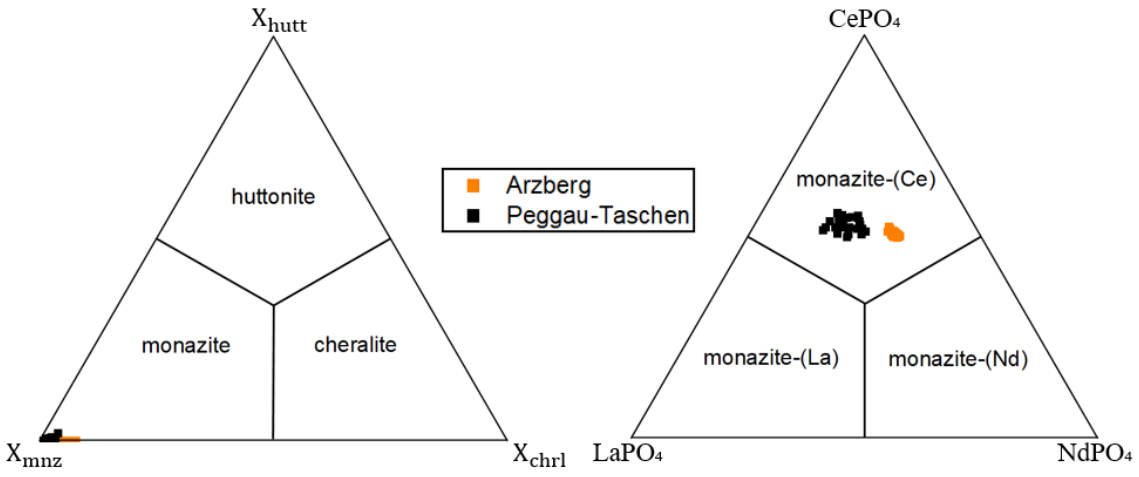

Figure 46: Classification of monazite based on microprobe data after Linthout (2007).

REE-fluorocarbonates are present at Kaltenberg-Burgstall and at the H1 section 2 drill core. They are consistently enriched in Ce_2O_3 and have more La_2O_3 than Nd_2O_3. Rarely low concentrations of up to 2.0 wt.% Y_2O_3 and up to 3.0 wt.% ThO_2 were detected using SEM. A more exact subdivision of REE-fluorocarbonates is not advisable from the available data because of problems to accurately analyse REE phases using the SEM. However, REE-fluorocarbonates are consistently CaO bearing, this could point to parasite or synchysite.

Allanite was observed in samples from both sections of the H1 drilling. It is always Ce_2O_3 bearing, whereas some also contain La_2O_3 and Nd_2O_3.

Xenotime was found at Arzberg as well as in the drill cores H1 section 1 & 2 and G7 section 1. It is rich in Y_2O_3 and contains small amounts of Dy_2O_3 but Gd_2O_3, Yb_2O_3, Er_2O_3, and EuO are not consistent and are only positively detected in some crystals.

3.3.6 HFSE Phases

Titanium bearing minerals occur as TiO_2, ilmenite, and titanite; as a distinction between the TiO_2 polymorphs anatase, brookite, and rutile is not possible using SEM data, TiO_2 minerals are generally referred to as rutile in this thesis.

Rutile is present at locations of sulphide mineralisation and drill cores equally, but at most locations it is Nb bearing. Only at Arzwaldgraben with its different lithological setting of a greenschist host rock this observation does not pertain. In both marble and carbonate phyllite Nb bearing rutile exists. Highest concentrations of 4.7 wt.% Nb_2O_5 were detected in the lower most sample of the H1 section 2 drill core at 423.2 m but apart from ore horizons it is present throughout this section. Elevated concentrations are also found in rutile from the G7 section 1 drill core reaching 3.2 wt.% Nb_2O_5, whereas it occurs in samples from footwall carbonate phyllite, sulphide mineralisation and breccia. Niobium-bearing rutile with up to 2.1 wt.% Nb_2O_5 is common at Kaltenberg-Burgstall but at Arzberg it was only detected in “ribbon chert” with a maximum of 1.0 wt.% Nb_2O_5. Nb-rutile is rare in samples from the H1 section 1 drill core with readings of 0.6 wt.% twice in the sulphide-poor carbonate phyllite at 318.7 m in the hanging wall of the mineralisation and at Peggau-Taschen with a single crystal containing 0.4 wt.% in the sulphide mineralisation.

Ilmenite is less common than rutile but forms generally larger crystals. Apart from the drill core G7 section 1 ilmenite was found at every location and in both H1 drill core sections. SEM data show that ilmenite often contains MnO. Only a single ilmenite crystal with 0.3 wt.% MnO at the sulphide mineralisation at 399.3 m of the H1 section 2 drill core and 1.9 wt.% MnO at the Arzwaldgraben was found. At Arzberg the highest concentrations of up to 2.4 wt.% were detected in ilmenite in the baryte rich mineralisation. At Kaltenberg-Burgstall MnO contents reach 1.1 wt.% and additionally some ilmenite crystals also contain low Nb_2O_5 concentrations up to 0.4 wt.%. The highest MnO concentrations within ilmenite of up to 4.4 wt.% are detected in the footwall of the mineralisation at the H1 section 1 drill core.

Titanite has occasionally low FeO concentrations of up to 2.3 wt.% and is limited to metatuffite and carbonate phyllite in the footwall of the sulphide mineralisation of the H1 section 1 drill core.

Zircon is present at the H1 drill core sample, in the G7 section 1 drill core, at Kaltenberg-Burgstall and within the Kalkrippe unit. HfO_2 concentrations up to 3.4 wt.% were detected.

Microprobe analysis of thorite from the H1 section 2 drill core shows that it contains up to 21.0 wt.% UO_2, and 5.1 wt.% Y_2O_3. PbO reaches a maximum of 0.7 wt.% but was not detected with most thorite crystals meaning that PbO loss occurred, which inhibits age dating using thorite.

Niobium phases are exclusively present at Kaltenberg-Burgstall. Four euxenite-(Y) crystals (general formula $(Y,Ca,Ce,U,Th)(Nb,Ta,Ti)_2O_6$) were analysed containing between 21.2-36.9 wt.% Nb_2O_5, 1.4-3.6 wt.% Ta_2O_5, 10.6-20.8 wt.% Y_2O_3, and 0.2-15.7 wt.% UO_2, plus small amounts of Dy_2O_3, Er_2O_3, and Yb_2O_3. Furthermore, the Y_2O_3 and UO_2 contents correlate negatively with each other meaning that with more Y_2O_3 less UO_2 is incorporated and generally higher concentrations of REE occur. However, only in UO_2 rich euxenite-(Y), Ta_2O_5 was detected, but the presence of SiO_2, CaO, as well as FeO indicates metamictization.

The second niobium mineral is columbite-(Fe) (general formula $(Fe,Mn)(Nb,Ta)_2O_6$). SEM data of 19 crystals shows that columbite-(Fe) is composed of 62.3-76.1 wt.% Nb_2O_5, 0.7-3.8 wt.% Ta_2O_5, 17.2-23.8 wt.% FeO, 0.3-1.5 wt.% MnO, 1.3-7.9 wt.% TiO_2, plus low concentrations of up to 0.9 wt.% Y_2O_3 and ZrO_2 in only few crystals.

3.3.7 Ore and Related Phases

The ore phases are sulphides, which are composed of mainly Pb, Zn, Cu, Ni, Ag, Co, As and S, or rarely tellurides. Ore related phases are iron sulphides and oxides.

SEM analysis of galena gives a mostly homogenous composition. Low Se concentrations of up to 1.9 wt.% in the H1 section 1 drill core and up to 0.9 wt.% in the G7 section 1 drill core were detected.

Compositional data of chalcopyrite gives maxima of 0.5 wt.% Cd in the H1 section 1 drill core and 2.0 wt.% In in the H1 section 2 drill core in the footwall of sulphide mineralisation of both sections. However, these EDX results are not realistic since LA-ICP-MS analysis showed that chalcopyrite from the locations Guggenbach and Arzberg has median In concentrations of 20 ppm (Melcher & Onuk, 2019).

Ag bearing phases are present as sulphide and telluride at the H1 section 2 drill core. These are argentopentlandite with up to 13.0 wt.% Ag and 21.4 wt.% Ni, and hessite containing up to 61.5 wt.% Ag.

Apart from argentopentlandite, Ni bearing sulphides include pentlandite with up to 41.7 wt.% Ni, 30.0 wt.% Fe and 9.2 wt.% Co, occurring in the G7 section 1 and H1 drill cores, as well as millerite with up to 58.2 wt.% Ni and 2.3 wt.% Fe present in the G7 and H1 section 1 drill cores. Furthermore, ullmannite with up to 26.0 wt.% Ni and 57.7 wt.% Sb exists at Kaltenberg-Burgstall and in the H1 section 2 drill core.

Sphalerite has up to 1.8 wt.% Cd in the H1 section 1 drill core, but concentrations are generally low, and most crystals have less than 0.5 wt.% Cd. Fe concentrations in sphalerite show differences between locations: crystals from the G7 section 1 drill core have less than 5.0 wt.% Fe and from Arzwaldgraben less than 2.0 wt.% Fe. A wider range of Fe concentrations is documented in H1 drill cores ranging between 1.6-10.3 wt.% at section 1 and between 0.5-10.6 wt.% in section 2. Relatively higher Fe concentrations are present in sphalerites at Kaltenberg-Burgstall with most values ranging between 1.6-8-9 wt.%, whereas the highest Fe concentrations of all measurements is 11.2 wt.% from a crystal from Kaltenberg-Burgstall. Sphalerites from Arzberg show two populations with different Fe and Cd concentrations. Low values are found in samples from the baryte rich mineralisation and Fe as well as Cd richer sphalerites exist in the

sulphide dominated mineralisation at Arzberg. Furthermore, a single sphalerite crystal from Peggau-Taschen has 2.8 wt.% Fe and from Kalkrippe unit has low Fe and Cd concentrations. Moreover, SEM data do not show a correlation between high Fe and elevated Cd concentrations in sphalerites (Fig.47).

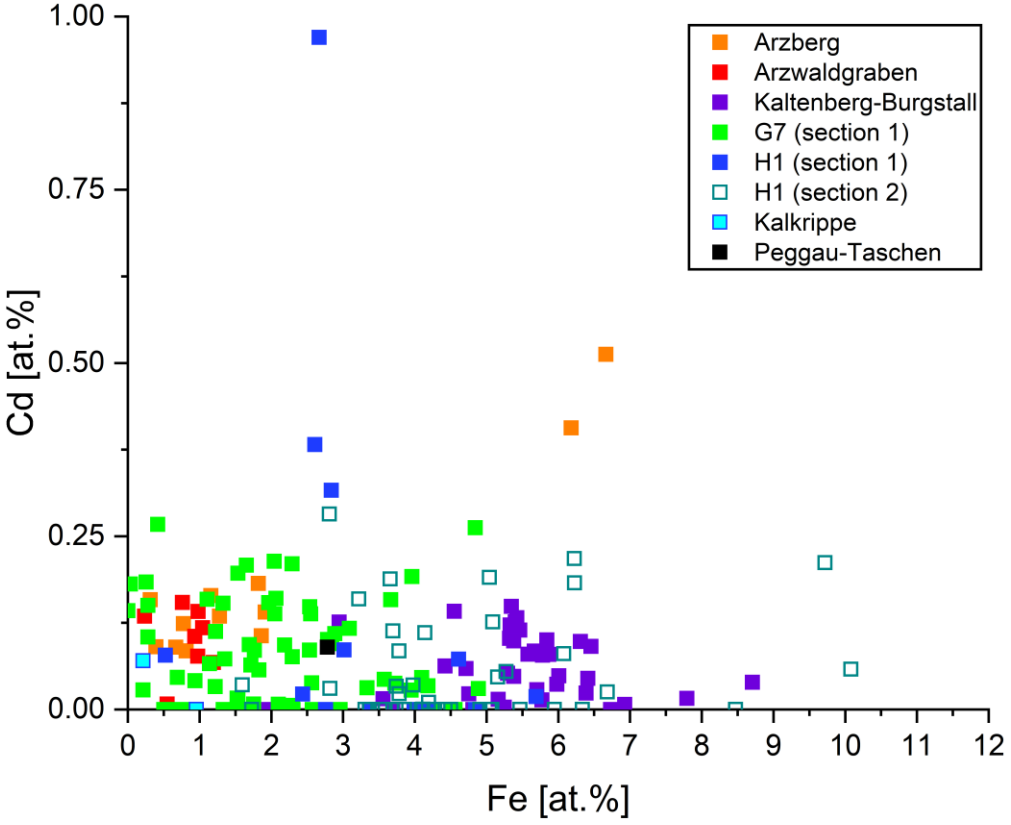

Figure 47: Cd vs. Fe concentrations in sphalerite from SEM analysis.

Pyrite is present at every location as well as drill core section and tends to incorporate more Co than Ni and As, with the maxima at 4.5 wt.% Co, 2.1 wt. Ni and 4.5 wt.% As (Fig.48). However, framboidal pyrite is different regarding Co, Ni and As, since the concentrations of these elements are distinct lower, but Co is still slightly more enriched than Ni and As. Cobalt shows a greater variability with higher concentrations in pyrite from the drill core sections, Arzberg, Arzwaldgraben and Peggau-Taschen. Elevated Ni and As concentrations are detected in pyrite from the G7 section 1 as well as both H1 drill cores, and from Arzberg, Arzwaldgraben plus from the Kalkrippe unit, where the highest As content in pyrite occurs. For most pyrites both Ni and As is below 0.5 wt.%. Compared to other locations with known sulphide mineralisation such as Arzberg and Arzwaldgraben, pyrites from Kaltenberg-Burgstall tend to have lower Co, Ni and As concentrations.

Pyrrhotite has lower Co, Ni and As than pyrite (Fig.48). The highest concentrations are 1.6 wt.% Co, 1.2 wt.% Ni and 1.9 wt.% As. It is present at Arzberg, Kaltenberg-Burgstall and the drill core sections, and has more Co with increasing Fe concentrations especially in samples of the H1 drill cores. Nickel and As concentrations are below 0.5 wt.% in most pyrrhotite crystals. The variability of Ni is generally less pronounced than of Co.

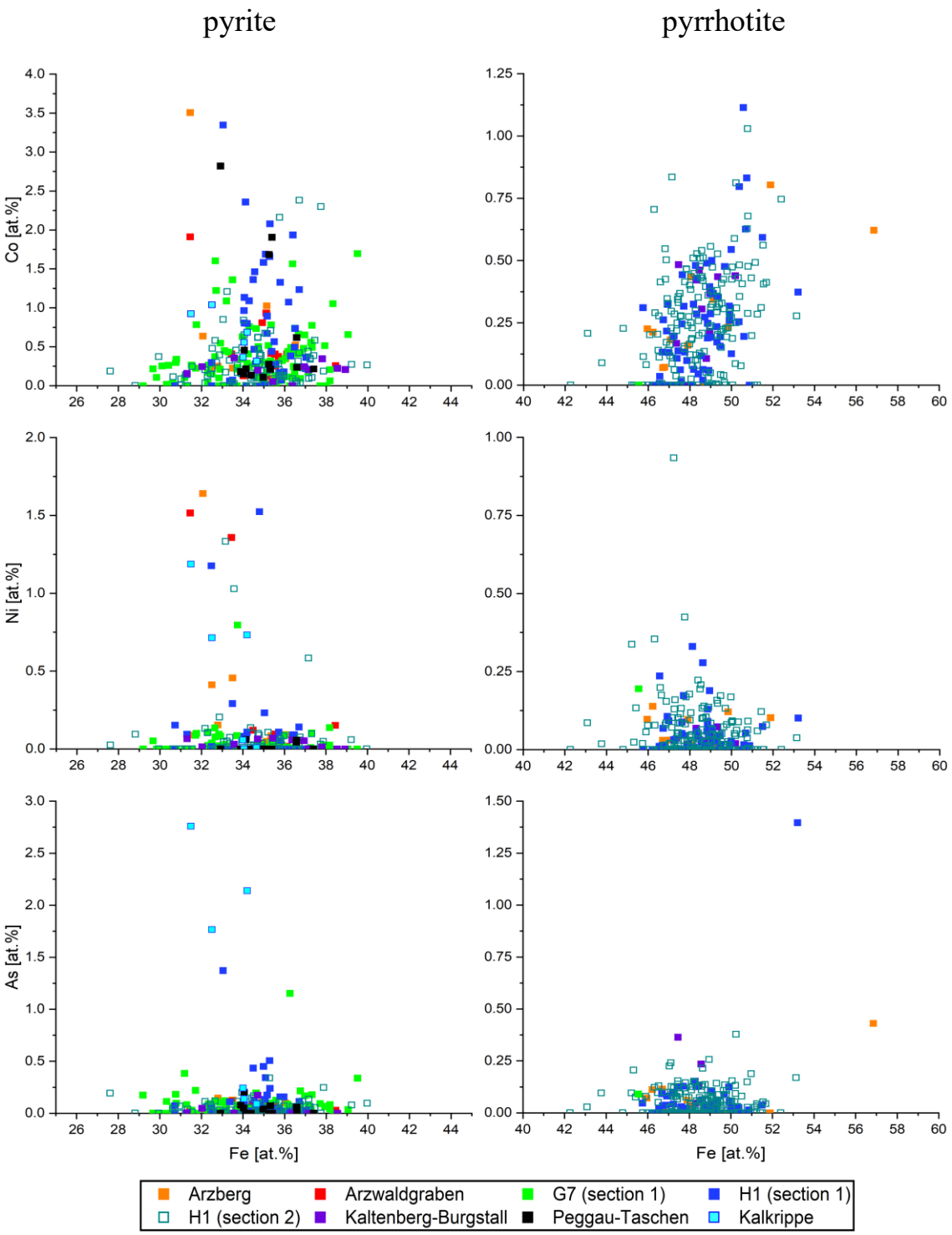

Figure 48: Co, Ni and As concentrations in pyrite and pyrrhotite plotted against Fe based on SEM data.

Another iron rich mineral is magnetite, which is present at Arzwaldgraben and in the baryte rich mineralisation at Arzberg. Besides, chromite with 1.9 wt.% TiO_2, 13.1 wt.% Al_2O_3, 39.8 wt.% Cr_2O_3, 10.2 wt.% MgO and 27.3 wt.% FeO was found as core within a magnetite crystal from Arzwaldgraben.

Arsenopyrite, gersdorffite and cobaltite are varieties of Fe, Ni and Co sulpharsenides that occur at Arzberg, Kaltenberg-Burgstall, in the H1 drill core sections as well as the Kalkrippe unit. These minerals show distinct differences of Fe, Ni and Co incorporation for different locations. In the H1 section 2 drill core these minerals have the widest range of chemical composition followed by crystals of the Kalkrippe unit. For the other locations compositional variations are less pronounced. The content and ratio of these three elements can be used as an indicator for formation temperatures, as Klemm (1965) introduced a ternary diagramm of this solid solution series (Fig.49). Applying this diagramm to the analysed crystals shows that those from the H1 section 2 drill core record the highest temperature values and fall within the temperature field 600-650°C, but also have the widest range as far as below 300°C. Crystals from the Kalkrippe unit reach almost 600°C and stretch to just below 400°C. High temperatures are also recorded for Kaltenberg-Burgstall and are within the 500-600°C field. The H1 section 1 drill core and samples from Arzberg show lower formation temperatures between approximatley 300-480°C. Besides, arsenopyrite from the H1 section 1 & 2 drill cores tend to have lower formation temperatures than cobaltite and gersdorffite. However, the resulting temperatures using the ternary diagramm by Klemm (1965) seem to be too high to represent conditions during deposit formation, and the wide span of temperatures might rather reflect temperature changes during metamorphism.

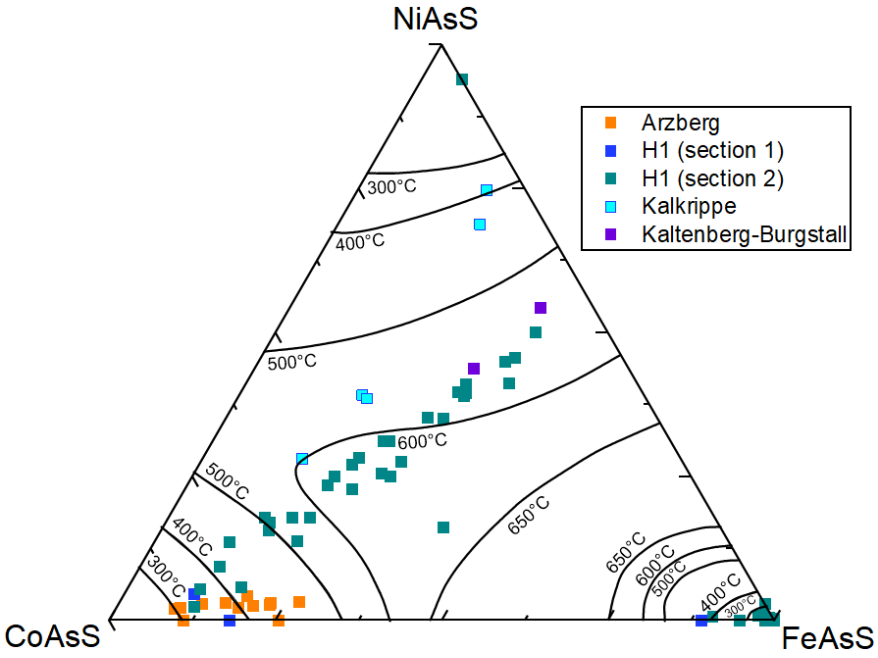

Figure 49: Ternary diagram of the CoAsS-NiAsS-FeAsS system for determining formation temperatures of sulpharsenides after Klemm (1965).

4 Discussion

In metasediments of the Schönberg Formation as part of the Schöckl nappe, hosting stratiform SEDEX-type Pb-Zn-Ag-Ba deposits, carbonates are very abundant. In and close to sulphide mineralisation, calcite as well as Fe and Mg rich carbonate varieties coexist. In order to distinguish between carbonates from background sedimentation and those related to deposit formation, the Kalkrippe marble unit can be used as a proxy for sedimentary input into the basin since it is calcite dominated as well as partly fossiliferous and so clearly part of the stratigraphic sequence, although it acts as an important marker unit for sulphide mineralisation in the western part of the deposit district, and sometimes hosts stratiform ore horizons (Weber, 1990). In the unmineralized part topographically uphill from the Silberberg adit the marble contains sporadic small sphalerite, galena, cobaltite, and pyrite crystals. The calcite in the Kalkrippe marble is poor in Mg, Mn, as well as Fe (<1.0 at.%). Rare dolomite is present containing 4.5 at.% Fe and 6.2 at.% Mg. If the carbonate composition of the Kalkrippe marble is compared to those of the section 1 from H1 and G7 drill cores, it becomes apparent that there is a distinct increase in Fe, Mg and Mn in carbonates forming a halo around sulphide mineralisation with the highest concentrations closest to ore and hence differing greatly from background sedimentation (Fig.50). Further, calcite contents decrease in the halo and are often only present within late veins, becoming surpassed by Fe rich ankerite and minor siderite or Fe-dolomite. Moreover, trends in chemical composition occur within individual carbonate mineral groups. Generally, dolomite is present in the more distal positions to the sulphide mineralisation compared to ankerite tending to be associated more closely with ore horizons and occurring in greater abundance in the inner alteration zone, whereas Mn incorporation is stronger in ankerite and increases approaching mineralised strata. Additionally, Fe concentrations in ankerite tend to be more elevated in sulphide ore. Similar trends are also recorded for siderite, which often occurs in close proximity to or within ore horizons. Its Mg and Mn concentrations show similar patterns as in dolomite-ankerite series carbonates with a depletion of Mg and an enrichment of Mn near mineralisation. If the ore horizons in the drill cores are considered to represent distal hydrothermal products (Lydon, 1995) due to their weak mineralisation, and locations with stratiform sulphide ore bodies like Arzberg, Arzwaldgraben or Kaltenberg-Burgstall are proximal to the feeder faults, then siderite shows a compositional zonation from a stronger Mn incorporation in the inner parts of the deposits and higher Mg contents in the periphery. Moreover, dolomite-ankerite series carbonates replicate this trend with ankerite being more common proximal to feeder systems than dolomite, which has a greater frequency distally. The increase of ankerite and siderite towards mineralized strata is also in alignment with geochemical data of drill core sections, which show a depletion of CaO as well as MgO near mineralisation and a concurrent MnO enrichment that can be attributed to carbonates. Besides, it should be noted that CaO+MgO concentrations of whole rock geochemical data is not sufficient to distinguish between marble and other lithologies alone since Fe-rich carbonates near ore horizons obscure high carbonate content derived from whole rock geochemistry.

In the context of stratiform SEDEX base metal deposits globally these findings fit well into observed alteration mineralogy since ferrous and manganiferous carbonates are a common feature of host rock alteration such as at the Lady Loretta and McArthur (HYC) deposits in Australia. Observations in the Graz Paleozoic are similar to Lady Loretta with an inner Mn rich siderite halo to an intermediate ankerite/ ferrous dolomite zone and dolomite at the outer rim of the alteration

zone with systematic changes from a CaO and MgO abundance to high MnO concentrations approaching the Pb/Zn ore body (Large & McGoldrick, 1998; Large *et al.*, 2000; Large *et al.*, 2004).

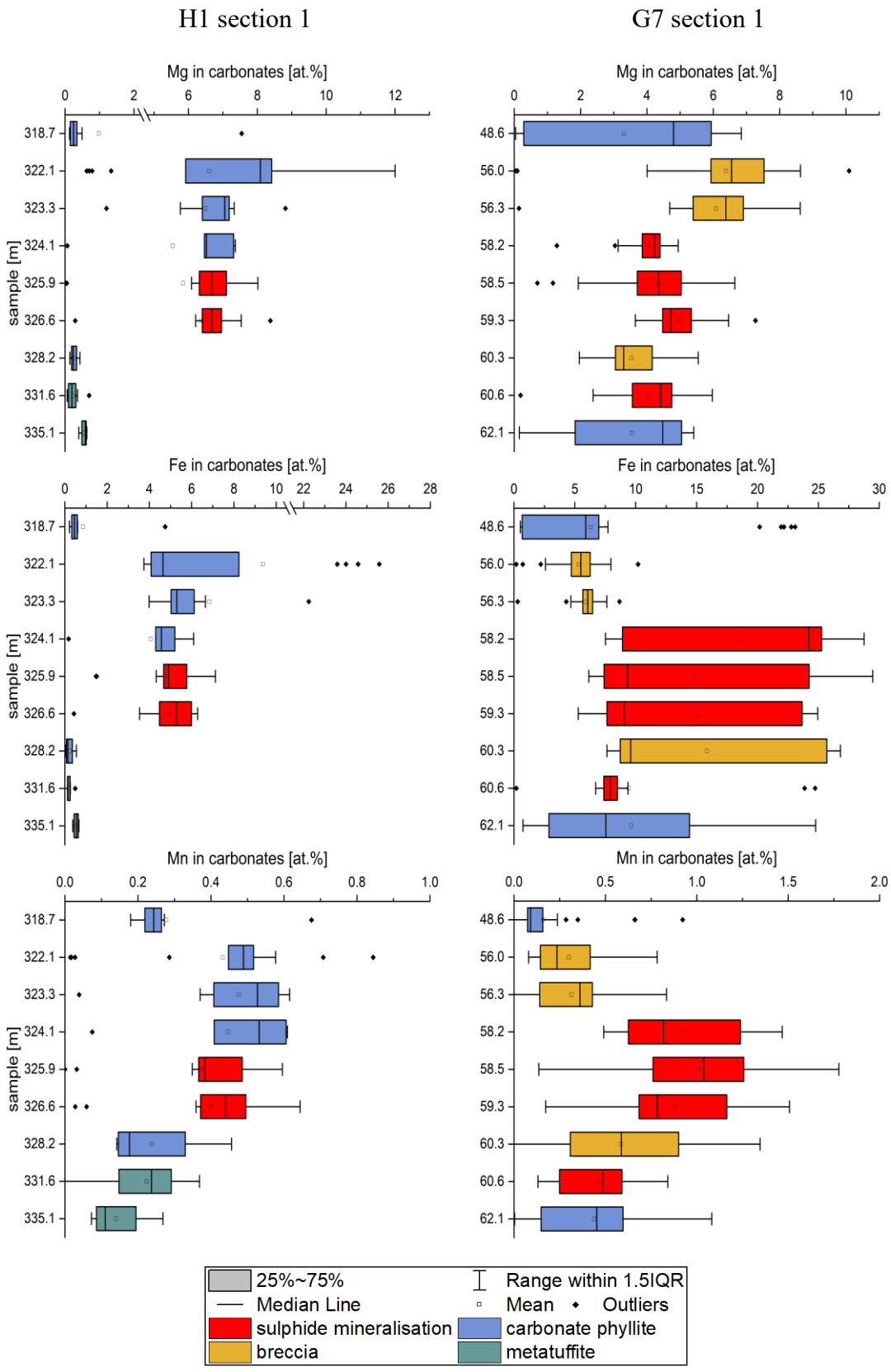

Figure 50: Fe, Mg and Mn variations in carbonates along the H1 section 1 and G7 section 1 drill cores.

Frequency estimations based on observations from SEM analysis show an abundance of albite with an association to sulphide mineralisation (Fig.51). The frequency distribution of albite in both sections of the H1 drill core exhibits medium to high contents in the footwall of ore horizons, whereas the frequency does not seem to be affected by lithological changes. In the H1 section 1 drill core albite occurs additionally in the hanging wall of the Pb/Zn horizon but below an Fe sulphide-rich layer at 315.6 m at the top of the profile. This iron sulphide-rich strata could represent a separate hydrothermal event additional to the main mineralisation of this drill core section, which caused albitization in the sediment below. This interpretation is supported by geochemical data showing Pb, As, Ba and MnO enrichment. Another indicator for this hypothesis is the decrease of albite content in the sulphide mineralisation and the immediate hanging wall meaning that the upper albite rich zone is not connected to the ore forming event itself. The comparison of the frequency estimation of albite and the Na_2O concentrations of the whole rock geochemistry highlights that the estimation correlates well with geochemistry and thus Na_2O can be used as a proxy for this alteration style. Besides, the paragonite component in white mica increases in zones of albite alteration. Albitization occurs also in the hanging wall at the Sullivan deposit in Canada, but there it formed as a result of fluid upflow in a convective cell due to gabbro dyke emblacement in unconsolidated sediments in the footwall of the ore body (Lydon, 2004a). At the Abra SEDEX deposit in Western Australia albitization is a common feature of the alteration zone proximal to mineralisation and is interpreted to be an early-stage alteration as well as distal in unconformably overlaying sediments as quartz-albite veins due to a protacted post-ore hydrothermal activity (Lampinen *et al.*, 2019; Pirajno *et al.*, 2016; Vogt & Stumpfl, 1987; Zi *et al.*, 2015). In the Graz Paleozoic albite alteration seems to be similar to the Abra deposit but different to the Sullivan deposit since it is likely related to the ore forming hydrothermal activity due to its close association with sulphide mineralisation and because it seems to be bound especially to the footwall of ore horizons indicating fluid flow in possibly unconsolidated sediments. However, albitization is not reported from many other Australian SEDEX deposits in the Mount Isa Inlier (Large *et al.*, 2004).

Potassium feldspar (orthoclase) is closely associated with sulphide mineralisation and can be considered as gangue phase since it occurs within thin sulphide-carbonate-quartz bearing veinlets associated with the sulphide in the H1 section 1 drill core and is present with Ba rich feldspars in the ore horizon in the H1 section 2 drill core. At Kaltenberg-Burgstall orthoclase is present in or in close proximity to sulphide mineralisation in small quantities.

The Ba feldspar varieties such as celsian and hyalophane occur in magnetite-rich host rocks at Arzwaldgraben, as thin layers in the sulphide mineralisation of the H1 section 2 drill core, and as disseminated individual crystals in the mineralisation at Peggau-Taschen. These feldspars are the first finds of this kind related to sulphide mineralisation in the Graz Paleozoic. However, they have been described from the Zamora SEDEX baryte deposit in Spain (Moro *et al.*, 2001) or the Jason deposit in Canada (Gardner & Hutcheon, 1985). At both locations celsian seems to have formed during diagenesis or metamorphism as an authigenic (idiomorphic) phase in chert and argillite as well as in beds of laminated sulphides and baryte, which could represent precipitates from an original Ba-Al-Si gel at the seafloor during diagenesis, and as a replacement of baryte indicated by spherical and relictic baryte inclusions in Ba feldspars (Gardner & Hutcheon, 1985; Moro *et al.*, 2001). For Ba feldspars in the Graz Paleozoic no evidence was found to support similar formation processes since no relictic baryte inclusions are present in celsian or hyalophane and the existence of Ba feldspars is not known from baryte rich layers. The only possible indicator

for baryte transformation to celsian could be tabular celsian crystals in the upper sulphide mineralisation at the H1section 2 drill core which based on their habit could reflect initial baryte crystals, therefore celsian could be pseudomorphs after baryte (Fig.36B).

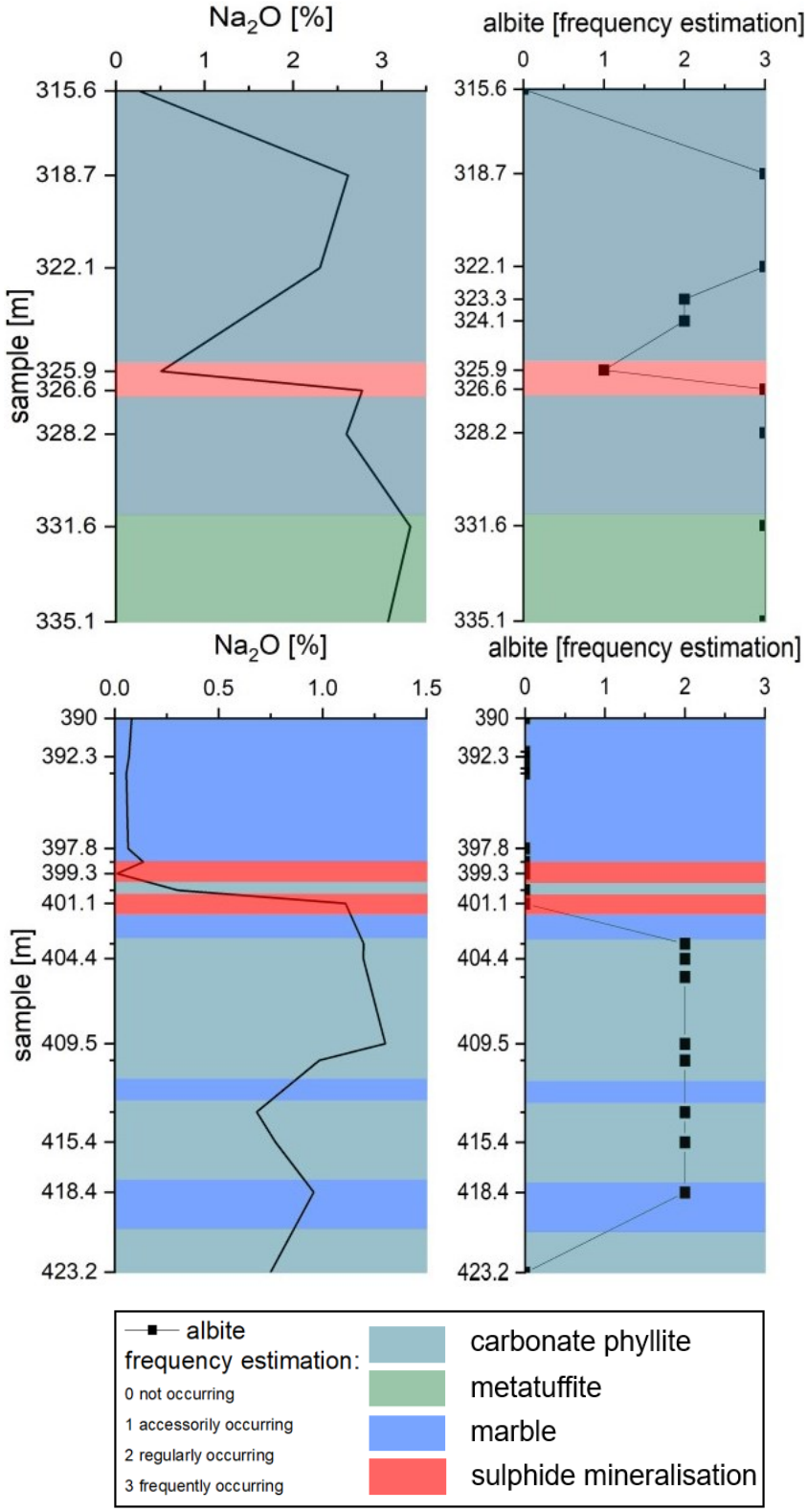

Figure 51: Comparison of Na_2O concentrations from whole rock geochemical data with frequency estimations of albite along H1 section 1 & 2 drill cores.

Whole rock geochemical data of Ba shows enrichments in the drill core sections, which cannot be attributed to Ba feldspars or baryte but rather caused by BaO incorporation into white mica reaching a maximum of 3.2 wt.% in the drill core of G7 section 1 (Fig.52), and 4.3 wt.% BaO at Kaltenberg-Burgstall. Higher BaO concentrations in white mica from 4.1 wt.% to 7.5 wt.% are found in baryte dominated mineralisation (e.g. at Arzberg, Arzwaldgraben or at the Ba feldspar layer in the H1 section 2 drill core). The maximum detected BaO concentration in white mica is 7.8 wt.% in the sulphide mineralisation at Peggau-Taschen. Furthermore, from the drill core sections it becomes clear that there is an association between BaO incorporation in white mica and sulphide mineralisation as well as a trend to higher BaO concentrations approaching ore horizons. Moreover, white mica shows compositional variations of MgO and FeO within the alteration halo. MgO increases in the outer alteration halo to 3.4 wt.% but shows a relative decrease of concentrations within alteration halos of sulphide mineralisation and a simultaneous increase of FeO of up to 14.6 wt.% at Arzberg, whereas drill core samples representing a more distal position to the centre of hydrothermal fluid expulsion tend to have lower MgO and especially FeO enrichments than for example those from Arzberg or Arzwaldgraben in proximity to the vent complex. Barium bearing muscovite with up to 10.3 wt.% BaO is also reported from the Dalradian Supergroup in Scotland occurring in a lateral extension of the SEDEX Ba-Zn deposits at Aberfeldy (Coats *et al.*, 1984). A similar situation could exist in the Graz Paleozoic with Ba-phengite and Ba-bearing stilpnomelane occurrences at ore deposits (e.g. Arzberg; Feichter, 2005) and in the periphery represented by drill core sulphide mineralisation. However, the question if Ba bearing white mica extends beyond ore horizons in the Graz Paleozoic like in the Dalradian Supergroup cannot be answered based on data presented in this thesis.

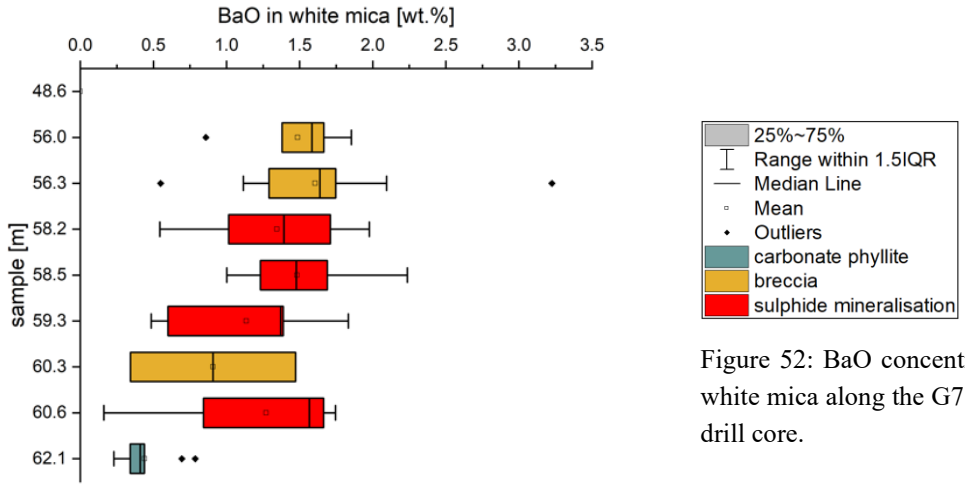

Figure 52: BaO concentrations in white mica along the G7 section 1 drill core.

Like white mica, chlorite has a similar zonation of MgO and FeO concentrations. Chlorite becomes enriched in FeO with increasing proximity to sulphide mineralisation and reaches a maximum of 44.0 wt.% FeO in sulphide ore, whereas concurrently MgO in chlorite decreases approaching ore horizons with concentrations ranging approximately between 8.0 wt.% and a minimum of 2.2 wt.% MgO at sulphide mineralisation. Chlorite in greater distances from ore horizons or in metatuffite in the footwall of the H1 section 1 drill core tends to contain below 35.0 wt.% FeO and from 9 to 18.4 wt.% MgO. Very similar zoning of FeO and MgO concentrations in chlorite was observed at the Rammelsberg deposit in Germany, where FeO concentrations in chlorite from ore horizons ranges between 37-46 wt.% and 2-7 wt.% MgO, in contrast to metasedimentary country rocks with 26-36 wt.% FeO and 9-19 wt.% MgO (Sperling & Walcher, 1990).

Various HFSE (Ti, Zr, Nb, Ta, Th and U) and REE rich minerals are associated with sulphide mineralisation. REE rich minerals, especially monazite, correlate well with whole rock geochemical Ce concentrations. This is exemplified by the H1 section 1 drill core where in the footwall of the sulphide mineralisation allanite occurs rarely, and Ce concentrations are low but with the onset of monazite at the ore horizon continuing to the hanging wall rocks of the section Ce concentrations increase distinctly. Furthermore, aggregates (pseudomorphs) contain calcite, chlorite, monazite, REE-fluorocarbonates, thorite, partly fluorapatite and pyrrhotite as well as galena, rarely allanite and in the zone of albitization in the H1 section 2 drill core sometimes also albite. Their deformed elongated and partly fragmented shape indicates a pre-deformational origin and their patchy looks with cluster of monazites and thorites seems to be the result of the in-situ decomposition of a larger earlier REE bearing mineral. The precursor phases were probably REE-silicates like allanite or epidote since calcite as the most abundant mineral in the aggregates indicates a high Ca content of the original mineral. In contrast to REE-silicates, the decomposition of monazite produces higher proportions of phosphates such as apatite, and often allanite (Schulz, 2021). HFSE phases are dominated by Ti minerals and whole rock geochemistry shows a trend to elevated HFSE concentrations at sulphide horizons. Furthermore, the type of Ti phases tends to be linked to the mineralogy of the host rock since ilmenite and titanite are present in calcite rich metapelite whereas rutile is often found in ankerite bearing rocks. The amount of Ti phases in the metasediment can be derived from Ti concentrations but the type of mineral (e.g. rutile or ilmenite) cannot be distinguished using whole rock geochemistry. The Ti and Nb concentrations partly correlate, indicating that Ti phases are also an important Nb carrier in these samples. Since there are no discrete Nb minerals present, Nb bearing rutile was often observed. Additionally, it is noteworthy that at Kaltenberg-Burgstall, grain sizes of abundant Nb bearing minerals as well as REE-fluorocarbonates are larger compared to other locations. Here, the highest whole rock geochemical concentrations of Nb (228 ppm), Ta (19 ppm), Ce (275 ppm), La (148 ppm), Nd (99 ppm), Th (20 ppm) and Zr (915 ppm) were measured. The Zr content is at least 2-3 times higher than Zr readings from other investigated sulphide mineralisations. The data indicate that HFSE and REE correlate and possibly have a common origin. Titanium concentrations are higher at locations especially where tuffogenous imprint on metasediments or metatuffite exists. Furthermore, the observed boundary of the albitization front in the H1 section 2 drill core showed that HFSE and REE minerals are more abundant in the alteration zone hinting to a relation between host rock alteration and both HFSE and REE phases. Airborne geophysical mapping in the Graz Paleozoic as well as underground geophysical measurements at the abandoned Arzberg mine showed γ-radiation anomalies of Th and U (as well as K) at Pb-Zn ore occurrences (Seiberl & Pistotnik, 1994; Römer *et al.*, 2006). These positive γ-radiation anomalies most probably originate from discrete Th and U minerals such as thorite as well as from the incorporation of radioactive elements into the lattice of REE and HFSE phases highlighting the spatial association of REE and HFSE minerals with mineralisation.

However, the question arises how these minerals formed since HFSE and REE enrichments are generally not widespread in SEDEX systems. There are two principal processes for HFSE and REE transport that are more likely to have been involved. Firstly, the initial hydrothermal activity forming the SEDEX mineralisation and secondly fluid infiltration during metamorphism are discussed. In any case the fluid must have had special properties in order to dissolve incompatible elements since these are considered to be immobile in most geologic settings. Most probably fluoride was involved to facilitate transport of HFSE and REE since these elements form strong complexes with fluoride (Migdisov & Williams-Jones, 2014; Wood, 2005). However, high total

fluoride concentrations in fluids do not necessarily enable REE and HFSE transport due to other elements (e.g. hydrogen) competing for fluoride. This decreases the free-fluoride activity and limits metal transport via fluoride complexes. Additionally, chloride is very relevant for REE transport as well but forms only very weak complexes with HFSE at room temperature (Migdisov & Williams-Jones, 2014; Wood, 2005). Anyhow, thin monazite veins indicate REE mobility at a certain point in time. For the sake of completeness, it must be mentioned that there is a third possibility to explain incompatible and REE bearing minerals in metapelites, namely terrigenous sedimentary input from an unknown Early Paleozoic basement. This would mean that these minerals reflect detritus of felsic plutonites since columbite group minerals are associated with evolved pegmatites from highly fractionated (granitic) melts (Cerny & Ercit, 2005). However, this option is discarded here because if it were detrital material from pegmatites a greater variety of HFSE minerals such as Nb and Ta phases plus cassiterite, tourmaline, and garnet as well as a greater spatial distribution of minerals with incompatible elements in the metasediments could be expected (Cerny *et al.*, 2012). For this reason, only the two plausible processes are discussed below:

- Hydrothermal fluids in SEDEX systems are saline residual brines from evaporated seawater rich in chloride (Emsbo, 2009). A fluoride component in the metalliferous fluid may trigger precipitation of HFSE and REE minerals at sulphide ore horizons in the Graz Paleozoic. However, fluoride would need to have come from an external source since it is not commonly found in the primary brine from seawater evaporation. Either brines penetrated deep into the basement where they came in contact with magmatic volatiles, or fluorine was leached from sediments, such as observed in coastal areas (Jia *et al.*, 2022). Limited volcanic activity in the depositional area is indicated by tuffogenic material. However, in both options fluoride intake is limited by the Ca concentration in the brine since the reaction of F with Ca precipitates fluorite. Compositional data of fluids enclosed in baryte from Arzwaldgraben show that hydrothermal fluids contained Ca (Tufar, 1978); however, Ca would decrease the free-fluoride activity considerably making metal transport with fluoride complexes only possible if fluoride is in excess to Ca. Hence, in most cases Ca and F cannot be transported simultaneously due to the formation of solid fluorite (Wood, 2005). Fluorite would also form if Ca-rich and fluoride bearing fluids mix or if fluoride-rich fluids interact with carbonate rich lithologies buffering the solution which would consequently lead to a precipitation of solid phases containing incompatible elements, whereas the reaction of fluoride bearing brines with phosphates like apatite from the sediment would have the same effect (Migdisov & Williams-Jones, 2014; Wood, 2005). However, fluorite was not found as evidence for the presence of fluoride in the hydrothermal fluid. The only indication that fluoride was present is F bearing minerals such as fluorapatite. If no fluoride was involved in the transport of incompatible elements, then the possibility of chloride complexes as carriers of HFSE cannot be ruled out completely since their stability increases with temperature, but it would need very high concentrations of these ligands and very low pH conditions (Wood, 2005). Moreover, if REE and HFSE deposition like REE-fluorocarbonate is a primary feature of hydrothermal activity then this would mean that relics of decomposed REE-silicates present as aggregates (pseudomorphs) containing REE-fluorocarbonates were decomposed possibly during alteration of the host sediment, whereas this could be signified by the existence of sulphides, such as galena or pyrrhotite, and albite in some of them. Furthermore, microprobe analysis of monazite in absence of pseudomorphs shows a median of 1.0 wt.% ThO_2 typical for monazite derived from hydrothermal fluids pointing to syn-mineralisation REE transport (Schandl & Gorton, 2004).

- The polymetamorphic history of the Schöckl nappe implies that the primary mineral composition of ore and host rocks is heavily influenced by metamorphic events (Hollinetz *et al.*, 2024). HFSE and REE mobilization and transport in metamorphic fluids was already observed at other locations such as the contact aureoles of the Bergell and Adamello intrusions (Italy), whereas fluoride acted as complexing ligand (Gieré, 1990). The main metamorphic overprint in the Schöckl nappe is related to the metamorphic HT/LP Permian event (Hollinetz *et al.*, 2024). Anatexis due to crustal thinning and the subsequent formation and emplacement of granitic and pegmatitic intrusions during the Permian in the Koralpe-Wölz nappe system underlaying the Graz Paleozoic could represent a source of fluoride in metamorphic fluids (Knoll *et al.*, 2023). However, at this point it can only be speculated how fluid movement in the metasediments took place. but pre-existing feeder faults of the SEDEX system or tectonic structures between formations may have acted as fluid pathways. Nevertheless, HFSE and REE bearing metamorphic fluids entering the sediments would equilibrate with fluorapatite in the sediment stripping off fluoride from the solution resulting in the precipitation of HFSE and REE due to the drastic solubility reduction (Rapp *et al.*, 2010; Migdisov & Williams-Jones, 2014; Wood, 2005). In this case it is assumed that the unique geochemistry of the sulphide mineralisation acted as a sink for incompatible elements. Furthermore, the decomposition of REE-silicates would have occurred during Permian metamorphism indicated by the presence of REE-fluorocarbonates within aggregates (pseudomorphs) formed by metamorphic fluids, whereas the formation of thorite could have caused a partitioning of Th and REE explaining low ThO_2 contents in monazite. Moreover, the breakdown of Ti-rich biotite by metamorphic fluids could have produced chlorite and small rutile crystals present interspersed in mica rich layers simultaneously (van Baalen, 1993).

The stronger enrichment pattern of LREE over HREE in ore and country rocks results probably from hydrothermal fractionation due to stability differences of REE-complexes. LREE complexes with fluoride are more stable than those with HREE. The mobility differences are even more drastic for chloride as ligand since LREE complexes are 1.5 orders of magnitude more stable at temperatures ≥250°C than those with HREE (Migdisov *et al.*, 2016). Europium must be viewed differently because its geochemical behaviour is decoupled from other REE since it is redox sensitive, occurs under hot reducing conditions as bivalent Eu compared to trivalent REE making it much more mobile with chloride complexes and it substitutes Ca^{2+} e.g. in feldspars and carbonates. The positive Eu anomalies in investigated samples are most probably a primary feature from deposit formation and are indicative for hydrothermal fluid interaction with host rocks (Migdisov *et al.*, 2016; Parr, 1992).

Fluorapatite accompanies both HFSE and REE minerals regularly, whereas all three are often associated with mica. The frequency of fluorapatite correlates well with whole rock geochemical P_2O_5 concentrations. The distribution of phosphate along drill core sections shows a distinct enrichment in the sulphide mineralisation and its proximal hanging wall where fluorapatite occurs commonly and was found to even form layer like aggregations. It is also observed, together with dolomite, as a halo surrounding sulphide bearing veins hinting to a connection to ore forming processes. However, the presence of fluorapatite is not exclusive to ore horizons and alteration halos since fluorapatite is present in other units of the Graz Paleozoic as well (Hollinetz *et al.*, 2024). Similar observations of fluorapatite associations with SEDEX mineralisation were made at the Howard's Pass district (Canada) but REE systematics revealed that the relation to ore is casual and that fluorapatite is of hydrogenous authigenic origin from phosphogenesis connected to paleoenvironmental conditions and not related to hydrothermal activity (Gadd *et al.*, 2016). Besides, phosphate in the hydrothermal fluid would inhibit REE transport due to the precipitation

of REE-phosphates (Migdisov & Williams-Jones, 2014). However, substantial evidence is not available to clarify the role of fluorapatite in this setting.

Sulphides are present disseminated and to a lesser extent in veinlets (stringers) throughout the alteration halo and even beyond as accessory sulphides in the Kalkrippe marble unit, whereas the frequency of sulphides tends to increase approaching sulphide horizons. Apart from ore horizons, sulphides are predominantly pyrite but pyrrhotite shows trends to higher frequencies in proximity to sulphide mineralisation and was found to surpass pyrite in samples of the mineralisation within the H1 drill core sections. However, no compositional trends that would indicate proximity to sulphide mineralisation was identified in any of the various Pb, Cu, Ni, Co or As sulphides. However, Ni sulphides like pentlandite as well as sulpharsenides exist predominantly in the alteration zone and are rare in ore horizons. In general, Fe content in sphalerite does not increase near sulphide ore. Only at the G7 section 1 drill core Fe concentrations in sphalerite are more elevated in sulphide mineralisation. A weak trend to a greater Co, Ni or As variability in iron sulphides exists close to ore horizons.

The combination of compositional data from carbonates, chlorite, white mica, and iron sulphides as well as whole rock geochemistry shows a zonation within the alteration zone both vertically, at small scale in drill core sections and laterally, at large scale centred proximal to feeder systems. The alteration zone of ore horizons in drill core sections is generally characterized by an Fe incorporation in carbonates, chlorite and white mica peaking at the sulphide mineralisation. Additionally, the outer rim of the alteration zone shows an enrichment of Mg in these minerals but approaching ore horizons Mg becomes depleted and in carbonates Mn and Fe concentrations rise. Further, pyrrhotite becomes more frequent approaching ore horizons and, in H1 drill core sections, supersedes pyrite, which is present throughout the alteration zone. This zoning is reproduced by whole rock geochemistry, which shows Mg as well as Ca depletion and an enrichment of Mn plus Fe(T) at sulphide mineralisation and a strong correlation of Fe(T) and Mn. If locations such as Arzberg and Arzwaldgraben are considered to be proximal to feeder faults acting as conduits for hydrothermal metalliferous fluids and weakly mineralised rocks of drill core sections representing distal hydrothermal products then it becomes apparent that there is a trend to higher Fe incorporation in chlorite, white mica and carbonates, which are also more manganiferous, in proximity to feeder systems than in distal areas resulting in a compositional gradient of alteration mineralogy from centre to periphery of sulphide ore deposition. This theory is supported by whole rock geochemistry exemplified by higher maximum MnO readings at Arzberg (1.5 wt.%) and Arzwaldgraben (1.6 wt.%) than from H1 section 1 (0.3 wt.%) and section 2 (0.7 wt.%) as well as G7 section 1 (0.7 wt.%) and section 2 (0.5 wt.%) drill cores. Moreover, BaO incorporation in white mica seems to follow this trend both vertically in drill core sections and laterally as well.

Finally, it should be noted that individual minerals of the investigated lithologies are impossible to identify macroscopically in most cases due to their fine-grained nature, hence alteration halos are only possible to recognise by the colouring of the metasediments. Rocks, especially carbonate phyllite and marble, containing ferrous carbonates or sulphides tend to exhibit beige, yellowish to reddish and brownish colours, whereas calcite rich barren lithologies are often characterized by blueish tints.

5 Conclusion

Investigation of alteration halos of stratiform SEDEX-type Pb-Zn-Ag-Ba mineralisation in the Graz Paleozoic as well as of drill core sections from an exploration project provided evidence of distinct mineralogical and geochemical changes surrounding ore horizons in fine-grained metasediments resulting in colour changes of host rocks. Observed hanging wall as well as footwall alteration indicates ore formation proximal to feeder systems of hydrothermal metalliferous fluids. The alteration halo has a diffuse character with the coexistence of primary sedimentation, alteration and metamorphic mineralogy. It was found that phases attributed to host rock alteration correlate well with whole rock geochemistry. Selected elements and their distribution allow for determining alteration phenomena and proximity estimations. The host rock alteration mineralogy of sulphide mineralisation in the Graz Paleozoic is largely in alignment with other base metal deposits of the SEDEX-type globally. In the following results of the study are summarized:

- The alteration zone is characterized by a general Fe enrichment, but there is a trend from a Mg-rich outer rim to an inner Mn-rich zone, where Fe enrichment is strongest as well, whereas the outer Mg rim still contrasts to unaltered country rocks. This is found to be the case in drill core sections with thin weakly mineralized horizons at small scale. On a larger scale the alteration zone is centred at sites of initial hydrothermal fluid exhalation like Arzberg with stronger Fe and Mn enrichments diminishing laterally to a less pronounced, but still recognisable, alteration zone at drill cores in the periphery. This zonation is reflected by compositional variations of carbonates, chlorite and white mica as well as by whole rock geochemistry. Carbonates associated with host rock alteration are enriched in Fe, Mg and Mn compared to unaltered host rock carbonates, whereas approaching ore horizons concentrations of these elements increase while Ca decreases. They occur predominantly as the ankerite-dolomite series plus minor siderite in the alteration halo. These carbonates are enriched in Mg in the outer alteration zone and increasingly more Fe and Mn rich closer to sulphide mineralisation indicated by a gradient from dolomite to ankerite, which shows stronger Mn incorporation than dolomite, from distal to proximal. In general, siderite occurs in the inner parts of the alteration halo closer to ore horizons, whereas the observation of decreasing Mg and increasing Mn concentrations like in dolomite and ankerite does also apply, whereas the median Mn values show a stronger incorporation in siderite compared to ankerite and dolomite. In contrast, sedimentary calcite has low Fe, Mg and Mn concentrations. Whole rock geochemistry follows carbonate composition trends with a depletion of CaO and MgO as well as an enrichment of MnO at sulphide mineralisation. This Mg and Fe zonation is also present in chlorite with a Mg enrichment in the outer alteration zone and a progressive increase of Fe as well as decrease of Mg concentrations closing in on ore horizons. The exact same trend is found in white mica. Additional incorporation of BaO in white mica was observed reaching highest concentrations in sulphide mineralisation. Furthermore, Fe enrichment in the alteration halo is also reflected by iron sulphides with an increasing ratio of pyrrhotite to pyrite proximal to mineralisation.
- Albite is only found in association with ore horizons. It forms a zone beneath sulphide mineralisation indicating fluid infiltration beneath the water sediment interface hinting to proximal sulphide deposition. Frequency distributions of albite in the host rock correlate well with Na_2O concentrations of whole rock geochemistry making it an ideal proxy to identify albitization in metasediments. Host rock lithology does not affect the grade of albitization.

- K-feldspar exists as gangue phase in sulphide-quartz-carbonate veinlets (stringers) in H1 section 1 drill core in the sulphide mineralisation and the immediate hanging wall. Additionally, it occurs in Ba-K feldspar rich layers in the sulphide mineralisation of the H1 section 2 drill core as well as accessorily in the ore horizons of the unnamed adit at Kaltenberg-Burgstall.
- The Ba feldspar celsian is accompanied by hyalophane forming layers in the sulphide mineralisation of the H1 section 2 drill core and is present disseminated in the sulphide mineralisation at Peggau-Taschen. Hyalophane is a common in magnetite-rich host rock at Arzwaldgraben. Both Ba rich feldspars are first finds connected to ore horizons in the Graz Paleozoic.
- Chondrite and average European shale REE normalised data shows distinct REE enrichments and Eu anomalies of ore and host rock. Further, there is a correlation between REE and HFSE.
- REE as well as HFSE minerals are associated with sulphide mineralisation and occur frequently in the alteration zone, often in mica rich layers. REE phases occur disseminated and are represented by abundant monazite, minor REE-fluorocarbonate as well as xenotime-(Y) and rare allanite. The frequency of LREE minerals, especially monazite, correlates well with whole rock Ce concentrations due to the dominance of Ce incorporation into these minerals. Observed disseminated HFSE minerals encompass phases containing Ti, Nb, Zr, Th and U. Titanium minerals are most common among this group and are dominated by partly Nb bearing rutile, minor ilmenite and titanite, whereas ilmenite as well as titanite occur in calcite rich lithologies and rutile in ferrous carbonate bearing rocks. Whole rock geochemical data shows a trend to HFSE enrichment at ore horizons. Discrete Nb minerals are columbite-(Fe) and euxenite-(Y) accompanying ore horizons in the unnamed adit at Kaltenberg-Burgstall. Zirconium occurs as zircon and the elements Th and U are present mainly as (urano-)thorite, which is often found together with REE minerals. Radiometric dating of monazite and thorite did not produce any acceptable results. Fluorapatite occurs regularly with REE and HFSE minerals. However, its relation to the HFSE minerals as well as to ore is unclear but it tends to be associated with mineralisation and its frequency correlates well with phosphate of the whole rock geochemistry, which is enriched at ore horizons. The presence of HFSE and REE minerals associated with sulphide mineralisation is enigmatic since they are usually not widespread in SEDEX-type mineralisation. Further research on the occurrence of incompatible element bearing minerals is needed to resolve this conundrum.
- Sulphides are present disseminated or within veinlets in the alteration zone. They encompass mainly galena, sphalerite, chalcopyrite, pyrite and pyrrhotite. Nickel sulphides such as pentlandite and sulpharsenides are only present in small quantities, which are predominantly found in the alteration zone but rarely in ore horizons. Argentopentlandite and hessite are only recorded from samples from the H1 section 2 drill core. Magnetite is present in the baryte rich ore horizon at the abandoned Arzberg mine and in samples from Arzwaldgraben. Baryte is absent in most investigated sulphide mineralisations.

These findings provide valuable information to deepen our understanding on mineralogical footprints of SEDEX deposits and can be utilised in mineral exploration vectoring as well as in identifying prospective areas not only in the Graz Paleozoic but also in fossil sedimentary basins worldwide.

6 References

Cave, B.W. (2022). Sediment-hosted Zn-Pb-Ag (+ Cu) deposits in the Mount Isa region: An epigenetic approach to mineralisation, Dissertation, University of Adelaide. p. 132.

Cerny, P. & Ercit, T.S. (2005). The classification of granitic pegmatites revisited. The Canadian Mineralogist, Vol. 43, No. 6, pp. 2005–2026.

Cerny, P., Teertstra, D.K., Chapman, R., Selway, J.B., Hawthorne, F.C., Ferreira, K., Chackowsky, L.E., Wang, X.-J. & Meintzer, R.E. (2012). Extreme fractionation and deformation of the leucogranite - pegmatite suite at Red Cross Lake, Manitoba, Canada. IV. Mineralogy. The Canadian Mineralogist, Vol. 50, No. 6, pp. 1839–1875.

Chapman, L.H. (2004). Geology and Mineralization Styles of the George Fisher Zn-Pb-Ag Deposit, Mount Isa, Australia. Economic Geology, Vol. 99, No. 2, pp. 233–255.

Coats, J.S., Fortey, N.J., Gallagher, M.J. & Grout, A. (1984). Stratiform barium enrichment in the Dalradian of Scotland. Economic Geology, Vol. 79, No. 7, pp. 1585–1595.

Deer, W.A., Howie, R.A. & Zussman, J. (2013), An introduction to the rock-forming minerals, Third edition 2013, The Mineralogical Society, London. p. 498.

Ebner, F. (1976). Die Schichtfolge an der Wende Unterkarbon/ Oberkarbon in der Rannach-Fazies des Grazer Paläozoikums. Verhandlungen der Geologischen Bundesanstalt, No. 2, pp. 65–93.

Ebner, F. & Sachsenhofer, R. (1991). Die Entwicklungsgeschichte des Steirischen Tertiärbeckens. Mitteilungen der Abteilung für Geologie, Paläontologie und Bergbau am Landesmuseum Joanneum, No. 49, p. 96.

Emsbo, P. (2000). Gold in Sedex Deposits. SEG Reviews, 2000, pp. 427–437.

Emsbo, P. (2009). Geologic criteria for the assessment of sedimentary exhalative (sedex) Zn-Pb-Ag deposits. US Geological Survey Open-File Report 2009–1209.

Farquhar, J., Wu, N., Canfield, D.E. & Oduro, H. (2010). Connections between Sulfur Cycle Evolution, Sulfur Isotopes, Sediments, and Base Metal Sulfide Deposits. Economic Geology, Vol. 105, No. 3, pp. 509–533.

Feichter, M. (2005). Die sedimentgebundene Pb-Zn-Ba-Lagerstätte Arzberg (Steiermark, Österreich): Mineralisation und Genese, Dissertation, Karl-Franzens-Universität Graz. p. 230.

Finlow-Bates, T. & Stumpfl, E. (1979). The copper and lead zinc silver orebodies of Mt. Isa Mine, Queensland; products of one hydrothermal system. Annales de la Societe Geologique de Belgique, 1979, pp. 497–517.

Flügel, H.W. (1975), Die Geologie des Grazer Berglandes: Erläuterungen zur Geologischen Wanderkarte des Grazer Berglandes 1:100.000; mit 47 Tabellen, Mitteilungen der Abteilung für Geologie, Paläontologie und Bergbau am Landesmuseum Joanneum, Sonderheft 1, Graz. p. 288.

Flügel, H.W. & Hubmann, B. (2000), Das Paläozoikum von Graz: Stratigraphie und Bibliographie, Schriftenreihe der Erdwissenschaftlichen Kommissionen / Österreichische

Akademie der Wissenschaften, Vol. 13, Verlag der Österreichischen Akademie der Wissenschaften, Wien. p. 118.

Freeze, A.C. (1966), On the origin of the Sullivan orebody: Kimberley, B.C., Tectonic history and mineral deposits of the western Cordillera, Canadian Institute of Mining and Metallurgy Special Publication, Vol. 8, pp. 263–293.

Fritz, H. (1991). Stratigraphie, Fazies und Tektonik im nordwestlichen Grazer Paläozoikum (Ostalpen). Jahrbuch der Geologischen Bundesanstalt, No. 134 (2), pp. 227–255.

Fritz, H., Ebner, F. & Neubauer, F. (1992). The Graz thrust-complex (Paleozoic of Graz), in Neubauer, F. (Ed.), ALCAPA Field Guide: The Eastern Central Alps of Austria, Geological evolution of the internal Eastern Alps and Carpathians and of the Pannonian Basin, June 27 - July 6, 1992, Graz, pp. 83–92.

Fritz, H. & Neubauer, F. (1988). Geodynamic aspects of the Silurian and Early Devonian sedimentation in the Paleozoic of Graz (Eastern Alps). Schweizerische mineralogische und petrographische Mitteilungen, No. 3, pp. 359–367.

Gadd, M.G., Layton-Matthews, D. & Peter, J.M. (2016). Non-hydrothermal origin of apatite in SEDEX mineralization and host rocks of the Howard's Pass district, Yukon, Canada. American Mineralogist, Vol. 101, No. 5, pp. 1061–1071.

Gardner, H.D. & Hutcheon, I. (1985). Geochemistry, mineralogy, and geology of the Jason Pb-Zn deposits, Macmillan Pass, Yukon, Canada. Economic Geology, Vol. 80, No. 5, pp. 1257–1276.

Gasser, D., Stüwe, K. & Fritz, H. (2010). Internal structural geometry of the Paleozoic of Graz. International Journal of Earth Sciences, Vol. 99, No. 5, pp. 1067–1081.

Gibson, G.M., Meixner, A.J., Withnall, I.W., Korsch, R.J., Hutton, L.J., Jones, L., Holzschuh, J., Costelloe, R.D., Henson, P.A. & Saygin, E. (2016). Basin architecture and evolution in the Mount Isa mineral province, northern Australia: Constraints from deep seismic reflection profiling and implications for ore genesis. Ore Geology Reviews, Vol. 76, pp. 414–441.

Gieré, R. (1990). Hydrothermal mobility of Ti, Zr and REE: examples from the Bergell and Adamello contact aureoles (Italy). Terra Nova, Vol. 2, No. 1, pp. 60–67.

Goodfellow, W.D. (2004). Geology, genesis and exploration of SEDEX deposits, with emphasis on the Selwyn basin, Canada, in Deb, M. and Goodfellow, W.D. (Eds.), Sediment-hosted lead-zinc sulphide deposits: Attributes and models of some major deposits in India, Australia and Canada, Narosa Publishing House, New Delhi, pp. 24–99.

Hardie, L.A. (1996). Secular variation in seawater chemistry: An explanation for the coupled secular variation in the mineralogies of marine limestones and potash evaporites over the past 600 m.y. Geology, Vol. 24, No. 3, p. 279.

Hasenhüttl, C. & Russegger, B. (1992). Niedriggradige Metamorphose im Grazer Paläozoikum. Jahrbuch der Geologischen Bundesanstalt, Vol. 1992, No. 135 (1), pp. 287–297.

Haskin, M.A. & Haskin, L.A. (1966). Rare Earths in European Shales: A Redetermination. Science, Vol. 154, No. 3748, pp. 507–509.

Hey, M.H. (1954). A new review of the chlorites. Mineralogical Magazine and Journal of the Mineralogical Society, Vol. 30, No. 224, pp. 277–292.

Hoggard, M.J., Czarnota, K., Richards, F.D., Huston, D.L., Jaques, A.L. & Ghelichkhan, S. (2020). Global distribution of sediment-hosted metals controlled by craton edge stability. Nature Geoscience, Vol. 13, No. 7, pp. 504–510.

Hollinetz, M.S., Huet, B., Schneider, D., A., McFarlane, C., Schuster, R., Rantitsch, G., Schantl, P., Iglseder, C., Reiser, M. & Grasemann, B. (2024). Pressure-temperature-time and REE-mineral evolution in low to medium grade polymetamorphic units (Austroalpine Unit, Eastern Alps).

Jia, C.P., Chen, Q., An, M.G., Zhi, C.L., Lou, S.W., Zhang, P.P., Li, Q.C., Zhang, Y.M., Han, S.Y. & Zheng, H.T. (2022). Fluoride-leaching simulation of aquifer sediment and its influence on groundwater fluoride levels along coastal plains. Water Supply, Vol. 22, No. 4, pp. 4133–4141.

Klemm, D.D. (1965). Syntheses and analyses in the ternary diagrams FeAsS-CoAsS-NiAsS and FeS2-CoS2-NiS2. Neues Jahrbuch für Mineralogie - Abhandlungen, Vol. 103, No. 3, pp. 205–255.

Knoll, T., Huet, B., Schuster, R., Mali, H., Ntaflos, T. & Hauzenberger, C. (2023). Lithium pegmatite of anatectic origin – A case study from the Austroalpine Unit Pegmatite Province (Eastern European Alps): Geological data and geochemical modeling. Ore Geology Reviews, No. 154. 105298, pp. 1–32.

Krebs, W. (1981). The geology of the Meggen ore deposit, in Wolf, K.H. (Ed.), Handbook of strata-bound and stratiform ore deposits, Elsevier, Amsterdam, pp. 510–549.

Kröll, A. & Heller, R. (1978). Die Tiefbohrung AFLING U1 in der Kainacher Gosau. Verhandlungen der Geologischen Bundesanstalt, No. 2, pp. 23–34.

Lampinen, H.M., Laukamp, C., Occhipinti, S.A. & Hardy, L. (2019). Mineral footprints of the Paleoproterozoic sediment-hosted Abra Pb-Zn-Cu-Au deposit Capricorn Orogen, Western Australia. Ore Geology Reviews, Vol. 104, pp. 436–461.

Large, R.R., Bull, S.W. & McGoldrick, P.J. (2000). Lithogeochemical halos and geochemical vectors to stratiform sediment hosted Zn–Pb–Ag deposits. Part 2. HYC deposit, McArthur River, Northern Territory. Journal of Geochemical Exploration, Vol. 68, No. 1-2, pp. 105–126.

Large, R.R., Bull, S.W., McGoldrick, P.J., Walters, S., Derrick, G.M. & Carr, G.R. (2005). Stratiform and Strata-Bound Zn-Pb-Ag Deposits in Proterozoic Sedimentary Basins, Northern Australia, in Hedenquist, J.W., Thompson, J.F.H., Goldfarb, R.J. and Richards, J.P. (Eds.), One Hundredth Anniversary Volume, Society of Economic Geologists, pp. 931–963.

Large, R.R. & McGoldrick, P.J. (1998). Lithogeochemical halos and geochemical vectors to stratiform sediment hosted Zn–Pb–Ag deposits, 1. Lady Loretta Deposit, Queensland. Journal of Geochemical Exploration, Vol. 63, No. 1, pp. 37–56.

Large, R.R., McGoldrick, P.J., Bull, S.W. & Cooke, D. (2004). Proterozoic Stratiform Sediment-hosted Zinc-Lead-Silver Deposits of Northern Australia, in Deb, M. and Goodfellow, W.D. (Eds.), Sediment-hosted lead-zinc sulphide deposits: Attributes and models of some major deposits in India, Australia and Canada, Narosa Publishing House, New Delhi, pp. 1–23.

Leach, D.L., Marsh, E., Emsbo, P., Rombach, C.S., Kelley, K.D. & Anthony, M. (2004). Nature of Hydrothermal Fluids at the Shale-Hosted Red Dog Zn-Pb-Ag Deposits, Brooks Range, Alaska. Economic Geology, Vol. 99, No. 7, pp. 1449–1480.

Leach, D.L., Sangster, D.F., Kelley, K.D., Large, R.R., Garven, G., Allen, C.R., Gutzmer, J. & Walters, S. (2005). Sediment-Hosted Lead-Zinc Deposits: A Global Perspective, in Hedenquist, J.W., Thompson, J.F.H., Goldfarb, R.J. and Richards, J.P. (Eds.), One Hundredth Anniversary Volume, Society of Economic Geologists.

Linthout, K. (2007). Tripartite division of the system $2REEPO_4$ - $CaTh(PO_4)_2$ - $2ThSiO_4$, discreditation of brabantite, and recognition of cheralite as the name for members dominated by $CaTh(PO_4)_2$. The Canadian Mineralogist, Vol. 45, No. 3, pp. 503–508.

Lowenstein, T.K., Hardie, L.A., Timofeeff, M.N. & Demicco, R.V. (2003). Secular variation in seawater chemistry and the origin of calcium chloride basinal brines. Geology, Vol. 31, No. 10, p. 857.

Lydon, J. (2004a). Genetic Models for Sullivan and other SEDEX deposits, in Deb, M. and Goodfellow, W.D. (Eds.), Sediment-hosted lead-zinc sulphide deposits: Attributes and models of some major deposits in India, Australia and Canada, Narosa Publishing House, New Delhi, pp. 149–190.

Lydon, J. (2004b). Geology of the Belt-Purcell basin and the Sullivan deposit, in Deb, M. and Goodfellow, W.D. (Eds.), Sediment-hosted lead-zinc sulphide deposits: Attributes and models of some major deposits in India, Australia and Canada, Narosa Publishing House, New Delhi, pp. 100–148.

Lydon, J.W. (1995). Exhalative Base Metal Sulphides, in Eckstrand, O.R., Sinclair, W.D. and Thorpe, R.I. (Eds.), Geology of Canadian Mineral Deposit Types, Geological Society of America, pp. 129–196.

Maghfouri, S., Hosseinzadeh, M.R., Lentz, D.R., Tajeddin, H.A., Movahednia, M. & Shariefi, A. (2021). Nature of ore-forming fluids in the Mehdiabad world-class sub-seafloor replacement SEDEX-type Zn-Pb-Ba-(Cu-Ag) deposit, Iran; constraints from geochemistry, fluid inclusions, and O-C-Sr isotopes. Journal of Asian Earth Sciences, Vol. 207, p. 104654.

Melcher, F. & Onuk, P. (2019). Potential of Critical High-technology Metals in Eastern Alpine Base Metal Sulfide Ores. BHM Berg- und Hüttenmännische Monatshefte, Vol. 164, No. 2, pp. 71–76.

Migdisov, A., Williams-Jones, A.E., Brugger, J. & Caporuscio, F.A. (2016). Hydrothermal transport, deposition, and fractionation of the REE: Experimental data and thermodynamic calculations. Chemical Geology, Vol. 439, pp. 13–42.

Migdisov, A.A. & Williams-Jones, A.E. (2014). Hydrothermal transport and deposition of the rare earth elements by fluorine-bearing aqueous liquids. Mineralium Deposita, Vol. 49, No. 8, pp. 987–997.

Moreno, C., González, F. & Sáez, R. (2019). Basin Evolution and Massive Sulfide Deposition at Rammelsberg (Germany): Updating the Subsidence Analysis. Minerals, Vol. 9, No. 1, p. 45.

Moro, M.C., Cembranos, M.L. & Fernandez, A. (2001). Celsian, (Ba,K)-feldspar and cymrite from SEDEX barite deposits of Zamora, Spain. The Canadian Mineralogist, Vol. 39, No. 4, pp. 1039–1051.

Nakamura, N. (1974). Determination of REE, Ba, Fe, Mg, Na and K in carbonaceous and ordinary chondrites. Geochimica et Cosmochimica Acta, Vol. 38, No. 5, pp. 757–775.

Neubauer, F., Friedl, G., Genser, J., Handler, R., Mader, D. & Schneider, D. (2007). Origin and tectonic evolution of Eastern Alps deduced from dating of detrital white mica: a review. Austrian Journal of Earth Sciences, No. 100, pp. 8–23.

Neubauer, F., Liu, Y., Dong, Y., Chang, R., Genser, J. & Yuan, S. (2022). Pre-Alpine tectonic evolution of the Eastern Alps: From Prototethys to Paleotethys. Earth-Science Reviews, Vol. 226. 103923, pp. 1–35.

Niggli, M. (1987). Geochemische Untersuchungen metamorpher Pb-Zn-Lagerstaetten und ihrer Nebengesteine, Dissertation, ETH Zurich. p. 190.

Onuk, P. (2018). High-tech metal potential of sphalerite from Eastern Alpine lead-zinc deposits and development of a matrix-matched sphalerite (ZnS) calibration material (MUL-ZnS-1) for calibration of in-situ trace element measurements by laser ablation inductively coupled plasma mass spectrometry (LA-ICP-MS), Dissertation, Montanuniversität Leoben. p. 196.

Parr, J.M. (1992). Rare-earth element distribution in exhalites associated with Broken Hill-type mineralisation at the Pinnacles deposit, New South Wales, Australia. Chemical Geology, Vol. 100, No. 1-2, pp. 73–91.

Pirajno, F., Mernagh, T.P., Huston, D., Creaser, R.A. & Seltmann, R. (2016). The Mesoproterozoic Abra polymetallic sedimentary rock-hosted mineral deposit, Edmund Basin, Western Australia. Ore Geology Reviews, Vol. 76, pp. 442–462.

Plimer, I. (2006). Hydrothermal alteration at Broken Hill. Broken hill exploration initiative: abstracts for the September 2006 conference. Geoscience Australia Record, No. 2006/21, pp. 138–144.

Polito, P.A., Kyser, T.K., Golding, S.D. & Southgate, P.N. (2006). Zinc Deposits and Related Mineralization of the Burketown Mineral Field, Including the World-Class Century Deposit, Northern Australia: Fluid Inclusion and Stable Isotope Evidence for Basin Fluid Sources. Economic Geology, Vol. 101, No. 6, pp. 1251–1273.

Rantitsch, G., Ebner, F., Russegger, B. & Weber, L. (1998). Kohlenstoff-Schwefel-Beziehungen in Schwarzschiefern der Schönberg Formation (Obersilur/Unterdevon des Grazer Paläozoikums, Österreich): ein Produktivitätsmodell zur Entstehung altpaläozoischer Schwarzschiefer. Mitteilungen der Abteilung für Geologie, Paläontologie und Bergbau am Landesmuseum Joanneum, No. 2, pp. 303–314.

Rantitsch, G., Sachsenhofer, R.F., Hasenhüttl, C., Russegger, B. & Rainer, T. (2005). Thermal evolution of an extensional detachment as constrained by organic metamorphic data and thermal modeling: Graz Paleozoic Nappe Complex (Eastern Alps). Tectonophysics, Vol. 411, No. 1-4, pp. 57–72.

Rapp, J.F., Klemme, S., Butler, I.B. & Harley, S.L. (2010). Extremely high solubility of rutile in chloride and fluoride-bearing metamorphic fluids: An experimental investigation. Geology, Vol. 38, No. 4, pp. 323–326.

Rodríguez, A., Weis, P., Magnall, J.M. & Gleeson, S.A. (2021). Hydrodynamic Constraints on Ore Formation by Basin-Scale Fluid Flow at Continental Margins: Modelling Zn Metallogenesis in the Devonian Selwyn Basin. Geochemistry, Geophysics, Geosystems, Vol. 22, No. 6. e2020GC009453, pp. 1–19.

Rohrhofer, S., Geringer, A., Melcher, F. & Schuster, R. (2024). Alteration Zones as Exploration Parameters for Stratiform Pb-Zn-Ag-Ba Deposits in the Graz Paleozoic (Eastern Alps, Austria). BHM Berg- und Hüttenmännische Monatshefte, Vol. 169, No. 10, pp. 567–573.

Römer, A., Bieber, G., Supper, R. & Motschka, K. (2006). Geophysikalische Untertagemessungen im Stollen Arzberg (Stmk) 2006. ÜLG28/05, Geologische Bundesanstalt Wien, Fachabteilung Geophysik. p. 46.

Russegger, B. (1996). Niedrigst- bis niedriggradige Metamorphose im südlichen Grazer Paläozoikum (Ostalpen). Jahrbuch der Geologischen Bundesanstalt, No. 139 (1), pp. 93–100.

Sangster, D.F. (2002). The role of dense brines in the formation of vent-distal sedimentary-exhalative (SEDEX) lead–zinc deposits: field and laboratory evidence. Mineralium Deposita, Vol. 37, No. 2, pp. 149–157.

Schandl, E.S. & Gorton, M.W. (2004). A textural and geochemical guide to the identification of hydrothermal monazite: criteria for selection of samples for dating epigenetic hydrothermal ore deposits. Economic Geology, Vol. 99, No. 5, pp. 1027–1035.

Schantl, P., Schuster, R., Krenn, K. & Hoinkes, G. (2015). Polyphase metamorphism at the southeastern margin of the Graz Paleozoic and the underlying Austroalpine basement units. Austrian Journal of Earth Sciences, Vol. 108, No. 2, pp. 219–238.

Schmid, S.M., Fügenschuh, B., Kissling, E. & Schuster, R. (2004). Tectonic map and overall architecture of the Alpine orogen. Eclogae Geologicae Helvetiae, Vol. 97, No. 1, pp. 93–117.

Schroll, E. (1997). Geochemische und geochronologische Daten und Erläuterungen, in Weber, L. (Ed.), Handbuch der Lagerstätten der Erze, Industrieminerale und Energierohstoffe Österreichs: Erläuterungen zur Metallogenetischen Karte von Österreich 1:500.000 unter Einbeziehung der Industrieminerale und Energierohstoffe. Archiv für Lagerstättenforschung der Geologischen Bundesanstalt, Geologische Bundesanstalt, Wien, pp. 395–537.

Schulz, B. (2021). Monazite Microstructures and Their Interpretation in Petrochronology. Frontiers in Earth Science, Vol. 9. 668566.

Schuster, R. & Stüwe, K. (2008). Permian metamorphic event in the Alps. Geology, Vol. 36, No. 8, p. 603.

Seiberl, W. & Pistotnik, J. (1994). Aerogeophysikalische Vermessung im Bereich von Semriach, Aero-Geophysik Österreich, Geologische Bundesanstalt Wien. p. 41.

Sperling, H. & Walcher, E. (1990). Die Blei-Zink-Erzlagerstätte Rammelsberg (ausgenommen Neues Lager), Geologisches Jahrbuch, Reihe D, Hannover. p. 3-154.

Taylor, R., Bradley, D. & Pisarevsky, S. (2009). Compilation of Mineral Resource Data for Mississippi Valley-Type and Clastic-Dominated Sediment-Hosted Lead-Zinc Deposits, Open-File Report 2009–1297. p. 42.

Tschelaut, W. (1985). Über das Alter der Arzberger Schichten und der Blei-Zink-Vererzung im Grazer Paläozoikum. Jahrbuch der Geologischen Bundesanstalt, No. 128 (2), pp. 241–243.

Tufar, W. (1978). Flüssigkeitseinschlüsse in Baryten aus dem Grazer Paläozoikum (Steiermark) und in Magnesiten von Radenthein (Kärnten). Mitteilungen der Abteilung für Mineralogie am Landesmuseum Joanneum, No. 46, pp. 27–37.

van Baalen, M.R. (1993). Titanium mobility in metamorphic systems: a review. Chemical Geology, Vol. 110, No. 1-3, pp. 233–249.

Vogt, J.H. & Stumpfl, E.F. (1987). Abra; a strata-bound Pb-Cu-Ba mineralization in the Bangemall Basin, Western Australia. Economic Geology, Vol. 82, No. 4, pp. 805–825.

Weber, L. (1990), Die Blei-Zinkerzlagerstätten des Grazer Paläozoikums und ihr geologischer Rahmen, Archiv für Lagerstättenforschung der Geologischen Bundesanstalt, Bd. 12, Geologische Bundesanstalt, Wien. p. 289.

Weber, L. (2005). Die silberführende Blei-Zinkerzlagerstätte von Arzberg (Oststeiermark). Joannea Geologie und Paläontologie, No. 7, pp. 9–23.

Wilkinson, J.J. (2014). Sediment-Hosted Zinc–Lead Mineralization, in Treatise on Geochemistry, Elsevier, pp. 219–249.

Wood, S.A. (2005). The aqueous geochemistry of zirconium, hafnium, niobium and tantalum, in Linnen, R.L. and Samson, I.M. (Eds.), Rare-element geochemistry and mineral deposits. Geological Association of Canada short course notes, Geological Association of Canada, Canada, pp. 217–268.

Yardley, B.W. (2005). 100th Anniversary Special Paper: Metal Concentrations in Crustal Fluids and Their Relationship to Ore Formation. Economic Geology, Vol. 100, No. 4, pp. 613–632.

Zi, J.-W., Rasmussen, B., Muhling, J.R., Fletcher, I.R., Thorne, A.M., Johnson, S.P., Cutten, H.N., Dunkley, D.J. & Korhonen, F.J. (2015). In situ U–Pb geochronology of xenotime and monazite from the Abra polymetallic deposit in the Capricorn Orogen, Australia: Dating hydrothermal mineralization and fluid flow in a long-lived crustal structure. Precambrian Research, Vol. 260, pp. 91–112.

Appendix

Table 2: Coordinates of sample locations.

Locality	Coordinates (WGS 84)	
	N	E
Haufenreith		
H1 drilling	47.269704	15.547609
Black shale	47.258658	15.528281
Arzberg	47.250496	15.519425
Arzwaldgraben	47.239072	15.279756
Großstübing		
Kalkrippe	47.207820	15.230050
Guggenbach (Übelbach)		
G7 drilling	47.210648	15.238254
Kaltenberg-Burgstall		
Unnamed Adit	47.234481	15.514558
Peggau-Taschen		
Unnamed Adit near Moarbründl creek	47.196.658	15.370.072
Wilhelm Adit at Mitteregg	47.201431	15.378792

Table 3: List of investigated samples for this thesis and the analysis performed.

Sample	Lithology	Whole Rock Geochemistry	Optical Microscopy	SEM	Microprobe	Sample	Lithology	Whole Rock Geochemistry	Optical Microscopy	SEM	Microprobe
H1 drill core						H1 drill core					
H1-314,6	carbonate phyllite	X				H1-397,2	marble	X			
H1-315,6	carbonate phyllite	X	X	X		H1-397,8	marble	X	X	X	
H1-316,4a	carbonate phyllite	X				H1-398,1	marble	X			
H1-316,4b	carbonate phyllite	X				H1-398,6	marble	X	X	X	
H1-317,7	carbonate phyllite	X				H1-399,3	sulphide ore	X	X	X	
H1-318,7	carbonate phyllite	X	X	X		H1-400,1	carbonate phyllite	X			
H1-319,7	carbonate phyllite	X				H1-400,3	carbonate phyllite	X	X	X	
H1-321,1	carbonate phyllite	X				H1-400,4	carbonate phyllite	X			
H1-322,1	carbonate phyllite	X	X	X		H1-401,1	sulphide ore	X	X	X	
H1-322,4	carbonate phyllite	X				H1-401,4	sulphide ore	X			
H1-323.3	carbonate phyllite	X	X	X		H1-401,9	sulphide ore	X			
H1-324,1	carbonate phyllite		X	X		H1-402,7	marble	X			
H1-325,4	carbonate phyllite	X				H1-403,2	marble	X			
H1-325,6	sulphide ore	X				H1-403,5	carbonate phyllite	X	X	X	
H1-325,9	sulphide ore	X	X	X		H1-403,8	carbonate phyllite	X			
H1-326,6	sulphide ore	X	X	X		H1-404,4	carbonate phyllite	X	X	X	
H1-327,1	sulphide ore	X				H1-405,5	carbonate phyllite		X	X	
H1-327,3	carbonate phyllite	X				H1-406,5	carbonate phyllite	X			
H1-327,9	carbonate phyllite	X				H1-407,6	carbonate phyllite	X			
H1-328,2	carbonate phyllite	X	X	X		H1-408,6	carbonate phyllite	X			
H1-328,4	carbonate phyllite	X				H1-409,5	carbonate phyllite	X	X	X	
H1-329,0	carbonate phyllite	X				H1-410,5	carbonate phyllite	X	X	X	
H1-330,3	carbonate phyllite	X				H1-411,5	carbonate phyllite	X			
H1-331,6	metatuffite	X	X	X		H1-412,5	marble	X			
H1-332,0	metatuffite	X				H1-413,6	carbonate phyllite	X	X	X	
H1-334,1	metatuffite	X				H1-414,3	carbonate phyllite	X			
H1-335,1	metatuffite	X	X	X		H1-415,4	carbonate phyllite	X	X	X	
H1-390,0	marble	X	X	X		H1-416,5	carbonate phyllite	X			
H1-392.0	marble	X	X	X		H1-417,5	carbonate phyllite	X			
H1-392,3	marble	X	X	X		H1-418,4	marble	X	X	X	
H1-393,0	marble		X	X		H1-420,4a	marble	X			
H1-393,3	marble	X	X	X		H1-420,4b	marble	X			
H1-394,2	marble	X				H1-421,3	carbonate phyllite	X			
H1-395,9	marble	X				H1-423,2	carbonate phyllite	X	X	X	

Sample	Lithology	Note	Whole Rock Geochemistry	Optical Microscopy	SEM	Microprobe	Sample	Lithology	Note	Whole Rock Geochemistry	Optical Microscopy	SEM	Microprobe
G7 drill core							Kaltenberg-Burgstall						
G7-46,2	carbonate phyllite		X				US13A	sulphide ore	upper ore horizon	X		X	
G7-47,2	carbonate phyllite		X				US13B	marble	hanging wall	X			
G7-48,6	carbonate phyllite		X	X	X		US15		upper part of adit		X	X	
G7-53,5	carbonate phyllite		X				US17	sulphide ore	upper part of adit	X	X		
G7-56	breccia		X	X	X		US18	sulphide ore	upper part of adit	X	X	X	
G7-56,3	breccia		X	X	X		Haufenreith						
G7-56,7	breccia		X				22 TB 01	black shale	Taubenbrunnen	X			
G7-58,2	sulphide ore		X	X	X		Peggau-Taschen (Moarbründl)						
G7-58,5	sulphide ore		X	X	X		MB01	black shale		X			
G7-59,3	sulphide ore		X	X	X		MB02	carbonate phyllite	hanging wall				
G7-60,3	carbonate phyllite		X	X	X		MB04	carbonate phyllite	hanging wall	X			
G7-60,6	sulphide ore		X	X	X		MB05	carbonate phyllite	hanging wall	X	X	X	
G7-62,1	carbonate phyllite		X	X	X		MB06	sulphide ore			X	X	
G7-63,7	carbonate phyllite		X				MB 07	sulphide ore		X	X		
G7-98,4	breccia		X				MB08	sulphide ore			X		
G7-99,6	breccia		X				MB 09	sulphide ore		X	X	X	X
G7-100,9	breccia		X	X			MB 10	sulphide ore		X	X	X	
G7-101,5	breccia		X	X			Peggau-Taschen (Mitteregg)						
G7-105,2	breccia		X	X			ME 02	carbonate phyllite	from dumps	X			
G7-106,9	carbonate phyllite		X				Arzwaldgraben						
G7-108,25	sulphide ore		X	X			22 AW 01	baryte ore	from dumps	X	X		
G7-110,5	breccia		X				22 AW 02	magnetite rich phyllite	from dumps		X	X	
G7-112,3	breccia		X	X			22 AW 03	sulphide ore	from dumps	X	X		
G7-114,7	breccia		X	X			22 AW 05	magnetite rich phyllite	from dumps	X	X	X	
G7-118,8	breccia		X	X			Kalkrippe						
G7-119,25	breccia		X				KR 01	marble		X	X	X	
Kaltenberg-Burgstall							Arzberg						
US01	marble	footwall	X	X			22 AB 01	"ribbon chert"	"Südostschlag"		X	X	
US02A	sulphide ore	lower ore horizon	X	X	X		22 AB 02	sulphide ore	backfill ("Unterbau")	X			
US02C	marble	lower ore horizon	X				22 AB 03	sulphide ore	backfill ("Unterbau")		X		
US03	marble	footwall	X	X	X		22 AB 04	sulphide ore	backfill ("Unterbau")	X	X	X	X
US05	marble			X			22 AB 05	sulphide ore	backfill ("Unterbau")	X	X	X	
US06	marble			X			22 AB 11	"ribbon chert"	at bottom of Arzberg shaft	X	X	X	
US07A	sulphide ore	upper ore horizon	X	X			22 AB 12	baryte ore	at seismograph station	X	X	X	
US07B	marble	hanging wall	X				21AB01	sulphide ore		X	X		
US09	marble	hanging wall	X	X	X		21AB02	sulphide ore		X	X		
US10	carbonate phyllite	interlayer	X	X	X		21AB03	sulphide ore		X	X		
US12	marble			X									

Table 4: Frequency estimations of occurring minerals in samples of the H1 section 1 drill core based on observations made during SEM analysis; X=accessorily occurring, XX=regularly occurring, XXX=frequently occurring.

H1 section 1 drill core																			
sample	lithology	note	siderite	calcite	ankerite	dolomite	phengite	chlorite	biotite	quartz	albite	orthoclase	tremolite	galena	sphalerite	chalcopyrite	pyrrhotite	pyrite	arsenopyrite
H1-315,6	carbonate phyllite	stringers			X		XX	XX		XX				X			XX	X	
H1-318,7	carbonate phyllite			XXX		X		XXX		XXX	XXX			X	X	XX		XX	
H1-322,1	carbonate phyllite	stringers	X			XX	XXX	XX		XX	XXX	X		X			XXX	XX	
H1-323,3	carbonate phyllite	stringers	X		X	XXX	XX			XXX	XX	X		X			XX	X	
H1-324,1	carbonate phyllite	stringers				XX	XXX	XX		XXX	XX	XX		X			XXX	X	X
H1-325,9	sulphide ore	stringers		X	X	XXX	XXX	X		XXX	X	X		X		X	XX	XX	
H1-326,6	sulphide ore	stringers			X	XX	XXX			XX	XXX	XX		XX	XXX		XXX		
H1-328,2	carbonate phyllite			XXX					XXX	X	XXX			X	X	X		XX	
H1-331,6	metatuffite			XXX				XX	XX	XX	XXX		XX	X	X	XX		XX	
H1-335,1	metatuffite			XXX				X	XX	X	XXX		XXX			XX		XX	

H1 section 1 drill core																				
sample	cobaltite	millerite	galena	sphalerite	chalcopyrite	pyrrhotite	pyrite	arsenopyrite	cobaltite	millerite	monazite	xenotime	rutile	ilmenite	titanite	fluorapatite	thorite	allanite	zircon	villamanínite
H1-315,6	X		X			XX	X		X		XX		XX			XX				
H1-318,7			X	X	X(X)		XX				X		XXX	XX		XX	X			
H1-322,1			X			XXX	XX				XX	X	XXX			XX	X	X		
H1-323,3			X			XX	X				XX		XX			XX			X	
H1-324,1	X		X			XXX	X	X	X		XX	X	XX			XX	X			
H1-325,9			X		X	XX	XX				XX		XXX			XX			X	
H1-326,6			XX	XXX		XXX					XX		XXX			XXX				
H1-328,2			X	X	X		XX							XX	XX					X
H1-331,6		X	X	X	XX		XX			X					XX	XX		X		
H1-335,1					XX		XX							XX	XX	X		X	X	

Table 5: Frequency estimations of occurring minerals in samples of the H1 section 2 drill core based on observations made during SEM analysis; X=accessorily occurring, XX=regularly occurring, XXX=frequently occurring, X(X)= frequency between X and XX.

H1 section 2 drill core																					
sample	lithology	note	siderite	calcite	ankerite	dolomite	phengite	chlorite	biotite	quartz	albite	celsian	hyalophane	orthoclase	galena	sphalerite	chalcopyrite	pyrrhotite	pyrite	arsenopyrite	cobaltite	gersdorffite
H1-390,0	marble			XXX		XX	XXX			XX					X		X		X	X	X	X
H1-392,0	marble	stringers		X		XXX	XXX	XX		XX					X	X	X	XX	X			
H1-392,3	marble	stringers		XXX		XXX	XX	X		XX								XX	X		X	X
H1-393,0	marble	stringers		XXX	X	XX	XX	XX		XX					X	XX	X	XXX	X	X		
H1-393,3	marble			XXX	X	XX	XX	XX		XXX					X		X	XX	XX	X(X)		
H1-397,8	marble			XXX			XX	XX		XX					X			XX	X	X(X)	X	X
H1-398,6	marble			XXX	X		XX	XX		XXX					X	X	X	XX	X		X(X)	X
H1-399,3	sulphide ore		X	XXX	XXX	X		XX		XXX		XXX		XX	XX	XX	X	XX	X			
H1-400,3	carbonate phyllite			XX			XXX	XXX		XX(X)					X	X	X	XX	XX		X	
H1-401,1	sulphide ore			XXX	XXX		XX	XX		XX		XXX	X	X	XXX	X	X	XXX	XX		X	
H1-403,5	carbonate phyllite	stringers		XXX	X	X	XXX	XX		XXX	XX				X	X		XXX	XX			
H1-404,4	carbonate phyllite	stringers		XXX	X		XX	XXX	X	XXX	XX				X	X	X	XX	XX			
H1-405,5	carbonate phyllite	stringers		XXX			XXX	XXX	X	XXX	XX				X	X		XX	XX			
H1-409,5	carbonate phyllite	stringers		XXX		X	XXX	XXX		XXX	XX			X	X	X	X	XX	X		X	
H1-410,5	carbonate phyllite	stringers		XX			XXX	XXX		XX	XX				X	X	X	XX	X			
H1-413,6	carbonate phyllite			XXX		XX	XX	X		XX	XX				X	X	X	X	X		X	
H1-415,4	carbonate phyllite			XXX			XXX	XXX		XXX	XX				X		X	X	XX		X	
H1-418,4	marble			XXX		X	XX	XX		XXX	XX				X	X	X	X	X		X	
H1-423,2	carbonate phyllite	stringers		XXX			XXX	XXX	X	XX					X	X	X	X(X)	X(X)			

H1 section 2 drill core																					
sample	ulmannite	hessite	argentopentlandite	baryte	monazite	REE-fluorocarbonate	xenotime	rutile	ilmenite	fluorapatit	Thorit	thorite	brannerite	uraninite	allanite	zircon	Anglesit	Cerussit	Glaukodot	pentlandite	Baddeleyit
H1-390,0					X			XX		XX						X(X)	X		X		
H1-392,0					XX			XX	XX	X	X	X				XX	X				
H1-392,3					X			XX	XX	X						X					
H1-393,0					X			X		XX	X	X				X					
H1-393,3					X			X	XX	XX	X				X	X					
H1-397,8	X	X						X	X	X								X			
H1-398,6	X	X			X			X	X	X	X(X)					X					
H1-399,3				X	XX				X	X											
H1-400,3					XX			XX		XX	X					XX					
H1-401,1			X		X			X	X	XX		X				X					
H1-403,5					X(X)		X	XX		XX	X	X				X					
H1-404,4	X				X(X)			XX		XX	X	X	X			X					
H1-405,5					XX	XX		XX		XX	X		X			X					
H1-409,5					X(X)	X(X)	X	XX		XX	X					X					
H1-410,5					X(X)			XXX		XX	X					X(X)					
H1-413,6					X	X		X(X)		X	X			X		X(X)				X	
H1-415,4					X			XX		X	X					X(X)				X	X
H1-418,4					X	X	X	X		X	X					X				X	
H1-423,2	X				X	XX	X	XXX		XXX	X				X	X					

Table 6: Frequency estimations of occurring minerals in samples of the G7 section 1 drill core based on observations made during SEM analysis; X=accessorily occurring, XX=regularly occurring, XXX=frequently occurring, X(X)= frequency between X and XX, XX(X)=frequency between XX and XXX.

G7 section 1 drill core												
sample	lithology	note	siderite	calcite	ankerite	dolomite	phengite	chlorite	quartz	albite	galena	sphalerite
G7-48,6	carbonate phyllite		X(X)	XXX	XXX	X	XXX	XX	XXX			X
G7-56,0	breccia			X	XXX	XXX	XXX		XXX		X	X
G7-56,3	breccia				XXX	XXX	XX		XXX		X	X
G7-58,2	sulphide ore		XX		XX		XX	XX	XXX		X	XX
G7-58,5-1	sulphide ore		XX		XX		XX	X	XXX		X	XXX
G7-58,5-2	sulphide ore		XX		XXX		XX(X)	X	XXX	X	X	XX
G7-59,3	sulphide ore		XX		XXX	X	X	X	XXX	X	X	XX
G7-60,3	breccia		XX		XXX		X	XX	XXX		X	X
G7-60,6	sulphide ore		X	X	XXX		XX		XXX		X	XX
G7-62,1	carbonate phyllite		X	X	XXX	X	XXX		XXX		X	X

G7 section 1 drill core										
sample	chalcopyrite	pyrrhotite	pyrite	millerite	monazite	xenotime	rutile	fluorapatite	zircon	pentlandite
G7-48,6	X		XX		X(X)	X	X	XX	X	
G7-56,0			XX(X)		X		X	X(X)	X	
G7-56,3	XX		XX(X)		X		X	X	X	
G7-58,2			XX		X		X	X		
G7-58,5-1			XX		X		X	X(X)		
G7-58,5-2			X(X)		X		X(X)	X(X)		
G7-59,3	X		X		X	X	X	X		
G7-60,3	X	X	XX		X		XX	X		
G7-60,6			X(X)		X(X)		XX	XX		
G7-62,1	X		XX	X	X(X)	X	X	X	X	X

Table 7: Frequency estimations of occurring minerals in samples of the unnamed adit at Kaltenberg-Burgstall based on observations made during SEM analysis; X=accessorily occurring, XX=regularly occurring, XXX=frequently occurring.

Unnamed Adit, Kaltenberg-Burgstall																	
sample	lithology	note	siderite	calcite	ankerite	dolomite	phengite	chlorite	quartz	albite	orthoclase	galena	sphalerite	chalcopyrite	pyrrhotite	pyrite	
US09	marble	profile across ore horizons		XXX	XX		XX	X	X	XX		XX	XX	X		X	
US13A	sulphide ore	profile across ore horizons	XX	X	XXX		X	XX	XXX			XXX	XXX			X	
US10	carbonate phyllite	profile across ore horizons		X	XXX		XXX	X	X	XX	X	X	X			X	
US02A	sulphide ore	profile across ore horizons	X		X		XXX	XXX	XXX	XX	X	XXX	XX		X	X	
US03	marble	profile across ore horizons	X	XXX			XX		X			X	X	X	X	X	
US15	marble			XXX			XXX		XX								
US18A	sulphide ore				XX	X	XX	X	XX			XXX	XX			XX	

Unnamed Adit, Kaltenberg-Burgstall																
sample	arsenopyrite	gersdorffite	ulmannite	baryte	monazite	REE-fluorocarbonate	rutile	ilmenite	fluorapatite	zircon	cerussite	columbite-(Fe)	euxenite-(Y)	coronadite	plumbojarosite	hetaerolite
US09		X			XX		X	XX	XX		X		X	X	X	X
US13A			X					XX			XX			XX	X	XX
US10					XX	X	X	XX	XX	X		X	X			
US02A							X	XX								
US03			X		X		X	XX	X	X						
US15	X			X	X		X		XX	X						
US18A											XX				X	

Table 8: Frequency estimations of occurring minerals in samples from the Arzberg mine based on observations made during SEM analysis; X=accessorily occurring, XX=regularly occurring, XXX=frequently occurring, X(X)= frequency between X and XX.

Arzberg													
sample	lithology	note	siderite	calcite	ankerite	dolomite	phengite	chlorite	biotite	quartz	galena	sphalerite	chalcopyrite
22AB01	"ribbon chert"	bottom of Arzberg shaft	X	XX	XX	X	XXX	X	X	XXX	X		
22AB04	sulphide ore	backfill	XX		XXX	X	XX	X		XX	X	XX	XXX
22AB05	sulphide ore	backfill	XX	XXX	XX	X	XX			XXX	XXX		X
22AB11	"ribbon chert"	"Südostschlag"		XXX		XX				XX	X		X
22AB12	baryte ore	next to seismograph station	XX	X	XX	XX	XX			XXX	XXX	XX	XX

Arzberg													
sample	pyrrhotite	pyrite	cobaltite	magnetite	baryte	monazite	xenotime	rutile	ilmenite	fluorapatite	zircon	cerussite	anhydrite
22AB01	X	X				X	X	X	XX	X			
22AB04	XXX	X	X			X	X		XX	XX	X		
22AB05	X	X						X	XX	X		X	
22AB11	X	X						X	X	X			
22AB12		X		XXX	XX				X(X)	X(X)			X

Table 9: Frequency estimations of occurring minerals in a sample from Kalkrippe based on observations made during SEM analysis; X=accessorily occurring, XX=regularly occurring, XXX=frequently occurring, X(X)= frequency between X and XX.

Kalkrippe, Guggenbach (Übelbach)												
sample	lithology	calcite	dolomite	phengite	quartz	galena	sphalerite	pyrite	cobaltite	monazite	fluorapatite	zircon
KR01	marble	XXX	X	X	X	X	X	X(X)	X	X	X	X

Table 10: Frequency estimations of occurring minerals in samples from Arzwaldgraben based on observations made during SEM analysis; X=accessorily occurring, XX=regularly occurring, XXX=frequently occurring, X(X)= frequency between X and XX, X(X)= frequency between X and XX.

.

Arzwaldgraben											
sample	lithology	note	siderite	calcite	ankerite	dolomite	phengite	chlorite	quartz	hyalophane	galena
22AW02	magnetite rich phyllite	from dumps		XX	X	X	XX	XX	XX	XX	XX
22AW05	magnetite rich phyllite	from dumps	XX				XXX		XXX	XX	X

Arzwaldgraben												
sample	sphalerite	chalcopyrite	pyrite	magnetite	baryte	monazite	rutile	ilmenite	fluorapatite	chromite	cerussite	coronadite
22AW02			X	XXX		X	X	X	X		X	
22AW05	X(X)	X	XX	XXX	XX	X(X)	X(X)		X(X)	X	X	X

Table 11: Frequency estimations of occurring minerals in samples from the unnamed adit near Moarbründl creek at Peggau-Taschen based on observations made during SEM analysis; X=accessorily occurring, XX=regularly occurring, XXX=frequently occurring, X(X)= frequency between X and XX, X(X)= frequency between X and XX, XX(X)=frequency between XX and XXX.

Peggau-Taschen (unnamed adit at Moarbründl)													
sample	lithology	note	calcite	ankerite	dolomite	phengite	chlorite	quartz	albite				
MB05	sulphide ore	upper part of ore horizon	XXX			XX	XX	XXX	XX				
MB06	carbonate phyllite		XXX			XX		XXX					
MB09	sulphide ore	upper part of ore horizon	XXX	X	X	XX	XX	XXX	X(X)				
MB10	sulphide ore		X	XXX	XXX	XX		XX	X(X)				

Peggau-Taschen (unnamed adit at Moarbründl)													
sample	celsian	barytocalcite	witherite	galena	sphalerite	chalcopyrite	pyrrhotite	pyrite	baryte	monazite	rutile	fluorapatite	cerussite
MB05				X		X		X	X	XX	X	X	
MB06								XX	X	X	X	X	
MB09				X				XX	X	XX	X	X(X)	X
MB10	X	X	X	X(X)	X	X(X)	X	XX(X)	X	X	X(X)	X	X

Table 12: Whole rock geochemistry of samples from the H1 drill core.

sample	Total S	SiO2	Al2O3	Fe2O3(T)	MnO	MgO	CaO	Na2O	K2O	TiO2	P2O5	LOI	Total	Sc	Be	V	Ba	Sr	Y	Zr
	%	%	%	%	%	%	%	%	%	%	%	%	%	ppm	ppm	ppm	ppm	ppm	ppm	ppm
Analysis Method	CS	FUS-ICP	FUS-ICP	FUS-ICP	FUS-ICP	FUS-ICP	FUS-ICP	FUS-ICP	FUS-ICP	FUS-ICP	FUS-ICP	GRAV	FUS-ICP	FUS-ICP	FUS-ICP	FUS-ICP	FUS-ICP	FUS-ICP	FUS-ICP	FUS-ICP
H1 drill core																				
H1-314,6	0.03	42.91	11.14	10.36	0.243	4.99	10.17	0.98	1.95	2.012	0.32	15.1	100.18	23	2	234	280	239	21	188
H1-315,6	2.21	54.44	13.42	8.37	0.192	2.56	6.01	0.26	3.93	1.888	0.34	7.24	98.65	16	3	176	677	174	24	233
H1-316,4a	0.79	46.17	12.39	10.26	0.254	3.98	7.91	0.21	2.96	2.107	0.34	11.33	97.91	23	2	242	404	188	29	214
H1-316,4b	0.81	46.45	12.59	10.34	0.256	4.04	7.96	0.22	3.03	2.103	0.36	11.34	98.69	24	3	247	411	188	30	216
H1-317,7	0.12	47.11	12.63	10.55	0.115	4.29	8.91	2.87	0.35	2.294	0.37	10.01	99.50	26	2	274	144	224	29	219
H1-318,7	0.13	46.8	12.62	11.12	0.14	5.91	8.75	2.62	0.03	2.271	0.32	9.61	100.19	27	2	269	29	273	26	201
H1-319,7	0.1	45.65	11.56	10.58	0.167	5.69	10.05	2.67	0.06	2.121	0.33	12	100.88	25	1	258	43	242	32	197
H1-321,1	0.04	49.1	12.51	10.48	0.125	5.22	7.11	3.25	0.05	2.296	0.35	9.52	100.01	24	1	250	33	209	26	219
H1-322,1	2.6	48.03	16.94	7.33	0.166	2.12	5.04	2.3	3.91	3.414	0.55	8.82	98.62	21	3	311	417	167	24	263
H1-322,4	4.11	41.4	15.51	11.83	0.182	3.14	6.91	0.53	4.64	2.664	0.91	10.68	98.40	12	3	161	466	186	35	341
H1-325,4	0.27	58.48	5.8	5.36	0.309	3.4	9.12	2.36	0.57	0.417	0.4	12.33	98.55	5	< 1	29	81	184	22	81
H1-325,6	2.31	42.05	17.75	8.98	0.194	2.49	6.61	2.02	4.41	4.37	0.59	9.22	98.68	23	3	390	501	209	33	343
H1-325,9	2.97	42.38	12.64	10.3	0.302	3.76	9.13	0.51	3.64	2.596	0.64	12.25	98.15	14	2	211	494	223	31	317
H1-326,6	2	42.33	15.24	7.19	0.275	2.91	8.35	2.78	3.46	3.349	0.86	10.63	97.37	16	2	262	588	227	31	368
H1-327,1	0.15	39.19	11.53	9.8	0.155	6.59	13.14	2.67	0.31	2.797	0.31	13.56	100.05	37	1	323	352	507	24	110
H1-327,3	0.4	31.54	9.98	10.04	0.198	6.34	18.11	1.76	0.51	2.435	0.28	17.32	98.51	30	1	291	278	572	18	90
H1-327,9	0.28	37.35	12.39	9.98	0.147	5.94	12.51	3.47	1.52	2.998	0.32	11.48	98.11	32	1	353	764	359	15	111
H1-328,2	0.42	37.23	11.88	10.43	0.154	7.93	13.63	2.6	1.34	2.622	0.25	11.45	99.52	33	1	335	631	439	14	96
H1-328,4	1.68	40.73	11.27	12.14	0.128	8.17	10.61	2.43	1.27	2.523	0.29	9.72	99.28	30	1	341	613	294	18	149
H1-329,0	0.07	37.16	8.36	8.27	0.217	6.35	18.66	2.05	2.42	2.103	0.21	14.64	100.44	34	1	269	1053	509	16	114
H1-330,3	0.14	42.68	10.23	10.72	0.161	9.71	11.3	2.51	1.47	2.58	0.29	8.64	100.29	36	1	305	627	261	18	144
H1-331,6	0.26	42.71	9.98	6.99	0.193	7.08	15.25	3.32	0.69	2.312	0.34	11.11	99.98	26	1	238	315	327	19	139
H1-332,0	0.5	45.56	9.18	9.08	0.155	8.82	12.14	2.76	0.84	2.72	0.47	7.85	99.58	36	1	297	340	262	20	163
H1-334,1	0.23	41.53	11.15	10.8	0.158	7.92	11.43	2.88	2.63	2.725	0.32	8.71	100.25	36	2	344	1008	315	19	159
H1-335,1	0.18	41.83	10.19	9.68	0.172	7.86	12.52	3.07	1.6	2.527	0.29	8.56	98.30	34	1	296	556	254	22	143

sample	Cr	Co	Ni	Cd	Cu	Zn	Ga	Ge	As	Rb	Nb	Mo	Ag	In	Sn	Sb	Cs	La	Ce	Pr
	ppm	ppm	ppm	ppm	ppm	ppm	ppm	ppm	ppm	ppm	ppm	ppm	ppm	ppm	ppm	ppm	ppm	ppm	ppm	ppm
Analysis Method	FUS-MS	FUS-MS	FUS-MS	FUS-MS	FUS-MS	FUS-MS	FUS-MS	FUS-MS	FUS-MS	FUS-MS	FUS-MS	FUS-MS	FUS-MS	FUS-MS	FUS-MS	FUS-MS	FUS-MS	FUS-MS	FUS-MS	FUS-MS
H1 drill core																				
H1-314,6	130	26	40		< 10	140	17	1	19	48	22	2	< 0.5	< 0.2	2	1.1	2.2	29.4	64.3	7.84
H1-315,6	80	44	70		40	< 30	19	3	19	97	25	7	< 0.5	< 0.2	2	0.7	4.2	41.5	83.1	9.1
H1-316,4a	120	27	40		20	80	19	1	63	76	25	< 2	< 0.5	< 0.2	2	0.6	3.3	29.8	66.3	8
H1-316,4b	120	28	30		20	70	18	1	66	78	25	< 2	< 0.5	< 0.2	2	0.7	3.4	29.8	65.8	7.93
H1-317,7	150	37	70		50	130	18	1	5	9	28	2	< 0.5	< 0.2	2	0.8	0.8	30.6	64.7	8.32
H1-318,7	180	36	80		10	120	19	3	10	< 2	24	< 2	< 0.5	< 0.2	2	1.5	< 0.5	28.2	65.3	7.4
H1-319,7	180	36	60		30	120	17	1	< 5	< 2	25	< 2	< 0.5	< 0.2	2	1.3	0.7	31.1	64.3	8.49
H1-321,1	130	33	50		10	140	18	1	< 5	< 2	26	2	< 0.5	< 0.2	2	1.3	< 0.5	29.4	64.8	7.98
H1-322,1	90	30	70		10	40	27	3	< 5	96	49	9	< 0.5	< 0.2	2	0.9	4.1	70.4	127	13.3
H1-322,4	20	25	90		60	< 30	22	< 1	< 5	115	62	4	< 0.5	< 0.2	2	1	4.5	50.2	108	13.3
H1-325,4	60	7	140		20	120	4	< 1	< 5	14	6	2	< 0.5	< 0.2	2	0.5	0.8	9.4	19.1	2.37
H1-325,6	60	21	70		60	30	25	< 1	< 5	110	55	3	< 0.5	< 0.2	2	1.1	4.1	54.6	113	14.1
H1-325,9	< 20	40	50		30	1540	19	2	< 5	90	52	2	< 0.5	< 0.2	2	1.4	3.7	74.2	144	15.1
H1-326,6	< 20	18	50		< 10	9230	25	3	< 5	86	65	3	< 0.5	0.2	3	1.1	3.6	50.4	108	12.3
H1-327,1	300	35	80		< 10	390	14	1	< 5	5	15	< 2	0.7	< 0.2	1	0.8	2.2	25.5	51.1	6.23
H1-327,3	210	35	60		10	40	13	< 1	< 5	6	14	< 2	< 0.5	< 0.2	1	0.6	1.9	23.5	47.1	5.71
H1-327,9	160	48	80		30	60	14	1	5	23	15	< 2	< 0.5	< 0.2	1	0.5	10.1	12.4	29.1	3.77
H1-328,2	270	57	100		30	50	15	2	7	24	14	< 2	< 0.5	< 0.2	1	1.5	11.6	12.8	28.7	3.61
H1-328,4	150	67	80		70	80	14	< 1	5	19	19	< 2	< 0.5	< 0.2	1	1.3	9.5	15.3	35.6	4.64
H1-329,0	580	40	140		60	80	11	1	< 5	40	15	< 2	< 0.5	< 0.2	1	0.5	16.8	13.3	30.5	4.03
H1-330,3	530	47	130		100	100	14	1	< 5	24	18	< 2	< 0.5	< 0.2	1	0.6	9.9	18.7	42.6	5.44
H1-331,6	280	26	90		60	60	11	2	5	13	20	< 2	< 0.5	< 0.2	1	0.6	4.5	20	45.8	5.19
H1-332,0	390	50	120		90	120	11	1	5	13	21	< 2	< 0.5	< 0.2	1	0.6	5.1	23.6	52.1	6.46
H1-334,1	520	52	140		140	90	15	1	< 5	40	23	< 2	< 0.5	< 0.2	1	0.5	15.7	17.5	40.5	5.42
H1-335,1	470	48	130		100	70	14	2	6	27	23	< 2	< 0.5	< 0.2	1	0.8	10.2	17.4	39.3	5.13

sample	Nd	Sm	Eu	Gd	Tb	Dy	Ho	Er	Tm	Yb	Lu	Hf	Ta	W	Tl	Pb	Bi	Th	U
	ppm	ppm	ppm	ppm	ppm	ppm	ppm	ppm	ppm	ppm	ppm	ppm	ppm	ppm	ppm	ppm	ppm	ppm	ppm
Analysis Method	FUS-MS	FUS-MS	FUS-MS	FUS-MS	FUS-MS	FUS-MS	FUS-MS	FUS-MS	FUS-MS	FUS-MS	FUS-MS	FUS-MS	FUS-MS	FUS-MS	FUS-MS	FUS-MS	FUS-MS	FUS-MS	FUS-MS
H1 drill core																			
H1-314,6	32.7	6.8	1.68	5.4	0.8	4.3	0.8	2.2	0.31	2	0.32	4.5	1.6	5	0.2	14	< 0.4	4.3	1.2
H1-315,6	34.6	6.9	1.56	5.3	0.8	4.6	0.9	2.6	0.38	2.3	0.33	5.8	2.1	3	0.4	12	< 0.4	5.6	3.9
H1-316,4a	33.3	7.1	1.73	6.3	1	6.3	1.1	3	0.4	2.5	0.39	5.1	1.8	5	0.3	87	< 0.4	5	1.4
H1-316,4b	33	7	1.74	6.3	1	6.3	1.1	3.1	0.38	2.5	0.39	5.3	1.8	3	0.3	93	< 0.4	5	1.4
H1-317,7	34.9	8.1	2.09	7.3	1.2	6.6	1.1	3	0.4	2.3	0.37	5.5	1.9	2	< 0.1	20	< 0.4	5.3	1.4
H1-318,7	32	7	2.01	5.8	1	5.3	1	2.7	0.39	2.3	0.34	5.3	1.8	< 1	< 0.1	8	< 0.4	4.7	1.3
H1-319,7	36.4	8.4	2.58	8	1.2	6.7	1.2	3	0.4	2.4	0.38	4.8	1.7	2	< 0.1	26	< 0.4	4.5	1.2
H1-321,1	33.2	7.3	2.01	6.2	1	5.4	1	2.7	0.35	2.2	0.34	5.4	1.9	6	< 0.1	12	< 0.4	5	1.4
H1-322,1	54.7	9.8	3.09	7.3	1	5.5	1	2.5	0.35	2.2	0.31	7	3.4	3	0.4	15	< 0.4	6	2.2
H1-322,4	55	11.2	2.91	8.6	1.3	7	1.3	3.5	0.48	3	0.45	6.5	4.1	13	0.4	16	< 0.4	5.6	1.9
H1-325,4	10.6	2.5	0.91	3.2	0.6	3.7	0.7	1.7	0.19	1.2	0.17	1.7	0.6	80	< 0.1	17	< 0.4	1.5	0.6
H1-325,6	57.6	11.7	3.25	9.6	1.3	7.1	1.2	3.2	0.42	2.5	0.4	8.2	3.8	17	0.4	184	< 0.4	5.2	1.9
H1-325,9	60.1	11.3	3.13	8.6	1.2	6.3	1.1	2.9	0.41	2.6	0.41	7.4	3.6	< 1	0.4	1500	< 0.4	4.9	1.6
H1-326,6	53.7	10.5	2.85	8.3	1.1	6.3	1.2	3.1	0.41	2.5	0.39	9.2	4.5	2	0.4	92	< 0.4	5.5	1.6
H1-327,1	26.2	5.2	2.9	5.3	0.9	4.8	0.8	2	0.22	1.3	0.2	2.9	1	< 1	< 0.1	273	< 0.4	1.4	0.5
H1-327,3	24.9	5.2	3.2	4.8	0.7	3.5	0.6	1.6	0.19	1	0.14	2.2	0.9	1	< 0.1	14	< 0.4	1	0.4
H1-327,9	17.8	3.9	1.33	3.8	0.5	3.1	0.5	1.4	0.18	1.1	0.17	2.8	1.1	< 1	0.2	9	< 0.4	1.4	0.4
H1-328,2	17.9	3.8	1.34	3.6	0.5	2.9	0.5	1.3	0.19	1.1	0.15	2.7	1	< 1	0.2	8	< 0.4	1.2	0.4
H1-328,4	21	4.7	1.4	4.5	0.7	3.9	0.7	1.9	0.24	1.5	0.23	3.8	1.3	33	0.1	12	< 0.4	1.8	0.6
H1-329,0	18.9	4.2	1.29	3.9	0.6	3.3	0.6	1.6	0.2	1.2	0.19	2.9	1.1	9	0.2	10	< 0.4	1.5	0.4
H1-330,3	24.6	5.1	1.62	4.7	0.7	4	0.7	1.8	0.25	1.5	0.24	3.4	1.4	13	0.1	8	< 0.4	2.1	0.6
H1-331,6	24.2	5.5	1.72	4.7	0.7	3.9	0.7	1.9	0.25	1.6	0.23	3.5	1.5	< 1	< 0.1	13	< 0.4	2.2	0.7
H1-332,0	28	5.8	1.88	5.1	0.8	4.2	0.8	2	0.27	1.6	0.25	3.9	1.6	6	< 0.1	15	< 0.4	2.7	0.7
H1-334,1	24.8	5.4	1.65	5	0.7	4.1	0.8	1.9	0.26	1.5	0.24	4	1.5	3	0.2	6	< 0.4	2.3	0.7
H1-335,1	23.1	5.7	1.94	5.3	0.8	4.5	0.8	2.2	0.28	1.8	0.27	3.8	1.6	< 1	0.1	6	< 0.4	2.1	0.7

sample	Total S	SiO2	Al2O3	Fe2O3(T)	MnO	MgO	CaO	Na2O	K2O	TiO2	P2O5	LOI	Total	Sc	Be	V	Ba	Sr	Y	Zr
	%	%	%	%	%	%	%	%	%	%	%	%	%	ppm	ppm	ppm	ppm	ppm	ppm	ppm
Analysis Method	CS	FUS-ICP	FUS-ICP	FUS-ICP	FUS-ICP	FUS-ICP	FUS-ICP	FUS-ICP	FUS-ICP	FUS-ICP	FUS-ICP	GRAV	FUS-ICP	FUS-ICP	FUS-ICP	FUS-ICP	FUS-ICP	FUS-ICP	FUS-ICP	FUS-ICP
H1 drill core																				
H1-390,0	< 0.01	24.51	8.3	4.26	0.225	4.29	26.58	0.06	3.11	1.234	0.34	26.41	99.32	9	2	121	479	192	21	172
H1-392,3	0.65	18.77	8.24	7.59	0.257	3.86	29.93	0.05	2.31	0.79	0.26	26.61	98.67	9	2	100	310	162	25	154
H1-393,3	1.2	14.1	4.06	7.72	0.244	3.37	36.82	0.04	0.79	0.245	2.8	27.74	97.93	4	< 1	168	135	257	50	120
H1-394,2	1.29	13.17	3.29	6.74	0.244	2.59	39.41	0.05	0.77	0.185	0.23	31.47	98.15	4	< 1	142	114	279	33	75
H1-395,9	0.19	10.65	3.52	6.38	0.226	1.73	41.72	0.02	0.37	0.332	0.22	34.12	99.29	4	< 1	33	109	243	26	67
H1-397,2	0.3	11.49	3.7	3.85	0.219	1.06	42.96	0.02	0.83	0.213	0.12	34.79	99.25	4	< 1	45	320	458	23	52
H1-397,8	0.12	9.16	3.2	3.92	0.233	0.77	43.79	0.04	0.64	0.214	0.14	36.04	98.15	4	< 1	41	365	279	23	48
H1-398,1	< 0.01	7.82	2.3	3.62	0.232	1.57	46.43	0.03	0.32	0.127	0.12	37.99	100.56	3	< 1	24	141	378	16	30
H1-398,6	0.08	21.22	9.35	3.99	0.179	1.44	33.1	0.1	2.38	0.47	0.16	27.61	100.00	9	2	90	4642	299	22	86
H1-399,3	0.81	60.12	2.86	6.26	0.272	0.83	13.23	0.01	0.25	0.103	0.07	12.89	96.90	3	< 1	19	14210	220	10	23
H1-400,1	0.22	35.39	6.1	8.09	0.472	5.38	18.49	0.09	1.65	0.377	0.07	23.54	99.65	5	2	40	2629	433	21	156
H1-400,3	0.86	45.02	16.91	5.78	0.073	1.91	12.18	0.27	4.4	0.77	0.08	10.68	98.07	17	4	127	4408	448	23	105
H1-400,4	0.29	32.78	8.39	9.09	0.544	5.59	17.33	0.12	2.22	0.471	0.08	22.93	99.55	7	3	57	4311	395	23	158
H1-401,1	3.21	42.99	9.06	13.49	0.714	2.32	10.59	0.97	1.94	0.412	0.11	11.15	93.75	8	3	59	12520	548	8	87
H1-401,4	1.79	34.22	12.52	5.67	0.169	1.59	15.46	0.81	2.63	0.497	0.1	11.67	85.34	11	4	78	11970	394	22	68
H1-401,9	0.25	37.49	7.86	6.89	0.253	4.49	18.33	0.11	2.26	0.466	0.1	21.92	100.17	6	3	49	3621	430	28	217
H1-402,7	0.04	13.8	3.97	4.04	0.195	1.35	41.13	0.02	0.82	0.235	0.14	34.1	99.80	4	< 1	40	811	401	19	63
H1-403,2	0.15	20.18	3.77	4.95	0.173	3.29	33.86	0.04	0.9	0.192	0.05	31.47	98.88	4	< 1	27	934	432	33	60
H1-403,5	0.7	31.71	11.6	5.24	0.083	2.58	23.07	0.95	2.54	0.555	0.1	19.98	98.41	10	2	76	862	679	26	105
H1-403,8	1.21	35.92	18.37	7.01	0.053	2.72	14.61	0.44	4.37	0.79	0.1	14.21	98.59	19	3	133	1300	629	27	103
H1-404,4	1.16	37.18	14.4	5.8	0.064	1.86	19.12	1.01	3.02	0.576	0.12	15.2	98.35	14	3	92	481	356	24	72
H1-404,4	0.87	45.52	19.27	6.21	0.035	2.53	8.96	1.33	4.06	0.824	0.16	10.55	99.45	19	3	125	670	290	16	104
H1-406,5	0.2	31.74	11.73	4.69	0.075	2.78	23.41	0.62	2.54	0.576	0.14	21.95	100.25	11	2	74	336	436	23	144
H1-407,6	0.13	38.94	17.01	4.07	0.055	2.18	16.28	0.47	3.99	0.801	0.14	15.95	99.89	15	3	115	469	271	17	169
H1-408,6	0.17	37.99	10	4.69	0.083	3.21	20.51	0.87	2.02	0.556	0.12	20.55	100.60	9	2	63	267	368	22	156
H1-409,5	0.43	48.22	15.22	5.23	0.052	3.09	10.02	1.14	3.19	0.728	0.12	11.51	98.52	13	3	99	375	207	26	200
H1-410,5	0.44	52.25	16.91	6.84	0.044	3.26	6.64	0.9	3.15	0.711	0.15	7.7	98.56	14	3	95	418	176	28	204
H1-411,5	0.02	32.97	10	4.57	0.108	2.95	23.97	0.65	1.98	0.544	0.1	22.84	100.68	9	2	65	276	353	17	162
H1-412,5	0.08	26.02	10.07	3.98	0.115	1.45	30.03	0.7	2.11	0.572	0.12	25.5	100.67	8	2	58	272	381	28	151
H1-413,6	0.09	29.96	9.75	3.93	0.088	1.77	27.47	0.52	1.93	0.467	0.09	23.22	99.20	9	2	58	216	417	19	106
H1-414,3	0.04	29.48	11.36	4.48	0.101	1.88	26.55	0.59	2.3	0.54	0.1	23.19	100.57	10	2	66	270	340	27	161
H1-415,4	0.08	31.11	11.66	4.75	0.092	2.05	25.49	0.61	2.25	0.553	0.09	21.86	100.52	11	2	72	233	413	17	114
H1-416,5	0.08	29.53	12.02	4.76	0.101	2.1	25.98	0.74	2.27	0.559	0.1	22.5	100.66	11	2	74	248	394	21	110
H1-417,5	0.06	33.75	9.95	4.61	0.099	2.91	23.6	0.56	2.05	0.544	0.1	22.44	100.61	9	2	66	279	381	19	156
H1-418,4	0.31	24.11	9.04	4.33	0.117	1.47	31.73	0.71	1.71	0.42	0.1	25.86	99.60	6	2	37	200	477	27	225
H1-420,4a	0.08	21.11	6.44	2.78	0.117	1.33	36.23	0.46	1.3	0.324	0.08	30.21	100.38	6	1	44	187	622	19	81
H1-420,4b	0.07	20.09	6.08	2.6	0.11	1.24	34.8	0.45	1.22	0.302	0.08	30.16	97.13	6	1	42	175	581	17	72
H1-421,3	0.06	42.72	17.62	5.21	0.058	2.23	12.73	0.74	3.73	0.799	0.11	13.57	99.52	15	3	109	495	294	17	186
H1-423,2	1.3	33.64	13.73	6.75	0.1	2.12	20.63	0.62	2.57	0.826	0.21	17.16	98.36	11	3	94	308	531	25	154

sample	Cr	Co	Ni	Cd	Cu	Zn	Ga	Ge	As	Rb	Nb	Mo	Ag	In	Sn	Sb	Cs	La	Ce	Pr
	ppm	ppm	ppm	ppm	ppm	ppm	ppm	ppm	ppm	ppm	ppm	ppm	ppm	ppm	ppm	ppm	ppm	ppm	ppm	ppm
Analysis Method	FUS-MS	FUS-MS	FUS-MS	FUS-MS	FUS-MS	FUS-MS	FUS-MS	FUS-MS	FUS-MS	FUS-MS	FUS-MS	FUS-MS	FUS-MS	FUS-MS	FUS-MS	FUS-MS	FUS-MS	FUS-MS	FUS-MS	FUS-MS
H1 drill core																				
H1-390,0	100	< 1	< 20		< 10	< 30	12	1	29	46	33	< 2	< 0.5	< 0.2	2	2.4	2.3	34.4	66.8	7.57
H1-392,3	70	< 1	< 20		20	30	11	< 1	< 5	40	21	< 2	< 0.5	< 0.2	1	< 0.5	1.7	27.5	54.3	6.12
H1-393,3	40	6	50		70	50	7	< 1	200	16	14	3	< 0.5	< 0.2	1	0.5	0.9	31.3	67.2	7.36
H1-394,2	60	5	50		50	50	5	< 1	686	14	6	< 2	< 0.5	< 0.2	< 1	1	0.6	37.6	72.6	8.25
H1-395,9	30	< 1	< 20		< 10	40	5	< 1	< 5	8	12	< 2	< 0.5	< 0.2	< 1	< 0.5	0.6	35.8	57.7	7.01
H1-397,2	< 20	6	20		30	90	5	< 1	16	20	5	2	< 0.5	< 0.2	1	< 0.5	1	40	69.7	8.21
H1-397,8	< 20	< 1	< 20		10	< 30	5	< 1	10	18	6	< 2	< 0.5	< 0.2	< 1	< 0.5	0.8	43.1	74.4	7.92
H1-398,1	< 20	< 1	< 20		20	40	3	< 1	< 5	11	3	< 2	< 0.5	< 0.2	< 1	0.6	< 0.5	22.1	35.4	4.16
H1-398,6	60	< 1	< 20		60	30	12	1	14	81	11	< 2	< 0.5	< 0.2	1	2.2	3.3	31.2	53.8	5.71
H1-399,3	< 20	< 1	< 20		30	190	5	1	< 5	5	2	< 2	2.2	< 0.2	< 1	2.9	< 0.5	20.3	32.7	3.33
H1-400,1	40	4	20		10	120	8	< 1	< 5	69	9	< 2	< 0.5	< 0.2	1	0.7	2.8	14.4	29.8	3.44
H1-400,3	90	14	40		30	90	23	2	< 5	169	18	< 2	< 0.5	< 0.2	2	0.9	6.6	33.2	69.4	7.28
H1-400,4	50	6	30		20	100	11	< 1	13	86	13	< 2	< 0.5	< 0.2	1	0.7	3.6	29.5	58.3	6.74
H1-401,1	50	18	40		190	140	17	1	< 5	62	10	< 2	< 0.5	< 0.2	1	2.6	2.3	34.4	57	6.37
H1-401,4	70	12	40		60	120	17	1	11	107	12	< 2	18.6	< 0.2	3	49.5	4.5	34.4	63.1	7.57
H1-401,9	40	3	20		10	120	10	< 1	< 5	89	12	< 2	< 0.5	< 0.2	2	0.5	3.6	28.8	56.4	6.43
H1-402,7	20	< 1	< 20		40	40	5	< 1	6	28	5	< 2	< 0.5	< 0.2	1	< 0.5	1.1	22.1	36.6	4.28
H1-403,2	20	< 1	< 20		< 10	50	5	< 1	< 5	32	5	< 2	< 0.5	< 0.2	1	1	1.5	31.8	60.6	7.05
H1-403,5	70	1	< 20		20	60	16	< 1	< 5	106	16	< 2	< 0.5	< 0.2	2	0.5	4.4	38.5	77.1	8
H1-403,8	100	15	50		30	130	24	< 1	< 5	176	19	< 2	< 0.5	< 0.2	3	1.1	7.2	36	70.6	8.24
H1-404,4	80	33	30		30	70	20	1	< 5	129	13	< 2	< 0.5	< 0.2	2	0.5	5.1	58	103	10.9
H1-404,4	100	18	40		30	120	24	< 1	< 5	171	18	< 2	< 0.5	< 0.2	2	0.7	7	31	62.6	7.08
H1-406,5	60	6	30		30	90	15	< 1	< 5	105	15	< 2	< 0.5	< 0.2	2	< 0.5	4.8	24.9	48.1	5.65
H1-407,6	90	10	40		30	120	22	1	5	163	22	< 2	< 0.5	< 0.2	4	0.6	6.6	28	52.4	5.92
H1-408,6	50	8	40		20	80	12	< 1	< 5	85	14	< 2	< 0.5	< 0.2	2	< 0.5	3.8	20.9	42.4	5.02
H1-409,5	80	12	30		30	100	20	2	< 5	145	18	< 2	< 0.5	< 0.2	2	0.5	6.3	42.6	86.7	9.39
H1-410,5	80	12	40		30	160	23	2	< 5	143	24	< 2	< 0.5	< 0.2	3	0.7	6.8	37.9	85.4	8.96
H1-411,5	50	4	30		30	90	12	< 1	< 5	91	18	< 2	< 0.5	< 0.2	2	< 0.5	4.1	23.8	47.2	5.45
H1-412,5	60	3	30		30	60	12	< 1	< 5	87	25	< 2	< 0.5	< 0.2	2	< 0.5	3.7	30.5	63.4	7.24
H1-413,6	50	< 1	< 20		20	60	13	1	< 5	91	13	< 2	< 0.5	< 0.2	2	< 0.5	3.9	21.5	46	4.97
H1-414,3	50	5	30		30	80	15	< 1	< 5	99	23	< 2	< 0.5	< 0.2	2	< 0.5	4.3	43.1	79.3	9.24
H1-415,4	60	3	20		40	90	16	1	< 5	101	14	< 2	< 0.5	< 0.2	2	< 0.5	4.7	20.6	37.7	4.38
H1-416,5	60	10	30		30	90	15	1	< 5	99	13	< 2	< 0.5	< 0.2	2	< 0.5	4.6	27.7	55.6	6.59
H1-417,5	50	8	30		30	80	12	< 1	< 5	93	16	< 2	< 0.5	< 0.2	2	< 0.5	4.3	17.6	38.8	4.6
H1-418,4	30	< 1	< 20		60	60	11	< 1	< 5	81	37	< 2	< 0.5	< 0.2	2	< 0.5	3.3	23.5	51.5	5.55
H1-420,4a	30	< 1	< 20		< 10	60	8	< 1	5	58	9	< 2	< 0.5	< 0.2	1	< 0.5	2.5	18.4	34.8	4.22
H1-420,4b	30	2	< 20		< 10	50	8	< 1	8	57	9	< 2	< 0.5	< 0.2	1	1.1	2.3	18.9	34.5	4.48
H1-421,3	90	11	40		20	120	24	2	5	174	28	< 2	< 0.5	< 0.2	4	< 0.5	7.5	32.4	64.7	7.17
H1-423,2	70	4	30		50	90	19	1	< 5	121	37	< 2	< 0.5	< 0.2	3	0.8	5.2	42.5	84	8.77

sample	Nd	Sm	Eu	Gd	Tb	Dy	Ho	Er	Tm	Yb	Lu	Hf	Ta	W	Tl	Pb	Bi	Th	U
	ppm	ppm	ppm	ppm	ppm	ppm	ppm	ppm	ppm	ppm	ppm	ppm	ppm	ppm	ppm	ppm	ppm	ppm	ppm
Analysis Method	FUS-MS	FUS-MS	FUS-MS	FUS-MS	FUS-MS	FUS-MS	FUS-MS	FUS-MS	FUS-MS	FUS-MS	FUS-MS	FUS-MS	FUS-MS	FUS-MS	FUS-MS	FUS-MS	FUS-MS	FUS-MS	FUS-MS
H1 drill core																			
H1-390,0	31.4	6.3	1.59	5.1	0.8	4	0.7	2	0.27	1.7	0.26	4.3	2.2	2	0.1	10	< 0.4	5.1	3.4
H1-392,3	25.2	5.3	1.22	4.4	0.7	4.2	0.9	2.5	0.36	2.3	0.37	3.6	1.4	< 1	0.2	37	< 0.4	5.6	1.7
H1-393,3	32.9	8.3	1.91	9.9	1.6	9.6	1.8	4.9	0.62	4.2	0.59	2.4	0.8	6	< 0.1	36	< 0.4	3.6	7.8
H1-394,2	33.1	7	1.75	6.5	1	5.7	1.1	3.1	0.44	2.9	0.43	1.8	0.3	5	< 0.1	29	< 0.4	3	1.6
H1-395,9	29	5.3	1.61	5.2	0.8	4.3	0.8	2.2	0.3	1.8	0.28	1.6	0.7	2	< 0.1	7	< 0.4	2.3	0.7
H1-397,2	33.1	6.4	1.87	5.3	0.8	3.9	0.7	2	0.27	1.6	0.24	1.2	0.3	< 1	< 0.1	11	< 0.4	3.1	1.1
H1-397,8	32.7	6.2	1.86	5.1	0.7	3.8	0.7	1.8	0.24	1.5	0.22	1	0.3	1	< 0.1	< 5	< 0.4	2.1	0.6
H1-398,1	17.1	3.2	1.24	3.1	0.4	2.2	0.4	1.2	0.17	1	0.16	0.7	0.2	2	< 0.1	7	< 0.4	1.6	0.3
H1-398,6	23.2	4.5	1.32	4.2	0.6	3.5	0.7	1.9	0.28	1.7	0.25	2.2	0.6	< 1	0.3	10	< 0.4	6	1.5
H1-399,3	13.6	2.3	0.69	1.9	0.3	1.7	0.3	0.9	0.14	0.9	0.14	0.5	0.2	< 1	< 0.1	4120	< 0.4	1.6	0.5
H1-400,1	14.1	3.1	0.69	3.3	0.6	3.6	0.7	2	0.28	1.8	0.28	3.8	0.6	5	0.2	30	< 0.4	6.6	1.6
H1-400,3	27.5	4.9	0.82	3.7	0.6	3.8	0.8	2.5	0.38	2.6	0.41	2.9	1.2	3	0.6	23	< 0.4	14	2.7
H1-400,4	26.9	5.4	1.04	4.9	0.7	4.1	0.8	2.3	0.32	2	0.28	3.9	0.8	5	0.3	51	< 0.4	8.5	2
H1-401,1	22	3.7	0.92	2.5	0.3	1.9	0.4	1.1	0.16	1	0.18	2.6	0.7	6	0.3	1470	< 0.4	8.9	1.6
H1-401,4	28.3	5.4	1.31	4.3	0.7	4.3	0.9	2.5	0.37	2.4	0.4	1.8	0.9	5	< 0.1	89200	2.5	11.1	2.3
H1-401,9	25.6	5.3	1.06	5	0.8	4.6	0.9	2.4	0.35	2.1	0.33	5.1	0.7	< 1	0.3	22	< 0.4	7.9	1.9
H1-402,7	17.6	3.5	1.2	3.2	0.5	3	0.6	1.6	0.22	1.4	0.21	1.6	0.3	2	0.1	8	< 0.4	3.2	1
H1-403,2	28.5	6.2	1.67	5.8	0.9	5	1	2.7	0.34	2	0.28	1.5	0.3	3	0.1	11	< 0.4	3.3	1.2
H1-403,5	32.1	6.1	0.86	4.8	0.8	4.4	0.9	2.4	0.35	2.3	0.33	2.8	0.9	< 1	0.4	8	< 0.4	10.6	2.4
H1-403,8	29.9	5.7	0.81	4.5	0.7	4.7	1	3	0.46	3.1	0.5	2.8	1.2	5	0.6	16	< 0.4	15.6	3.4
H1-404,4	42.5	8.5	1.71	6.6	1	5.1	0.9	2.4	0.32	2.1	0.32	2	0.8	2	0.4	9	< 0.4	11	2.6
H1-404,4	26.6	4.7	0.79	3.5	0.5	3.2	0.6	1.7	0.24	1.5	0.22	2.6	1.2	2	0.6	9	< 0.4	15.3	3.1
H1-406,5	21.7	3.8	0.75	3.5	0.6	3.8	0.8	2.2	0.3	2	0.31	3.5	1	1	0.4	14	< 0.4	9.3	2.5
H1-407,6	22.6	3.9	0.89	3.2	0.5	2.8	0.6	1.7	0.27	1.8	0.27	4.1	1.3	6	0.6	16	< 0.4	12.4	3.2
H1-408,6	19.7	3.6	0.56	3.3	0.6	3.6	0.7	2.1	0.29	1.8	0.29	4	1	13	0.3	15	< 0.4	8.2	2
H1-409,5	36.6	7	1.1	5.1	0.8	4.8	1	2.8	0.39	2.4	0.38	5.6	1.3	< 1	0.6	15	< 0.4	12.9	3.3
H1-410,5	33.6	6.3	0.7	4.3	0.8	4.6	0.9	2.9	0.42	2.6	0.41	5.3	1.6	1	0.6	17	< 0.4	14.3	3
H1-411,5	21.1	4	0.66	3.1	0.5	2.9	0.6	1.7	0.26	1.7	0.25	3.9	1.1	1	0.4	13	< 0.4	9.2	2
H1-412,5	28.8	5.4	0.99	4.7	0.8	4.9	0.9	2.6	0.37	2.3	0.34	3.3	1.7	3	0.3	10	< 0.4	8.6	1.5
H1-413,6	20.6	4	0.69	3.4	0.6	3.5	0.7	2	0.27	1.6	0.25	3	0.9	< 1	0.3	14	< 0.4	7.9	1.6
H1-414,3	34.7	6.8	1.46	5.6	0.8	4.7	0.9	2.5	0.33	2.1	0.31	3.8	1.4	2	0.3	12	< 0.4	8.9	1.8
H1-415,4	17.6	3.3	0.63	2.5	0.4	2.9	0.6	1.7	0.25	1.6	0.26	3	0.9	< 1	0.4	9	< 0.4	9.4	1.6
H1-416,5	25.4	4.4	0.66	3.5	0.6	3.6	0.7	2.1	0.31	1.9	0.28	2.9	0.9	< 1	0.4	11	< 0.4	9.3	1.5
H1-417,5	17.8	3.1	0.52	2.8	0.5	3.1	0.7	2	0.28	1.9	0.29	3.8	1	2	0.4	20	< 0.4	8.6	2.2
H1-418,4	22.5	4.8	0.71	4	0.7	4.3	0.9	2.5	0.35	2.3	0.32	5.8	3	< 1	0.3	14	< 0.4	9.8	2.1
H1-420,4a	16.8	3.4	0.96	3.2	0.5	3	0.6	1.5	0.21	1.2	0.18	1.9	0.5	3	0.2	14	< 0.4	5.2	1.2
H1-420,4b	17	3.7	1.06	3.5	0.6	3.2	0.6	1.6	0.22	1.4	0.2	1.9	0.6	2	0.3	17	< 0.4	5.8	1.2
H1-421,3	25.6	3.7	0.65	3	0.4	2.7	0.6	1.9	0.29	2	0.3	4.2	1.8	3	0.7	13	< 0.4	13.5	2.7
H1-423,2	32.6	6.4	1.14	5	0.8	4.6	0.9	2.4	0.35	2.2	0.31	3.6	2.4	< 1	0.5	16	< 0.4	11.7	2

Table 13: Whole rock geochemistry of samples from the G7 drill core.

sample	Total S	SiO2	Al2O3	Fe2O3(T)	MnO	MgO	CaO	Na2O	K2O	TiO2	P2O5	LOI	Total	Sc	Be	V	Ba	Sr	Y	Zr
	%	%	%	%	%	%	%	%	%	%	%	%	%	ppm	ppm	ppm	ppm	ppm	ppm	ppm
Analysis Method	CS	FUS-ICP	FUS-ICP	FUS-ICP	FUS-ICP	FUS-ICP	FUS-ICP	FUS-ICP	FUS-ICP	FUS-ICP	FUS-ICP	GRAV	FUS-ICP	FUS-ICP	FUS-ICP	FUS-ICP	FUS-ICP	FUS-ICP	FUS-ICP	FUS-ICP
G7 drill core																				
G7-46,2	0.06	69.03	1.67	1.48	0.033	0.58	14.44	0.1	0.33	0.07	< 0.01	12.88	100.61	2	< 1	13	58	580	12	31
G7-47,2	0.13	27.89	5.38	3.98	0.143	1.76	31.63	0.2	1.21	0.228	0.06	28.18	100.66	5	< 1	34	264	1342	19	63
G7-48,6	0.17	42.61	10.8	5.26	0.142	2.13	17.47	0.41	2.28	0.457	0.11	18.72	100.39	10	2	70	237	509	28	91
G7-53,5	0.03	23.08	4.72	9.7	0.519	8.11	21.6	0.08	1.23	0.219	0.12	30.34	99.72	5	2	44	3483	360	17	110
G7-56	0.54	49.83	6.65	6.94	0.362	4.25	12.26	1.05	1.29	0.25	0.12	16.68	99.68	3	2	28	2406	233	12	122
G7-56,3	2.84	46.93	8.34	8.99	0.356	3.92	11.25	0.27	2.11	0.493	0.14	14.8	97.60	4	3	52	4372	215	17	250
G7-56,7	0.56	62.61	10.33	4.47	0.216	1.66	6.59	1.58	2.02	0.479	0.19	9.61	99.76	2	3	36	4202	162	17	238
G7-58,2	4.3	51.48	5.23	11.28	0.521	1.96	5.82	0.2	1.06	0.597	0.22	9.48	87.85	2	1	19	1840	130	14	145
G7-58,5	5.13	42.83	12.6	8.37	0.343	1.83	4.32	0.34	2.79	1.273	0.26	9.53	84.49	2	3	42	5209	120	22	339
G7-59,3	2.08	46.81	3.95	12.22	0.7	2.93	9.78	0.1	0.7	0.677	0.26	12.76	90.89	3	1	45	1184	165	14	84
G7-60,3	2.25	51.81	6.8	16.3	0.477	2.56	7.54	0.08	0.63	1.296	0.59	10.24	98.32	4	1	67	1034	145	15	145
G7-60,6	1.91	54.28	7.9	5.96	0.331	1.8	7.43	0.31	1.92	1.124	0.29	10.64	91.99	3	3	45	3104	148	22	230
G7-62,1	0.44	39.03	13.15	9.24	0.425	3.39	11.85	0.3	3.63	0.675	0.14	17.64	99.47	13	3	109	1162	192	18	121
G7-63,7	< 0.01	12.39	3.67	4.69	0.378	2.21	40.05	0.07	1.01	0.192	0.09	35.92	100.67	4	< 1	38	298	715	13	44
G7-98,4	0.15	42.8	20.62	5.87	0.178	2.03	7.22	1.67	5.24	1.708	0.37	12.17	99.88	4	6	89	561	167	43	544
G7-99,6	0.1	34.93	13.81	10.58	0.427	2.78	12.09	1.22	3.36	2.659	1.16	17.3	100.32	9	4	149	380	285	33	335
G7-100,9	0.99	32.57	13.38	10.72	0.227	2.86	13.71	2.31	2.7	2.457	1.29	16.14	98.36	9	3	142	387	282	33	308
G7-101,5	0.05	33.64	12.43	8.18	0.314	2.59	16.19	2.08	2.49	2.371	0.96	19.11	100.36	8	3	131	307	326	31	320
G7-105,2	0.06	37.37	13.85	11.85	0.302	3.42	10.18	2.18	2.53	2.795	1.06	15.13	100.67	10	3	164	354	347	30	218
G7-106,9	0.07	53.75	14.8	4.96	0.13	1.85	6.43	2.67	3.04	1.531	0.37	10.11	99.64	3	3	50	799	222	33	452
G7-108,25	2.04	36.23	13.35	16.38	0.506	2.24	7.8	0.89	2.41	1.018	0.29	13.52	94.63	2	4	35	499	236	25	391
G7-110,5	0.29	37.34	13.69	6.56	0.237	2.21	15.89	3.19	2.26	0.883	0.22	18.25	100.73	2	4	54	456	403	21	341
G7-112,3	0.08	39.92	10.08	8.29	0.29	3.67	13.51	1.75	2.11	0.75	0.21	19.19	99.77	3	3	56	331	341	27	353
G7-114,7	0.34	38.71	3.6	5.56	0.084	1.4	26.22	0.17	0.93	0.183	0.1	23.34	100.30	4	< 1	24	105	504	16	29
G7-118,8	< 0.01	30.05	11.5	7.31	0.237	2.67	20.15	0.82	3.06	2.049	0.56	21.92	100.33	8	2	156	270	199	22	166
G7-119,25	0.05	26.51	9.51	7.86	0.273	2.4	23.82	0.63	2.61	1.714	0.4	24.89	100.62	7	1	134	202	216	17	142

sample	Cr	Co	Ni	Cd	Cu	Zn	Ga	Ge	As	Rb	Nb	Mo	Ag	In	Sn	Sb	Cs	La	Ce	Pr
	ppm	ppm	ppm	ppm	ppm	ppm	ppm	ppm	ppm	ppm	ppm	ppm	ppm	ppm	ppm	ppm	ppm	ppm	ppm	ppm
Analysis Method	FUS-MS	FUS-MS	FUS-MS	FUS-MS	FUS-MS	FUS-MS	FUS-MS	FUS-MS	FUS-MS	FUS-MS	FUS-MS	FUS-MS	FUS-MS	FUS-MS	FUS-MS	FUS-MS	FUS-MS	FUS-MS	FUS-MS	FUS-MS
G7 drill core																				
G7-46,2	90	< 1	260		< 10	30	2	< 1	< 5	16	2	2	< 0.5	< 0.2	< 1	< 0.5	0.9	5.1	11.1	1.53
G7-47,2	30	< 1	20		< 10	50	7	< 1	< 5	60	8	< 2	< 0.5	< 0.2	1	< 0.5	5.2	13	25.4	2.94
G7-48,6	60	< 1	< 20		10	60	15	< 1	< 5	115	15	< 2	< 0.5	< 0.2	2	0.5	4.5	26	54.5	5.81
G7-53,5	40	< 1	60		< 10	70	7	< 1	< 5	43	8	< 2	< 0.5	< 0.2	1	< 0.5	2	15.4	30.8	3.51
G7-56	< 20	3	< 20		< 10	90	8	< 1	6	45	21	< 2	< 0.5	< 0.2	1	0.9	2.2	24.4	42	4.09
G7-56,3	30	14	30		580	140	12	1	17	74	49	2	< 0.5	< 0.2	2	3.3	3.4	48	78	7.86
G7-56,7	60	7	140		10	490	11	1	6	69	53	2	< 0.5	< 0.2	1	0.7	3.2	36.9	61.9	6.09
G7-58,2	< 20	22	< 20		60	54400	12	2	< 5	39	41	< 2	< 0.5	2.7	3	0.9	1.8	25.7	49.6	5.06
G7-58,5	< 20	32	< 20		20	87700	24	2	< 5	102	93	< 2	< 0.5	< 0.2	3	0.8	4.6	15.6	29.7	3.36
G7-59,3	< 20	24	< 20		10	31600	9	1	5	27	17	< 2	< 0.5	0.4	1	< 0.5	1.1	35.5	67.7	6.69
G7-60,3	< 20	11	< 20		< 10	370	12	2	< 5	26	34	< 2	< 0.5	< 0.2	1	0.5	1.3	24.1	52.6	6.22
G7-60,6	< 20	12	< 20		40	34500	14	1	< 5	73	71	2	< 0.5	0.3	2	0.9	2.8	64.6	106	9.71
G7-62,1	70	12	30		10	50	19	< 1	11	136	14	< 2	< 0.5	< 0.2	2	1.6	4.7	32.9	64.1	6.75
G7-63,7	20	2	< 20		20	40	5	< 1	5	37	5	< 2	< 0.5	< 0.2	1	< 0.5	1.5	14.4	26	3.06
G7-98,4	< 20	6	< 20		< 10	30	27	1	< 5	139	142	< 2	< 0.5	< 0.2	2	1.1	6.1	108	196	20.7
G7-99,6	20	14	60		10	130	20	< 1	< 5	88	77	< 2	< 0.5	< 0.2	2	0.6	4	59.5	120	13.7
G7-100,9	< 20	13	20		< 10	60	21	< 1	< 5	76	80	< 2	< 0.5	< 0.2	2	0.5	3.8	41.1	97.7	11.5
G7-101,5	< 20	9	< 20		< 10	60	16	< 1	< 5	64	72	< 2	< 0.5	< 0.2	2	0.6	3	68.8	129	13.8
G7-105,2	< 20	19	< 20		10	60	20	1	< 5	72	75	< 2	< 0.5	< 0.2	2	0.7	3.4	58.5	119	15.3
G7-106,9	< 20	7	30		< 10	180	18	1	5	76	108	< 2	< 0.5	< 0.2	2	0.7	3.8	53.5	107	12.7
G7-108,25	< 20	36	30		240	5720	23	1	37	56	115	< 2	< 0.5	< 0.2	1	0.7	4.3	58.7	114	11.9
G7-110,5	< 20	< 1	< 20		10	50	18	< 1	< 5	48	115	< 2	< 0.5	< 0.2	2	< 0.5	3.5	30	65.2	6.79
G7-112,3	20	3	40		20	130	12	< 1	9	46	73	< 2	< 0.5	< 0.2	2	0.9	4.9	47.3	84.9	9.61
G7-114,7	< 20	< 1	< 20		20	100	5	< 1	< 5	37	6	< 2	< 0.5	< 0.2	1	0.8	1.4	15.1	28.4	3.25
G7-118,8	< 20	13	< 20		< 10	40	14	< 1	6	75	33	< 2	< 0.5	< 0.2	1	< 0.5	3.9	27	57.4	6.61
G7-119,25	< 20	20	< 20		40	80	11	< 1	< 5	63	28	< 2	< 0.5	< 0.2	1	< 0.5	3	23.1	47	6.13

sample	Nd	Sm	Eu	Gd	Tb	Dy	Ho	Er	Tm	Yb	Lu	Hf	Ta	W	Tl	Pb	Bi	Th	U
	ppm	ppm	ppm	ppm	ppm	ppm	ppm	ppm	ppm	ppm	ppm	ppm	ppm	ppm	ppm	ppm	ppm	ppm	ppm
Analysis Method	FUS-MS	FUS-MS	FUS-MS	FUS-MS	FUS-MS	FUS-MS	FUS-MS	FUS-MS	FUS-MS	FUS-MS	FUS-MS	FUS-MS	FUS-MS	FUS-MS	FUS-MS	FUS-MS	FUS-MS	FUS-MS	FUS-MS
G7 drill core																			
G7-46,2	7.6	2.3	0.6	2.1	0.3	1.7	0.3	0.9	0.13	0.8	0.12	0.6	0.1	155	< 0.1	9	< 0.4	1.3	0.2
G7-47,2	13.2	3.4	1.33	3.4	0.5	3.1	0.6	1.5	0.22	1.4	0.2	1.5	0.5	8	0.2	42	< 0.4	4	1.2
G7-48,6	23.9	5.2	1.12	4.6	0.8	4.8	0.9	2.6	0.36	2.2	0.33	2.4	0.9	8	0.5	12	< 0.4	8.1	1.8
G7-53,5	14.4	3	1.02	3	0.5	3	0.6	1.6	0.22	1.3	0.19	1.6	0.4	25	0.1	40	< 0.4	3	0.7
G7-56	15.1	2.8	0.82	2.3	0.4	2.3	0.4	1.2	0.17	1.1	0.17	2.3	1.8	< 1	0.2	78	< 0.4	3.7	1.3
G7-56,3	25.2	3.5	0.9	3.1	0.5	3.5	0.7	2	0.31	2.1	0.33	5.4	4	4	0.3	50	< 0.4	7.2	2.7
G7-56,7	20.2	3.1	0.87	2.8	0.4	2.6	0.6	1.6	0.24	1.6	0.25	4.6	4.3	78	0.3	64	< 0.4	6	2.8
G7-58,2	21.1	4.6	1.46	3.3	0.6	2.9	0.5	1.4	0.19	1.2	0.16	3.2	3	< 1	0.2	40	< 0.4	3.5	1
G7-58,5	15.4	3.9	1.32	3.7	0.6	4.1	0.9	2.5	0.35	2.3	0.31	7.8	7	< 1	0.4	22	< 0.4	7.4	2.3
G7-59,3	26.7	5.2	1.99	3.9	0.6	2.9	0.5	1.2	0.16	1	0.13	1.9	1.1	< 1	0.1	17	< 0.4	1.9	0.8
G7-60,3	28.1	6.3	2.11	4.8	0.6	3.2	0.5	1.4	0.19	1.1	0.15	3.5	2.1	< 1	< 0.1	18	< 0.4	3.2	1.1
G7-60,6	34.2	6	1.95	4.9	0.8	4.3	0.8	2.2	0.31	2	0.29	5.4	6.1	8	0.3	353	< 0.4	7	2.4
G7-62,1	26	4.8	0.98	3.7	0.6	3.4	0.6	1.9	0.28	1.7	0.25	3.2	1	< 1	0.6	10	< 0.4	8.8	2.5
G7-63,7	12.5	2.3	0.59	2.2	0.3	2	0.4	1.1	0.16	1.1	0.17	0.9	0.3	3	0.1	9	< 0.4	2.3	0.7
G7-98,4	71.6	12.4	3.53	9.2	1.3	7.7	1.4	4.1	0.57	3.5	0.5	9.9	8.9	5	0.4	< 5	< 0.4	14.1	3.8
G7-99,6	55	10.6	3.48	8.6	1.2	6.5	1.1	3.1	0.43	2.5	0.37	6.4	4.5	31	0.2	13	< 0.4	7.7	2.4
G7-100,9	54	10.8	3.02	8.6	1.2	6.6	1.2	3.2	0.41	2.5	0.37	7.2	4.5	< 1	0.2	11	< 0.4	6.7	2.5
G7-101,5	52.8	10	2.98	7.5	1.1	5.9	1.1	2.8	0.38	2.3	0.34	7	4.2	13	0.2	6	< 0.4	7	2.2
G7-105,2	60.8	11.6	3.49	8.9	1.2	6.8	1.1	3	0.42	2.7	0.41	5.3	4.8	2	0.2	< 5	< 0.4	7.3	2.1
G7-106,9	47.4	9.2	2.72	7.2	1.1	6.4	1.2	3.3	0.46	3	0.47	9	8.1	16	0.3	21	< 0.4	9.3	2.2
G7-108,25	45.2	8.2	2.43	5.5	0.8	4.5	0.9	2.5	0.36	2.3	0.35	9.1	7.9	< 1	0.2	132	< 0.4	8.8	3
G7-110,5	28	5.3	1.64	3.6	0.6	3.9	0.8	2.2	0.32	2.1	0.31	7	7.5	< 1	0.1	7	< 0.4	9.4	2.5
G7-112,3	33.6	6	1.94	4.9	0.8	4.8	0.9	2.7	0.38	2.6	0.42	6.5	5.5	16	0.2	6	< 0.4	7.7	3.3
G7-114,7	14.2	3.3	1.28	3.1	0.5	2.8	0.5	1.3	0.17	1	0.16	0.6	0.3	< 1	0.1	19	< 0.4	3.4	1.2
G7-118,8	28.6	5.9	1.89	5.2	0.8	4.3	0.8	2.1	0.28	1.7	0.23	3.9	2.1	< 1	0.2	6	< 0.4	2.5	0.7
G7-119,25	25.3	5.5	1.77	4.4	0.7	3.7	0.7	1.7	0.22	1.4	0.22	3.3	1.8	< 1	0.2	8	< 0.4	2.3	0.6

Table 14: Whole rock geochemistry of samples from Kaltenberg-Burgstall, Haufenreith, Peggau-Taschen, Arzwaldgraben, Kalkrippe, and Arzberg.

sample	Total S	SiO2	Al2O3	Fe2O3(T)	MnO	MgO	CaO	Na2O	K2O	TiO2	P2O5	LOI	Total	Sc	Be	V	Ba	Sr	Y	Zr
	%	%	%	%	%	%	%	%	%	%	%	%	%	ppm	ppm	ppm	ppm	ppm	ppm	ppm
Analysis Method	CS	FUS-ICP	FUS-ICP	FUS-ICP	FUS-ICP	FUS-ICP	FUS-ICP	FUS-ICP	FUS-ICP	FUS-ICP	FUS-ICP	GRAV	FUS-ICP	FUS-ICP	FUS-ICP	FUS-ICP	FUS-ICP	FUS-ICP	FUS-ICP	FUS-ICP
Kaltenberg-Burgstall																				
US01	0.18	15.34	4.78	3.11	0.345	1.2	41.09	0.06	1.47	0.274	0.15	32.31	100.13	4	2	50	4577	454	18	65
US02A	2.85	42.31	13.54	7.79	0.124	1.41	1.37	0.44	4.06	0.662	0.11	5.74	77.56	< 1	4	13	4871	71	23	483
US02C	0.11	50.43	23.27	7.71	0.049	1.65	0.71	0.41	7.4	1.177	0.22	4.16	97.19	1	8	27	8810	42	37	829
US03	0.22	14.98	4.44	3.65	0.317	1.22	40.81	0.05	1.43	0.231	0.08	32.75	99.96	4	2	37	3130	663	16	52
US07A	4.28	25.06	8.87	8.18	0.497	1.89	8	0.47	2.66	0.509	0.07	6.06	62.27	1	3	15	4779	220	20	334
US07B	0.9	41.38	20.75	7.87	0.187	1.66	3.36	0.49	6.49	1.262	0.09	5.16	88.70	1	8	28	11750	109	36	915
US09	0.05	26.73	7.37	4.15	0.361	1.55	33.32	0.3	2.03	0.372	0.11	17.46	93.75	2	2	26	2568	735	26	231
US10	0	54.54	19.08	5.03	0.167	1.71	4.1	2.72	5.23	0.91	0.17	6.58	100.24	< 1	6	15	3090	127	27	616
US13A	8.77	11.35	2.14	10.13	0.537	1.4	5.28	0.15	0.34	0.076	0.02	0.47	31.89	< 1	< 1	< 5	470	171	8	52
US13B	0.38	51.87	16.54	9.4	0.27	1.63	4.51	1.57	4.41	0.77	0.15	6.61	97.73	1	5	21	6266	135	28	522
US17	2.71	27.04	6.95	11.94	0.873	3.48	11.12	0.47	1.4	0.393	0.09	16.44	80.20	1	2	11	3261	284	17	256
US18	5.74	25.13	6.41	10.54	0.324	1.49	4.14	0.2	2.03	0.379	0.06	2.71	53.41	1	2	14	3007	114	14	221
Haufenreith																				
22 TB 01	< 0.01	51.25	26.05	6.14	0.021	2.18	0.28	1.44	4.38	1.065	0.14	6.6	99.55	25	5	191	739	514	23	133
Peggau-Taschen																				
MB01	0.31	53.6	21.97	10.8	0.017	2.69	0.47	1.32	2.62	0.931	0.26	5.1	99.78	22	4	157	492	280	39	92
MB04	0.1	28.62	15.93	6.82	0.236	2.27	17.68	0.61	3.79	3.503	0.88	18.36	98.70	21	3	358	709	411	28	256
MB05	1.47	52.09	11.39	9.24	0.146	0.94	10.16	2.02	1.87	1.45	0.35	7.67	97.33	13	3	135	6352	112	26	200
MB 07	10.2	14.95	0.47	6.43	0.387	1.79	6.58	0.01	0.12	0.073	0.01	8.21	39.03	2	< 1	12	325600	1821	3	8
MB 09	1.95	35.5	6.88	10.08	0.463	2.3	19.63	0.68	1.28	0.812	0.19	17.16	94.98	9	1	87	12510	507	20	108
MB 10	3.38	18.59	3.11	14.8	0.802	3.95	24.42	0.14	0.57	0.442	0.07	23.78	90.67	6	< 1	66	7608	1394	14	48
ME 02	1.37	24.68	12.69	26.22	0.629	4.78	8.61	0.36	1.64	2.589	0.56	14.5	97.26	18	2	309	5864	160	25	228
Arzwaldgraben																				
22 AW 01	10.4	24.91	0.57	1.14	0.017	0.03	0.05	0.12	0.14	0.128	0.03	0.96	28.10	1	< 1	11	355900	4031	< 1	9
22 AW 03	3.94	31.35	4.35	26.2	1.598	0.26	0.06	0.05	1.78	1.132	0.09	5.99	72.86	9	1	127	109200	641	7	67
22 AW 05	0.22	49.51	9.2	22.46	0.859	0.83	0.46	0.55	3.26	2.376	0.38	6.33	96.22	22	2	260	9247	99	14	139
Kalkrippe																				
KR 01	< 0.01	8.41	3.13	2.57	0.232	0.4	46.08	0.11	0.7	0.149	0.06	37.2	99.04	3	< 1	24	489	444	13	33
Arzberg																				
22 AB 02	0.04	36.22	14.92	7.63	0.217	1.5	16.01	1.78	5.07	2.31	0.63	14.12	100.41	10	2	177	1399	202	26	252
22 AB 04	8.13	22.13	7.27	32.45	1.174	2.28	5.28	0.05	2.59	1.48	0.27	15.66	90.63	10	2	147	1960	46	15	88
22 AB 05	2.06	29.97	2.4	20.88	1.229	2.39	11.76	0.02	0.64	0.421	0.08	17.87	87.66	3	< 1	46	316	128	13	27
22 AB 11	0.18	14.17	6.36	4.07	0.332	3.26	35.63	0.06	2.41	0.977	0.29	31.48	99.04	4	1	85	1267	563	10	113
22 AB 12	8.48	33.86	2.34	4.07	0.197	0.5	0.97	0.03	0.7	0.346	0.07	3.65	46.73	3	< 1	34	185600	2289	3	34
21AB01	6.53	36.67	0.66	29.52	1.213	1.98	3.28	0.02	0.05	0.105	0.02	6.17	79.69	1	< 1	17	90280	629	6	10
21AB02	9.87	27.15	1.16	44.59	1.529	2.81	2.77	0.06	0.17	0.046	< 0.01	10.74	91.03	2	< 1	34	37480	583	10	9
21AB03	8.28	28.1	5.48	43.84	0.353	3.39	1.01	< 0.01	0.24	0.715	0.16	6.48	89.77	5	< 1	64	1448	50	8	43

sample	Cr	Co	Ni	Cd	Cu	Zn	Ga	Ge	As	Rb	Nb	Mo	Ag	In	Sn	Sb	Cs	La	Ce	Pr
	ppm	ppm	ppm	ppm	ppm	ppm	ppm	ppm	ppm	ppm	ppm	ppm	ppm	ppm	ppm	ppm	ppm	ppm	ppm	ppm
Analysis Method	FUS-MS	FUS-MS	FUS-MS	FUS-MS	FUS-MS	FUS-MS	FUS-MS	FUS-MS	FUS-MS	FUS-MS	FUS-MS	FUS-MS	FUS-MS	FUS-MS	FUS-MS	FUS-MS	FUS-MS	FUS-MS	FUS-MS	FUS-MS
Kaltenberg-Burgstall																				
US01	30	2	16	< 0.5	17	80	7	< 1	6	35	10	< 2	0.5	< 0.2	1	1.1	1.1	19.8	34	4.39
US02A	< 20	8	13	25.5	41	6310	21	1	< 5	89	125	< 2	75.3	0.3	3	94.4	6.5	72.2	141	14.7
US02C	< 20	3	9	1	5	599	36	2	< 5	150	207	< 2	3.8	< 0.2	4	7.2	10.3	103	192	21.1
US03	20	2	10	0.8	20	189	7	< 1	30	32	8	< 2	0.4	< 0.2	1	7.1	1.1	20.4	33.9	4.4
US07A	< 20	8	9	48.5	68	11300	15	< 1	< 5	55	91	39	> 100	0.3	2	138	2.9	44.1	82.1	8.76
US07B	< 20	6	8	6.2	54	1600	35	2	< 5	140	228	< 2	25.6	< 0.2	5	37.7	7	148	275	28.7
US09	< 20	3	6	3.4	5	618	11	< 1	11	43	63	< 2	1.3	< 0.2	1	6.3	1.7	44.8	88.9	8.57
US10	< 20	2	4	< 0.5	11	142	27	2	< 5	185	174	< 2	< 0.3	< 0.2	3	1.1	16.9	98.2	177	19.3
US13A	< 20	11	15	124	13	25300	5	< 1	< 5	7	14	< 2	> 100	0.8	1	> 200	0.7	9.8	19.2	2.22
US13B	< 20	5	8	11.1	15	3260	24	2	< 5	95	142	< 2	4.6	< 0.2	3	6.1	8.4	78.1	143	15.8
US17	< 20	8	10	35.6	102	8870	12	< 1	< 5	29	73	< 2	63.4	0.3	1	79.3	1.4	36.1	68.2	7.29
US18	< 20	12	15	69.7	62	11700	10	< 1	< 5	59	59	< 2	> 100	0.3	2	180	8.8	42.7	78.3	8.3
Haufenreith																				
22 TB 01	150	12	< 20		< 10	80	36	2	5	219	23	< 2	< 0.5	< 0.2	4	2.2	7.9	34.6	75.7	7.71
Peggau-Taschen																				
MB01	120	18	61	< 0.5	18	206	30	2	26	120	21	< 2	<0.3	< 0.2	3	2.6	5.2	50.2	95.1	11.5
MB04	260	44	104	< 0.5	42	38	24	1	140	129	73	< 2	< 0.3	< 0.2	2	1.7	5.8	54.9	108	13.2
MB05	50	327	32	< 0.5	8	60	16	< 1	7	49	29	4	< 0.3	< 0.2	4	0.9	3.6	30.3	63.4	7.98
MB 07	< 20	8	< 20		40	6320	2	< 1	< 5	3	< 1	< 2	3.1	< 0.2	< 1	3.1	< 0.5	3	7.1	0.96
MB 09	20	26	30		30	260	9	< 1	< 5	31	14	< 2	< 0.5	< 0.2	1	0.9	1.4	17.7	36.7	4.78
MB 10	< 20	38	40		120	140	5	< 1	11	15	6	2	0.7	0.2	1	1.5	0.7	12.8	25.9	3.43
ME 02	30	23	60		30	230	23	2	< 5	37	33	2	0.7	< 0.2	1	3.3	2.4	74.1	128	14.7
Arzwaldgraben																				
22 AW 01	< 20	8	< 20		30	5480	3	< 1	< 5	3	< 1	< 2	19.1	< 0.2	< 1	14.3	< 0.5	0.6	1.4	0.2
22 AW 03	120	117	70		500	38300	63	11	6	34	8	< 2	41.9	< 0.2	1	29.1	1.5	3.4	11	1.57
22 AW 05	280	81	150		100	9480	24	5	17	70	20	< 2	2.9	< 0.2	1	13.6	2.2	10	28.4	4.2
Kalkrippe																				
KR 01	< 20	< 1	20		30	60	4	< 1	16	31	4	< 2	< 0.5	< 0.2	1	0.7	2	13.3	23.2	2.93
Arzberg																				
22 AB 02	< 20	10	30		< 10	< 30	22	< 1	< 5	97	48	< 2	< 0.5	< 0.2	2	0.7	6.5	28.1	68	7.9
22 AB 04	60	298	740		15600	180	10	2	254	59	17	2	10.4	0.2	2	1.3	2.1	7.4	19.7	2.93
22 AB 05	20	24	60		120	30	6	< 1	< 5	16	5	< 2	16.1	0.2	< 1	68.9	1	14.3	26.3	3.31
22 AB 11	< 20	< 1	< 20		< 10	460	10	< 1	< 5	25	24	< 2	< 0.5	< 0.2	1	1.6	1.3	24.8	54.1	6.16
22 AB 12	< 20	15	< 20		240	19000	8	2	< 5	14	5	< 2	36	0.3	1	31.3	< 0.5	4.1	8.8	0.99
21AB01	< 20	15	19	81.3	32	22100	6	2	< 5	< 2	2	< 2	3.6	1.1	2	1.7	< 0.5	3.3	10.4	1.73
21AB02	< 20	36	35	37	20	9860	13	2	8	7	2	< 2	1.7	0.3	117	1.2	0.8	6.6	19.4	2.98
21AB03	< 20	84	88	242	39	69700	36	3	7	4	10	8	21.4	0.9	1	1.1	< 0.5	10	24.2	3.25

sample	Nd	Sm	Eu	Gd	Tb	Dy	Ho	Er	Tm	Yb	Lu	Hf	Ta	W	Tl	Pb	Bi	Th	U
	ppm	ppm	ppm	ppm	ppm	ppm	ppm	ppm	ppm	ppm	ppm	ppm	ppm	ppm	ppm	ppm	ppm	ppm	ppm
Analysis Method	FUS-MS	FUS-MS	FUS-MS	FUS-MS	FUS-MS	FUS-MS	FUS-MS	FUS-MS	FUS-MS	FUS-MS	FUS-MS	FUS-MS	FUS-MS	FUS-MS	FUS-MS	FUS-MS	FUS-MS	FUS-MS	FUS-MS
Kaltenberg-Burgstall																			
US01	17.4	4	1.26	3.3	0.5	3.2	0.6	1.7	0.23	1.5	0.23	1.4	0.6	< 1	0.1	638	< 0.4	3.3	2.9
US02A	50.5	7.7	1.89	5.5	0.8	4.8	0.9	2.6	0.4	2.5	0.43	10.6	9.4	2	0.2	192000	< 0.4	11.8	3.3
US02C	69.5	11.4	2.99	7.3	1.1	6.5	1.3	4	0.59	3.8	0.58	16	13.6	3	0.5	8300	< 0.4	19	5.1
US03	17.2	3.6	1.15	3.1	0.5	2.8	0.6	1.6	0.22	1.4	0.2	1.3	0.4	1	< 0.1	697	< 0.4	3.2	0.6
US07A	30.2	5.1	1.45	4.1	0.7	4.4	0.9	2.5	0.36	2.3	0.38	7.2	6.7	2	0.5	243000	< 0.4	7.4	2.4
US07B	99.1	15.4	3.73	10.5	1.5	8.1	1.5	4.2	0.64	4.1	0.68	19	16.8	3	0.2	51000	< 0.4	19.5	6.2
US09	30.8	5.3	1.76	4.6	0.7	4.6	0.9	2.6	0.35	2.2	0.34	4.5	3.9	1	< 0.1	2120	< 0.4	5.4	2.2
US10	62.2	9.9	2.53	6.5	0.9	5.1	1	2.7	0.4	2.5	0.37	11.8	18.9	4	1	119	4.6	14	3.3
US13A	8.3	1.7	0.68	1.8	0.3	2	0.3	0.9	0.13	0.8	0.11	1	1	2	0.7	476000	< 0.4	1.7	0.5
US13B	52.3	8.7	2.33	6.1	0.9	5.1	1	2.9	0.42	2.7	0.4	10	9.3	1	0.3	8500	< 0.4	12.8	3.2
US17	25.7	4.4	1.38	3.7	0.6	3.7	0.7	1.9	0.25	1.7	0.26	5.1	5.9	1	< 0.1	135000	< 0.4	6.6	2.2
US18	30	4.8	1.33	3.7	0.6	3.2	0.6	1.6	0.23	1.5	0.24	4.8	4.6	< 1	0.6	317000	< 0.4	6.1	2.1
Haufenreith																			
22 TB 01	30	5.6	0.9	4	0.6	3.8	0.7	2.1	0.3	1.8	0.26	3.7	1.5	< 1	1.1	27	< 0.4	14.8	2.8
Peggau-Taschen																			
MB01	42.2	8.4	1.51	6.9	1.1	6.7	1.3	3.6	0.5	3.1	0.44	2.3	1.3	2	0.6	6	< 0.4	17.7	2.5
MB04	49.2	9.9	2.61	7.5	1.1	5.7	1	2.7	0.34	2	0.27	5.9	4.2	2	0.5	10	< 0.4	6.4	8.6
MB05	31.2	6.6	1.74	5.9	0.9	5.1	0.9	2.5	0.34	2.1	0.32	4.3	1.8	1	0.1	14	< 0.4	4.7	1.4
MB 07	4.3	0.6	< 0.05	0.8	0.1	0.7	0.1	0.3	< 0.05	0.2	0.03	< 0.2	< 0.1	< 1	< 0.1	8440	< 0.4	0.1	< 0.1
MB 09	20.9	4.9	1.75	4.8	0.7	4.4	0.8	2.2	0.27	1.8	0.28	3	0.9	5	0.1	1170	< 0.4	2.8	0.9
MB 10	14.5	3.5	1.87	3.5	0.5	3.1	0.5	1.4	0.17	1	0.17	1.2	0.4	3	< 0.1	3520	< 0.4	1.1	0.4
ME 02	53.4	8.8	3.18	7.3	1	5.7	1	2.9	0.38	2.4	0.38	6.2	2.3	4	0.3	36	< 0.4	2.9	2
Arzwaldgraben																			
22 AW 01	1.1	< 0.1	< 0.05	0.1	< 0.1	0.1	< 0.1	< 0.1	< 0.05	< 0.1	0.01	< 0.2	< 0.1	< 1	< 0.1	> 10000	< 0.4	< 0.1	< 0.1
22 AW 03	8.6	1.9	< 0.05	2	0.3	1.4	0.3	0.7	0.1	0.6	0.08	1.8	0.9	< 1	0.1	20600	< 0.4	0.6	0.3
22 AW 05	21.3	5.3	2.69	4.4	0.6	3.3	0.6	1.6	0.2	1.2	0.17	3.6	1.4	< 1	0.2	7570	< 0.4	1.7	0.5
Kalkrippe																			
KR 01	12.2	2.7	0.61	2.7	0.4	2.4	0.4	1.2	0.17	1	0.16	0.8	0.2	< 1	0.1	21	< 0.4	2.3	1.4
Arzberg																			
22 AB 02	34.7	7.7	2.23	6.5	1	5.5	1	2.6	0.36	2.1	0.33	6.1	2.8	< 1	0.3	45	< 0.4	4.2	1.7
22 AB 04	14	3.5	1.82	3.6	0.5	3.4	0.6	1.7	0.23	1.4	0.22	2.3	1	5	< 0.1	283	< 0.4	1.3	1.4
22 AB 05	15.5	3.4	2.91	2.9	0.4	2.2	0.4	0.9	0.11	0.6	0.1	0.5	0.3	< 1	0.1	78400	< 0.4	0.4	0.3
22 AB 11	25.8	4.3	1.58	3.2	0.4	2.2	0.3	0.9	0.12	0.7	0.11	2.5	1.2	< 1	< 0.1	38	< 0.4	2.1	1.4
22 AB 12	4.6	0.7	< 0.05	0.8	0.1	0.6	0.1	0.3	0.05	0.3	0.06	0.6	0.2	< 1	0.1	142000	< 0.4	0.7	0.2
21AB01	7	1.7	< 0.05	1.4	0.2	1	0.2	0.3	< 0.05	0.3	0.04	< 0.2	< 0.1	2	< 0.1	273	< 0.4	0.1	< 0.1
21AB02	13.1	3	0.8	2.4	0.4	2	0.3	0.7	0.1	0.5	0.07	< 0.2	0.5	< 1	< 0.1	1170	< 0.4	0.3	< 0.1
21AB03	13.3	3.1	1.05	2.7	0.4	1.9	0.3	0.8	0.1	0.6	0.08	1	0.5	1	< 0.1	553	< 0.4	0.7	0.2